

**A Numerical Based Determination of Stress Intensity Factors for Partially
Cracked Flexural I-shaped Cross-sections**

Eshwari Someshwara Korachar

Thesis submitted to the faculty of the Virginia Polytechnic Institute and State
University in partial fulfillment of the requirements for the degree of

MASTER OF SCIENCE
In
CIVIL ENGINEERING

Matthew H Hebdon, Chair

Matthew R Eatherton

Ioannis Koutromanos

February 25, 2019

Blacksburg, Virginia

Keywords: Stress Intensity Factor, Geometry Factor, Edge Crack, Full-width Crack, Linear
Elastic Fracture Mechanics, Fracture

Copyright © 2019, Eshwari Someshwara Korachar

A Numerical Based Determination of Stress Intensity Factors for Partially Cracked Flexural I-shaped Cross-sections

ABSTRACT

The AASHTO LRFD design specifications and the AASHTO manual for bridge evaluation are consistently revised using knowledge of previous bridge failures. Although modern steel structures are designed to resist fatigue cracking from service loads, cracks in the tension flanges of steel bridge girders have been observed as a result of stress concentrations, design errors, welding quality control, and vehicular impacts. Cracks can grow in size with time and active cyclic live loads and may result in a member fracture. Fracture is a dangerous limit state which occurs with little to no warning. One method to quantify the stress field in the vicinity of a crack tip is by calculating the Stress Intensity Factor (SIF) around the crack tip. Finding SIFs for a cracked geometry may help an engineer to determine the fracture potential based on crack dimensions found during the inspection. Rolled I-beam and steel plate girders are extensively used as bridge superstructure members to efficiently carry live loads. This research was focused on determining Stress Intensity Factors (SIFs) of partially cracked I-sections using Finite Element Analysis. Two different tension flange crack profiles were studied: edge cracks, and full-width cracks. The SIF solutions were further used to study the fracture behavior and stress redistribution in the partially cracked flexural I-shaped members.

A Numerical Based Determination of Stress Intensity Factors for Partially Cracked Flexural I-shaped Cross-sections

GENERAL AUDIENCE ABSTRACT

Steel is one of the fundamental materials used in the construction of bridge structures, and steel girder bridges are one of the most common types of bridge structures seen in the United States. Past bridge failures have helped engineers to understand shortcomings in design specifications, and AASHTO codes have been developed and revised over the years to reflect an improved understanding and evolution of engineering behavior. Engineers must make sure that a design is robust enough for functional use of the component during its service life. It is also equally important to understand the potential chances of failure and make the structure strong enough to overcome any failure mechanisms. Fracture is one structural failure mode which occurs with little to no warning and hence is very dangerous. One efficient way to quantify the stress field in the vicinity of a crack tip is by calculating the Stress Intensity Factor (SIF) around a crack tip. Fracture literature is available which describes different methods of determining SIFs for cracked members. However, there are no solutions available to find a SIF of a partially cracked flexural I-shaped members. This research was focused on determining Stress Intensity Factors and studying the fracture behavior of partially cracked I-sections using Finite Element Analysis. The resulting SIF solutions were further used to study the fracture behavior and stress redistribution in partially cracked flexural I-shaped members.

Table of Contents

List of Figures	vi
List of Tables	ix
CHAPTER 1: Introduction	1
1.1 Background	1
1.2 Objective and Scope	7
CHAPTER 2: Literature Review	10
2.1 Fracture Mechanics	10
2.2 Numerical Techniques.....	12
2.3 Experimental and Analytical Research Studies on Fracture Mechanics.....	19
2.4 Fracture Resilience and Redundancy	29
CHAPTER 3: Analytical Methods.....	32
3.1 Modeling	32
3.1.1 Benchmark Study	39
3.1.2 Model Types.....	41
3.2 Parametric Study	52
3.2.1 Edge Crack Geometries.....	54
3.2.2 Full-width Crack Geometries	57
CHAPTER 4: Results and Discussion	60
4.1 Benchmark Study	60

4.2 Model Types.....	63
4.3 Parametric Study – Edge Crack Geometry	68
4.4 Parametric Study – Full-Width Crack Geometry	79
4.5 Fracture Behavior of Edge Cracked Specimens.....	86
4.6 Stress Redistribution in a Partially Cracked Flexural I-shaped Member	92
CHAPTER 5: Conclusions and Summary	101
5.1 Conclusions.....	101
5.2 Future Work and Recommendation	103
References.....	106
APPENDIX A.....	109
A.1 Model Development	109
APPENDIX B	118
B.1 Handbook Solution for Benchmark Study Specimens	118

List of Figures

Figure 1: Built-up Steel Plate Girders (Top), Rolled I-beam Girder (Bottom)	2
Figure 2: Relationship between Stress Cycles and Crack Length	3
Figure 3: Crack Tip Singularity	4
Figure 4: Fracture modes	5
Figure 5: Crack Geometries Located in the Tension Flange of an I-shaped Member	7
Figure 6: Rectangular Quarter-point Element, Triangular, and Collapsed Singular Finite Element	13
Figure 7: One Dimensional Three Node Element.....	14
Figure 8: Quarter Point Element	15
Figure 9: (a) 2-D (b) 3-D Singular Finite Elements.....	16
Figure 10: Assigning Collapsed Quarter-point Elements in ABAQUS.....	17
Figure 11: Relation between Fracture Stress and Crack Size	20
Figure 12: (a) Two-tip web crack (b) Symmetric three-tip crack.....	21
Figure 13: Shape Classification of the Specimens.....	23
Figure 14: Cracked I-beam Geometry	24
Figure 15: FE Data Points and Curve Fit.....	25
Figure 16: Creating V-notch in the Test Specimens	27
Figure 17: Refined Meshing at the Crack Tip	28
Figure 18: Flexural I-shaped Member with Edge Crack, and Full-width Crack Profile	32
Figure 19: Partition around the Crack Line (Top), Schematic Diagram of Partition around the Crack tip (Bottom)	35
Figure 20: Typical Generated Mesh (top), Schematic Diagram of Circular Mesh (Bottom)	36
Figure 21: History Output Request	37
Figure 22: Typical Picked-set of a Contour	38
Figure 23: History Output.....	38
Figure 24: Half Symmetric Plate Model with Edge Crack Profile	40
Figure 25: Specimen B2 Model	41
Figure 26: (a) Built-up Member, (b) I-shaped member	42
Figure 27: Trapezoidal Loading.....	44

Figure 28: Symmetric Model with Trapezoidal Loading	45
Figure 29: (a) Elevation and (b) Cross-sectional View of an Edge Crack Configuration in an I-shaped member	46
Figure 30: (a) Elevation and (b) Cross-sectional View of an Edge Crack Configuration in an Axially Loaded Plate.....	47
Figure 31: Edge Crack Plane in the Tension Flange.....	47
Figure 32: Fine Meshing around the Crack Line in the Tension Flange of the I-shaped member	48
Figure 33: (a) Elevation and (b) Cross-sectional View of a Full-Width Crack Configuration in an I-shaped member.....	50
Figure 34: (a) Elevation and (b) Cross-sectional View of a Full-Width Crack Configuration in an Axially Loaded Plate.....	50
Figure 35: Full-width Crack Plane in the Tension Flange	51
Figure 36: Structured Mesh in the Partially Cracked Flexural I-shaped Member (Top), Fine Mesh along the Full-width Crack Line in the Tension Flange (Bottom).....	52
Figure 37: Edge Cracked Plate: (a) Elevation View (b) Cross-sectional View	53
Figure 38: Partially Cracked Flexural Member Cross-sections.....	54
Figure 39: Cross-Sectional Stress Profiles of Rectangular Beam Models.....	62
Figure 40: Cross-sectional Stress Profiles of the I-shaped member	64
Figure 41: Partially Cracked I-shaped member with an Edge Crack.....	65
Figure 42: Local Stress Concentration around the 3 inch Edge Crack in an I-shaped member ...	65
Figure 43: Stress Concentration in a 3 inch Edge Crack Axial Member.....	66
Figure 44: Stress Contours in a Partially Cracked flexural I-shaped member with a Full-width Crack	67
Figure 45: Localized Stress near the Full-width Crack in a flexural I-shaped member	67
Figure 46: Stress Concentration in Flexural Member with Crack Growth.....	72
Figure 47: Cross-Sectional Stress Profiles of Flexural Member with Different Crack Lengths ..	73
Figure 48: Shift in Neutral-Axis of Flexural Member with Increasing Crack Length	73
Figure 49: Geometry Factor ' β ' for a flexural I-shaped member with an Edge Crack Profile.....	77
Figure 50: Geometry Factor ' β ' for an Axially Loaded Plate with an Edge Crack Profile	78
Figure 51: Geometry Factor ' β ' for an Edge Crack Profile	79

Figure 52: Geometry Factor ‘ β ’ for a flexural I-shaped member with a Full-width Crack Profile	84
Figure 53: Geometry Factor ‘ β ’ for an Axially Loaded Plate with a Full-width Crack Profile ...	85
Figure 54: Geometry Factor ‘ β ’ for Full-width Crack Profile	86
Figure 55: Temperature Shift between ‘ K_{Id} ’ & ‘ K_{Ic} ’	87
Figure 56: Fracture Stress vs Crack Length Relation for Higher ($228.5 \text{ ksi}\sqrt{\text{in}}$), and Lower-bound Fracture Toughness ($80 \text{ ksi}\sqrt{\text{in}}$)	90
Figure 57: (a) Built-up Member (b) Partially Cracked flexural I-shaped member	93
Figure 58: Structured Mesh along the Cross-section of the Tension Flange	94
Figure 59: Detailed View of the Elements above the Full-width Crack Line	94
Figure 60: Cross-sectional Stress Profile of the Partially Cracked flexural I-shaped member with a Full-width Crack	95
Figure 61: Paths along the Flange Width (Top), Detailed View of the Elements (Bottom)	96
Figure 62: (a) Built-up Section (b) flexural I-shaped member with Full-width Crack	99
Figure 63: Typical Failure Assessment Diagram	105
Figure 64: Quarter portion of the tension plate	109
Figure 65: X-axis symmetry	110
Figure 66: Y-axis symmetry	110
Figure 67: Tension loading	111
Figure 68: Seam line representing the edge crack	112
Figure 69: Crack Creation	113
Figure 70: Edit crack options	114
Figure 71: Crack-tip Singularity	115
Figure 72: History Output Request	116
Figure 73: History Output	117
Figure 74: Visualization of Edge Cracked Plate	117

List of Tables

Table 1: Axial Specimen Matrix.....	39
Table 2: Bending Specimen Matrix	41
Table 3: Flange Thickness Variation for Edge Crack Profile.....	55
Table 4: Web Height Variation for Edge Crack Profile	55
Table 5: Tension Flange Width Variation for Edge Crack Profile	56
Table 6: Edge Crack Length Variation for Edge Crack Profile.....	57
Table 7: Tension Flange Width Variation for Full-width Crack Profile	58
Table 8: Web Height Variation for Full-width Crack Profile.....	58
Table 9: Tension Flange Thickness Variation for Full-width Crack Profile	59
Table 10: Full-width Crack Profile Variation for Full-width Crack Profile	59
Table 11: Benchmark Study Results.....	61
Table 12: Variation of SIF with the Tension Flange Thickness	69
Table 13: Variation of SIF with the Web Height.....	70
Table 14: Variation of SIF with Tension Flange Width	71
Table 15: Variation of SIF with Edge Crack Length.....	74
Table 16: Specimen Matrix for Edge Crack Profile	76
Table 17: Variation of SIF with Tension Flange Width	80
Table 18: Variation of SIF with the Web Height.....	80
Table 19: Variation of SIF with the Tension Flange Thickness	81
Table 20: Average SIF values for a Specific Crack Length	82
Table 21: Specimen Matrix for Full-width Crack Profile.....	83
Table 22: Fracture Stress Values for Higher Fracture Toughness Value ($228.5 \text{ ksi}\sqrt{\text{in}}$).....	89
Table 23: Fracture Stress Values for Lower-bound Fracture Toughness Value ($80 \text{ ksi}\sqrt{\text{in}}$)	90
Table 24: FE Stress Calculations	97
Table 25: FE Stress Calculation.....	100

CHAPTER 1: Introduction

1.1 Background

There have been several cases of bridge failures in the past and some of the primary reasons for these failures are material defects, design errors, loading uncertainties, and construction deficiencies (Roylance, 2001). The AASHTO LRFD Design Specifications and the AASHTO Manual for Bridge Evaluation have been improved over the past few decades with a deep understanding of the previous bridge failures. The engineer has to make sure that the design is robust enough for the effective functioning of the different individual components during its service life. It is also important for them to understand the potential chances of failure and make the structure strong enough to overcome any failure mechanisms (Grandt, 2004).

Steel girder bridges are one of the most common types of bridge structures seen in the US. Girders can be either a rolled I-shape member or a built-up member and are extensively used as bridge superstructure members to efficiently carry live loads. Figure 1 shows a riveted built-up girder with web plates, flange angles, and cover plates (Top), and rolled I-beam girder (Bottom). A structural member comprising of steel plates and angles connected using either bolts or welds is called a built-up member.

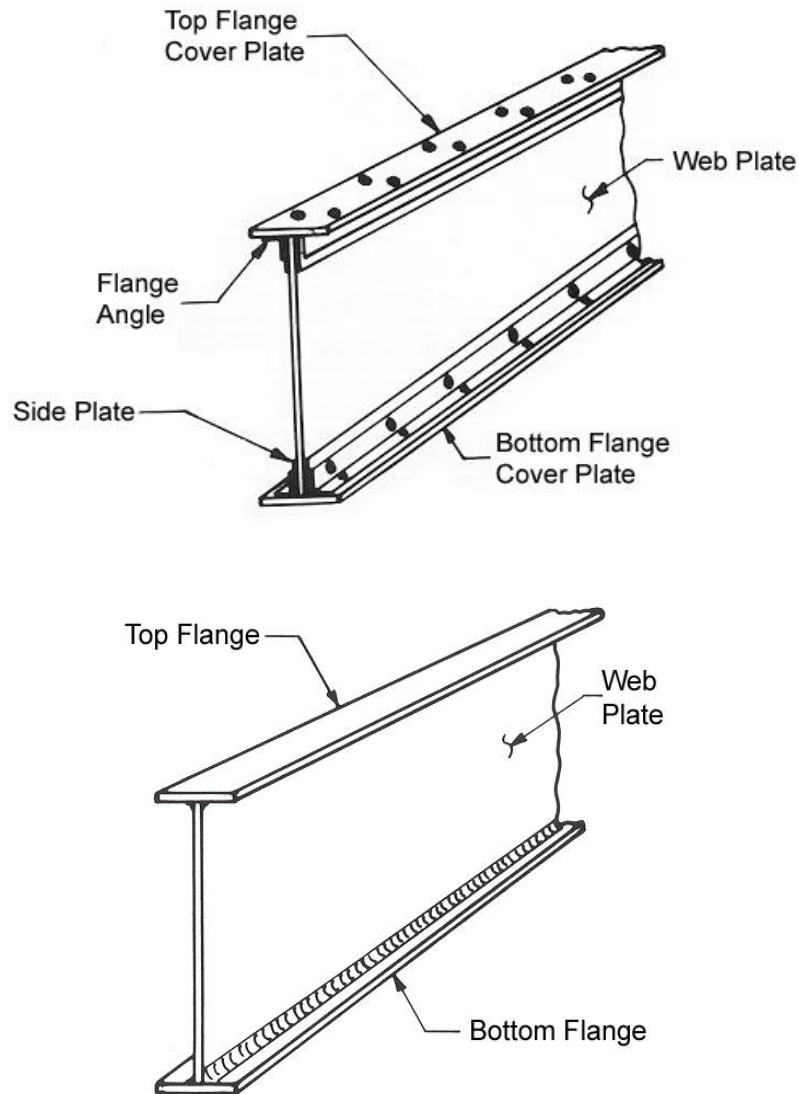


Figure 1: Built-up Steel Plate Girders (Top), Rolled I-beam Girder (Bottom) (Ohio Department of Transportation, 2008)

Although modern steel structures are typically designed to prevent fatigue, cracks which may reduce the fatigue life of steel sections can form and grow due to material defects, construction errors, member geometry, stress concentrations, and vehicular impacts. For example, in the case of an overpass type bridge with low clearance, overheight vehicles may impact the bottom portion of the steel girder, resulting in damage and potential cracks or crack initiation points. Moreover, bridge structures are subjected to continuous live load cycles from

moving vehicles. These load cycles can cause an existing flaw or crack to grow in size and eventually result in failure. With time and continuously acting fatigue load cycles, a crack may reach critical crack length and cause the member fracture (Roylance, 2001) as shown in Figure 2.

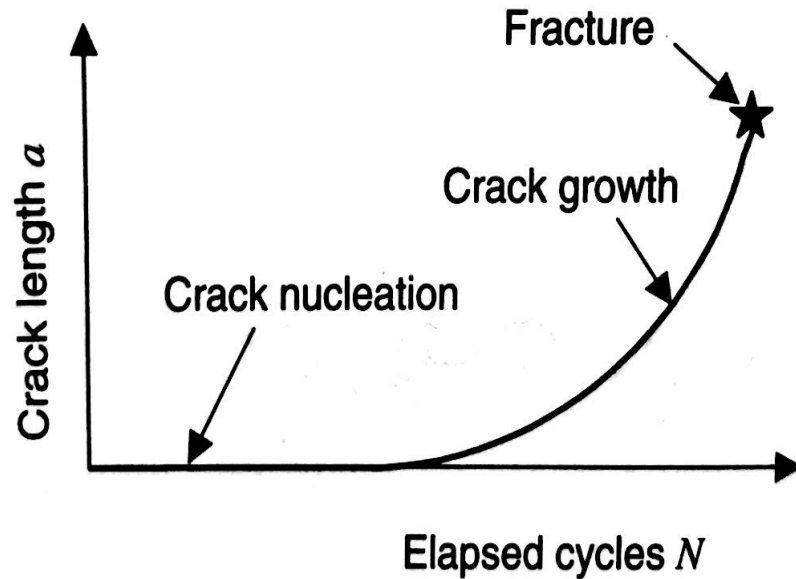


Figure 2: Relationship between Stress Cycles and Crack Length (Grandt, 2004)

The field of fracture mechanics involves the study of the behavior of cracked members under applied loading conditions. “Fracture toughness”, is a measure of resistance offered by a component to crack growth, and is a material property. Hence, it is important to choose the material properties as per the requirements. Generally, the material should be strong, stiff (modulus of elasticity), and have resistance to fracture, fatigue, and corrosion (Grandt, 2004). Other factors which contribute to the study of fracture resilience are member geometry and type of loading since they have a direct influence on the crack growth behavior.

According to the theory of linear elasticity, for a very sharp crack, the theoretical stress at the crack tip is equal to infinity, which is called “crack tip singularity”, (Figure 3). However,

it is not possible to have infinite stress in real materials. Localized stress concentrations can be observed at the crack tip. In ductile materials such as steel, the material will start to yield due to these high stresses at the crack tip, and plastic deformation will occur creating a plastic zone around the crack tip (Figure 3). The plastic deformation will blunt the cracks, which means the cracks will have some non-zero radius, thus removing the crack tip singularity in the member. It should be noted that fracture can occur without any plastic deformation even though the applied stress is well below the yield stress (Grandt, 2004).

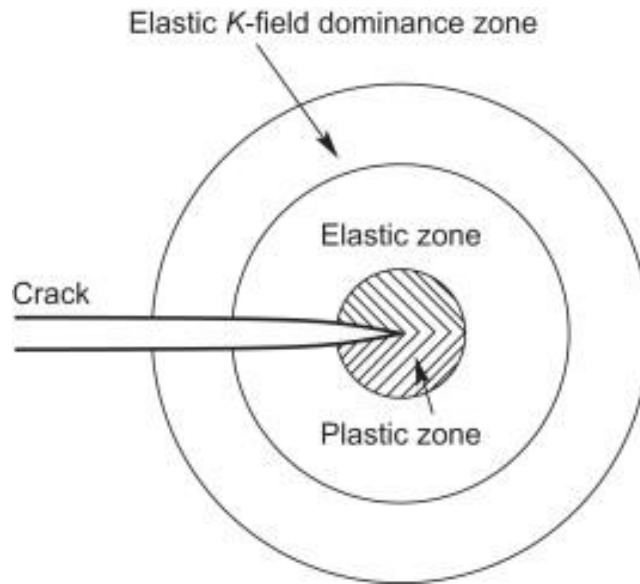


Figure 3: Crack Tip Singularity (Sun and Jin, 2012)

The size of this plastic zone limits the application of Linear Elastic Fracture Mechanics (LEFM). The Stress Intensity Factor (SIF) equation which is developed assuming the linear elastic material behavior, should be altered to include any plasticity in the member. If the size of the plastic zone is small compared to the size of the member, the changes in the SIF equations will be insignificant (Barnby, 1971). Usually, most of the bridge structural members are elastic in behavior. Also, the cracked steel sections such as W-shapes, the material behavior at the member level will be mostly elastic. Hence, LEFM analysis can be applied to study the

crack growth in a member (Courtin, Gardin et al., 2005). Moreover, bridge structures are more susceptible to brittle fractures because of the cold environmental conditions in which they can exist during winter months. Considering these aspects, LEFM is used to determine the SIF equations for the current research.

In LEFM there are three modes of failure which depend on the loading pattern. Mode I or ‘opening mode’ is related to tension loading which causes the crack faces to open perpendicular to each other. Mode II & III are related to shear loading which causes the crack faces to slide relative to each other as shown in Figure 4.

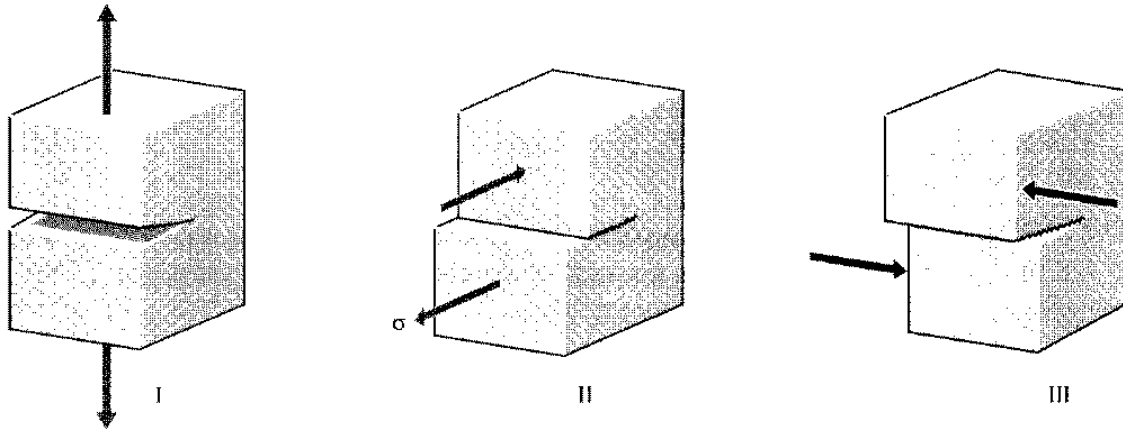


Figure 4: Fracture modes (Roylance, 2001)

One of the efficient ways to measure stress in the vicinity of the crack tip is by calculating the Stress Intensity Factor (SIF). SIF is one of the fundamental terms used in LEFM and is denoted by ‘K’. The general expression for SIF is given by equation 1.

$$K = \beta\sigma\sqrt{\pi a} \quad (1)$$

where ‘ β ’ is the geometry factor, ‘ σ ’ is the far-field stress, and ‘ a ’ is the crack length. This equation can be applied to calculate the SIF of any arbitrary geometry and crack profile, with a unique geometry factor, ‘ β ’. The geometry factor ‘ β ’ depends on the cross-sectional

dimensions and crack length of the considered geometry. The SIF, 'K' can be expanded to all the three modes of failure and sometimes even to the mixed modes of failures where both tension and shear loadings are measured. Mode I is most common in primary structural elements with tensile stresses longitudinal to the member, such as is present in plate girders. In this study, Mode I loading will be evaluated and ' K_I ' will be the SIF related to mode I or opening mode.

In order to determine the potential chances of structural failure, it is very important for an engineer to analyze the flaw criticality. SIF values can help to characterize the crack as critical or sub-critical. If the crack is critical, the member should be examined for any potential chances of fracture. Structural failure due to fracture can be very sudden without any plastic deformation, which means with no warning. If the crack is not critical, the remaining fatigue life can be calculated, because the crack will have slow steady growth with continuously load cycles (Sherman, 2016).

There has been much work conducted in the field of fracture mechanics and previous research has resulted in many different empirical formulas to determine the SIF of the various member and crack geometries. There are handbook solutions available which have SIF equations for several crack configurations (Grandt, 2004), (Tada, Paris et al., 2000). However, a search of relevant literature found no solutions available for calculating the SIF of partially cracked flexural I-shaped members.

1.2 Objective and Scope

The two objectives of the research study are: first, to analytically determine the SIF for both (a) an edge crack, and (b) a full-width crack in the tension flange of an I-shaped member, and second, to study the stress distribution of the partially cracked flexural I-shaped members.

In steel members, regions with high tensile stresses are more prone to fatigue crack formations, e.g., the tension flange of an I-shaped member. Hence, in this study, two crack geometries located in the tension flange of flexural members were studied. The first crack geometry was an edge crack, while second crack geometry was a full-width crack, as shown in Figure 5.

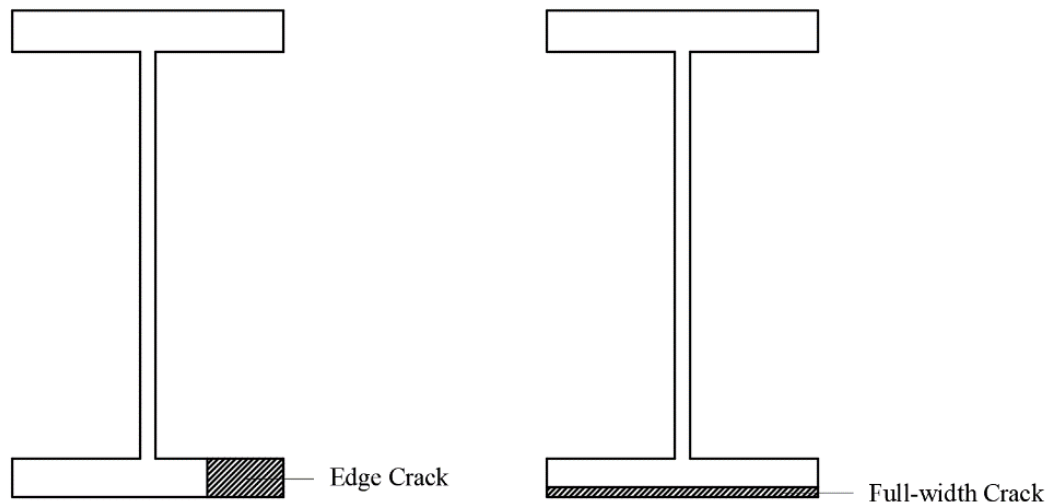


Figure 5: Crack Geometries Located in the Tension Flange of an I-shaped Member

The study was conducted in three phases. In the first phase, two FE models of 46' long partially cracked I-shaped member were developed. The first flexural member model had an edge crack in the tension flange. An edge crack was selected because it has similar geometry to common edge cracked plates loaded in tension, and for such flaws, common practice is to

treat the bottom flange as such. For flexural members, the tension flange represents the location with the largest tensile stress, and therefore the largest strain energy release rate. A crack will grow in size when the strain energy release rate exceeds the energy required to form new crack surfaces (Griffith, 1921).

The second flexural member model had a full-width crack in the tension flange. The crack was assumed to be all the way through the width of the tension flange and partially through the flange thickness. This crack profile was selected because of its similarity to mechanically fastened built-up girders with a failed single cover plate (Hebdon, Bonachera Martin et al., 2017). Such a geometry was theorized to have the potential to describe the stress state for members with single component failure. Afterward, the tension flange of the flexural I-shaped member was separately analyzed as an axially loaded plate with edge crack and full-width crack geometries. This was done because the behavior of the tension flange of an I-shaped flexural member is similar to the axial plate under tension. For the analysis, the same loading conditions as used in the tension flange of the flexural I-shaped member were applied. The obtained SIFs were further compared to the available handbook solutions of the edge cracked plates.

In the second phase, parametric studies were performed to determine the geometry factor, ' β ' for both (a) an edge crack, and (b) a full-width crack in a partially cracked I-shaped member. The resulting geometry factors were then compared with solutions widely accepted for uniaxial loaded plates with edge cracks. The geometry factor, ' β ' is a dimensionless term which is a function of crack length and other cross-sectional dimensions of the member. For the case of an I-shaped geometry, the variation of SIF was studied for parameters including tension flange thickness, tension flange width, web height, and crack length. From the obtained

results, parameters which had a significant influence on the SIF were used to develop an analytical equation for the geometry factor ' β ' for both the crack configurations considered in the study. The geometry factor ' β ' was further used to calculate the SIF in the vicinity of the crack tip.

In the third phase, the SIF solutions were used to study the fracture behavior of the specimens with edge crack profile. Both the I-shaped member and plate models were analyzed and a relation between the fracture stress and crack length was determined. Using this relationship, the fatigue crack growth behavior under the given loading condition was studied. Also, the critical crack length to cause the member fracture under given loading conditions were interpreted from the results.

Furthermore, a study comparing the stress redistribution of an I-shaped member with a full-width crack, and a built-up section with a failed cover plate was conducted. The stress increase in the tension flange of the I-shaped member due to the presence of a full-width crack was determined using cross-sectional stress values. In a cracked structural steel member, since the crack plane is not able to carry the load, and the presence of crack will reduce the net area of the section, the net-sectional stress is affected in the region immediately adjacent to the crack. A study was conducted to compare characteristics of a built-up I-shaped member with a failed cover plate to a solid I-shaped member with a full-width crack profile.

CHAPTER 2: Literature Review

2.1 Fracture Mechanics

Fracture mechanics can be classified into experimental fracture mechanics and computational fracture mechanics. The former method includes experimental studies, where specimens are tested to find fracture load/stress, critical crack length, or fracture toughness. The latter method involves the use of numerical techniques such as the Finite Element Method (FEM), and Boundary Element Method (BEM).

Some of the early works in the field of Fracture Mechanics was conducted by Griffith and Irwin. The early application to study crack parameters was based on the energy release rate. It was found that a crack will grow in size when the strain energy release rate (G) is greater than or equal to the energy required to form new crack surfaces (Griffith, 1921). A crack extension force ' G ' was derived, as shown in equation 2, where ' U ' is the elastic strain energy stored in a cracked member, and ' A ' is the crack area.

$$G = \frac{\delta U}{\delta A} \quad (2)$$

Later work derived a relation between the crack extension force ' G ' and SIF ' K ', based on the amount of elastic work required to close the crack tip, as given in equation 3 (Irwin 1957).

$$G \propto K^2 \quad (3)$$

Linear-Elastic Fracture Mechanics (LEFM) and Elastic-Plastic Fracture Mechanics (EPLM) are the two concepts used in Fracture Mechanics to study the crack parameters, which depend on the member material behavior. In the field of structural engineering, it is very common to assume linear elastic material behavior. The application of LEFM is limited by the

size of the plastic zone around the crack. Although there will be plastic material behavior at the tip of the crack, the member level material behavior will be mostly elastic. Therefore, LEFM can be used to determine the crack parameters.

Irwin proposed the term SIF, ‘K’ in 1957 (Irwin 1957), and the stress field in the vicinity of a crack can be measured in terms of SIF. For example, an elliptical notch will have stress as given by equation 4 (Grandt, 2004) at the crack tip. As the notch becomes very sharp (zero radius) the stress becomes infinite, which is called the “crack tip singularity”.

$$\sigma_{tip} = \lim_{\rho \rightarrow 0} \sigma \left(1 + 2\sqrt{\frac{a}{\rho}} \right) = \sqrt{\infty} \quad (4)$$

where ‘ ρ ’ is the notch radius and ‘a’ is the crack length

Using this relationship, an equation for the SIF was formulated, which is given by equation 5 (Grandt, 2004).

$$K_I = \lim_{r \rightarrow 0} \sqrt{2\pi r} \sigma_{tip} \quad (5)$$

σ_{tip} is found to depend on $r^{-1/2}$, where ‘r’ is the distance measured from the crack tip. When ‘r’ is equal to crack length ‘a’, the SIF equation becomes as given in equation 6.

$$K = \beta \sigma \sqrt{\pi a} \quad (6)$$

where ‘a’ is the crack length, ‘ σ ’ is the far-field stress, and ‘ β ’ is the geometry factor.

Another term commonly used in LEFM is the Stress Concentration Factor, ‘ K_t ’. ‘ K_t ’ gives a measure of the localized stress increase around the crack tip and is defined as the ratio of

local stress to remote or far-field stress. It depends on the geometry of the member and the alignment of the crack.

The stress field in the vicinity of the crack tip can be found using equation 632. The SIF depends on the crack configuration, type of loading, and cross-sectional geometry (Aliabadi, 2002), and the value of SIF determines the behavior of the crack (Critical or Sub-critical). A critical crack is one which may cause member fracture. Several studies have been conducted in the past and SIF solutions for common crack geometries are documented in handbooks (Grandt, 2004). Common crack geometries include an edge cracked plate, a double-edge cracked plate, a center cracked plate, a plate with radial cracks emanating from the hole, and an edge cracked rectangular beam.

2.2 Numerical Techniques

The Finite Element method (FE) is one of the most common methods used for the analysis of new crack configurations (Grandt, 2004). In numerical fracture mechanics, the crack growth behavior can be studied by calculating the crack parameters including SIF, Crack Tip Opening Displacement (CTOD), and J-integral. FE program packages like ABAQUS and ANSYS are specially designed to calculate the crack parameters using these above-mentioned approaches (Schreurs, 2012).

Previous researchers in the field mechanics have used special Finite Elements that have built-in square-root singularity in the calculation of SIF. According to the theory of linear elasticity, the stress at the crack tip is singular (infinite), which is called as crack tip singularity. Barsoum introduced the usage of quarter-point elements to incorporate the crack tip singularity and explains that the singularity in these elements can be achieved by placing the mid-side

node at the quarter point from the tip of the crack (Barsoum, 1976). Schreurs described the quarter point elements as “standard 8-node quadrilateral or 6-node triangular elements, where two mid-side points are repositioned towards one corner node, such that they divide the side in the ratio 1:3” (Schreurs, 2012), as shown in Figure 6.

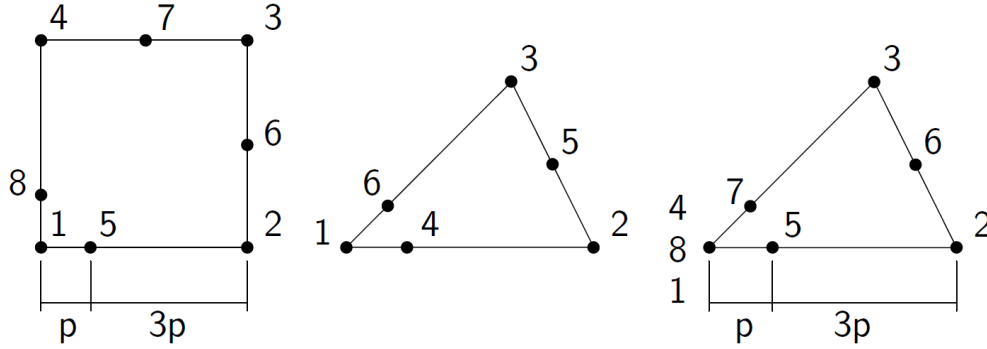


Figure 6: Rectangular Quarter-point Element, Triangular, and Collapsed Singular Finite Element (Schreurs, 2012)

Fracture literature has shown that using special finite elements that have built-in square-root singularity will improve the accuracy of the numerical results near the crack tip (Barsoum, 1976). These elements help to simulate the strain singularity which agrees with the theory of linear fracture mechanics (Aliabadi, 2002). The concept of crack tip singularity for a one-dimensional 3-node element is explained below. Figure 7 shows a three node element defined in the local coordinate system ($-1 \leq \xi \leq 1$), while in the global coordinate system node 1 is at the origin ($x=0$), and node 2 is at ‘L’ (length of the element).

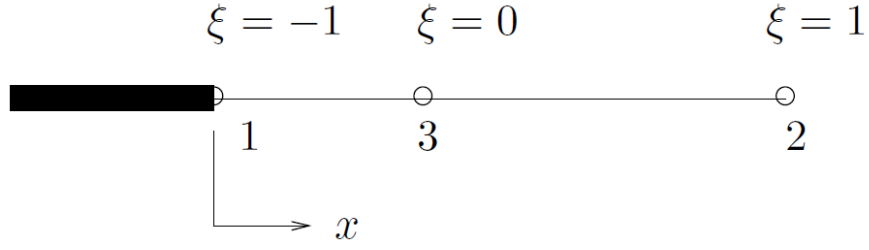


Figure 7: One Dimensional Three Node Element (Schreurs, 2012)

In FEA, the shape functions help us to define the deformed shape of an element at nodal points. The shape functions should satisfy displacement compatibility, and achieve constitutive relationships (Grandt, 2004). Further, these functions can be used to solve problems with applied load and the boundary condition. ABAQUS software uses these element shape functions for the analysis (ABAQUS 6.14 Documentation, 2014).

For a three-node element (Figure 7) there will be three shape functions, one for every node. It is denoted by N_i , where 'i' is the node number.

$$\text{Node 1: } N_1 = \xi (\xi - 1)$$

$$\text{Node 2: } N_2 = \xi (\xi + 1)$$

$$\text{Node 3: } N_3 = (\xi^2 - 1)$$

The position of any point in the global co-ordinate can be interpreted using equation 7.

$$x = \frac{1}{2} \xi (\xi - 1) x_1 + \frac{1}{2} \xi (\xi + 1) x_2 - (\xi^2 - 1) x_3 \quad (7)$$

For, $x_1 = 0$ and $x_2 = L$, equation 7 becomes,

$$x = \frac{1}{2} \xi (\xi + 1) L - (\xi^2 - 1) x_3 \quad (8)$$

Similarly, the displacement at any point along the x-direction can be interpreted using the nodal displacements u_1 , u_2 , and u_3 , using equation 7.

$$u = \frac{1}{2}\xi(\xi-1)u_1 + \frac{1}{2}\xi(\xi+1)u_2 - (\xi^2-1)u_3 \quad (9)$$

The strain can be calculated by taking the derivative of the displacement field. For a three-node element, the strain is given by equation 10.

$$\frac{du}{d\xi} = \left(\xi - \frac{1}{2}\right)u_1 + \left(\xi + \frac{1}{2}\right)u_2 - 2\xi u_3 \quad (10)$$

To convert the strain from local coordinate to global co-ordinate we can use the following equation 11.

$$\frac{du}{dx} = \frac{du/d\xi}{dx/d\xi} \quad (11)$$

If we apply this concept to a quarter point element, where the node 3 is at a distance of $L/4$ from the crack tip, as shown in Figure 8. For $x_1 = 0$, $x_2 = L$, and $x_3 = L/4$, equation 7 becomes,

$$x = \frac{1}{2}\xi(\xi+1)L - (\xi^2-1)\frac{L}{4} \quad (12)$$

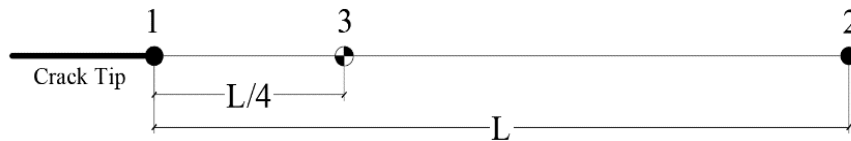


Figure 8: Quarter Point Element

The relationship between ‘ ξ ’ and ‘ x ’ is given by $\xi+1=\sqrt{\frac{4x}{L}}$. Further, differentiating

equation 12 with respect to local co-ordinate ‘ ξ ’ gives,

$$\frac{dx}{d\xi} = \frac{1}{2}(\xi+1)L = \sqrt{xL} \quad (13)$$

Using equation 11 & 13, we can show the strain singularity at the crack tip. At the crack tip, $x=0$, and $\xi=-1$, for which equation 14 becomes infinite, which proves the crack tip singularity property.

$$\frac{du}{dx} = \frac{du/d\xi}{\sqrt{xL}} \quad (14)$$

This proof of strain singularity can also be applied to 2-D and 3-D models. Figure 9 shows a 2-D and 3-D singular quarter-point elements. Barsoum has shown the proof of crack tip singularity property of 2-D eight-noded quadrilateral elements, 2-D six-noded triangular elements, 3-D twenty-noded cubic elements, and 3-D prism elements (Barsoum, 1976).

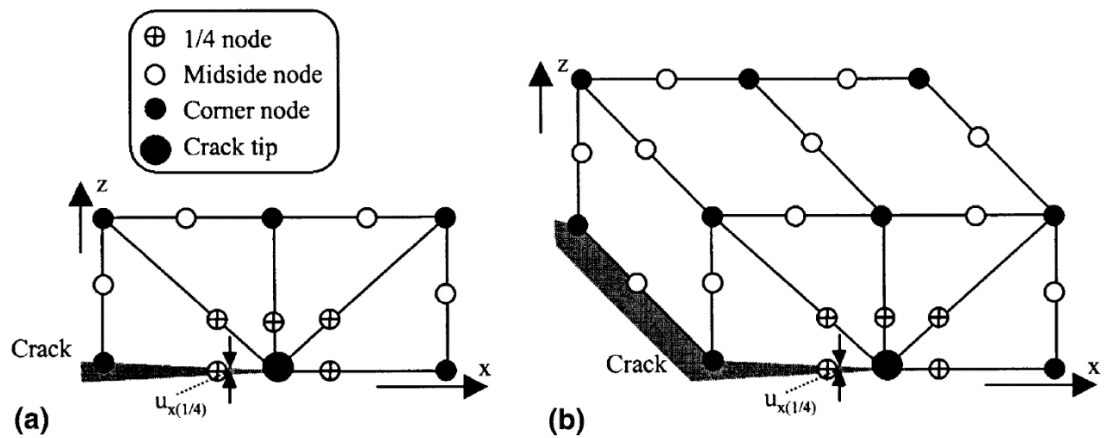


Figure 9: (a) 2-D (b) 3-D Singular Finite Elements (Courtin, Gardin et al., 2005)

In ABAQUS software, under the interaction tool, we have the option to assign quarter-point elements. Interaction module: Special → Crack → Edit → Singularity → Mid-side node parameter = 0.25 (Figure 10). Using these elements around the crack line helps to achieve strain singularity at the crack tip (ABAQUS Analysis User's Manual, 2006).

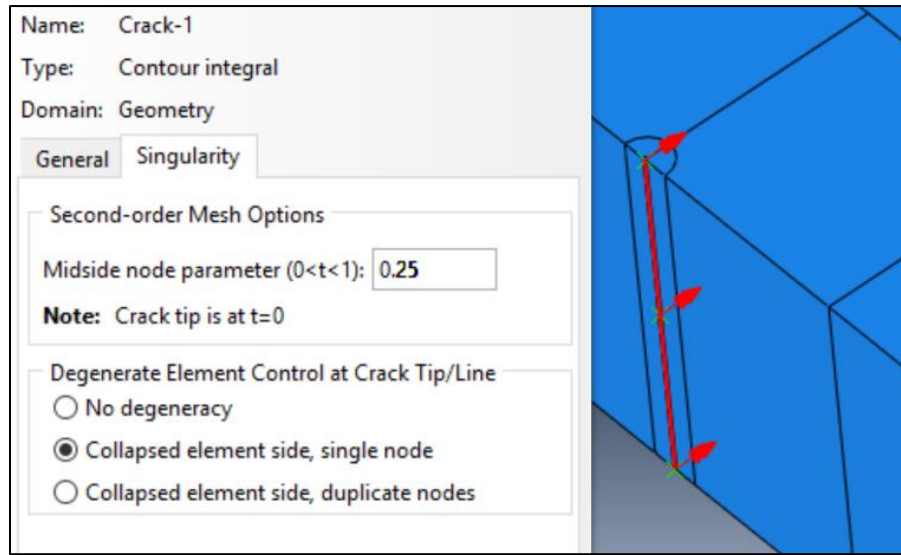


Figure 10: Assigning Collapsed Quarter-point Elements in ABAQUS

However, for the analysis, total strain energy and stiffness should be finite. According to Hibbitt, the stiffness of a 2-D rectangular or a 3-D cubic quarter-point elements was found to be singular at the crack tip (Barsoum, 1976). While the results obtained using 2-D triangular or 3-D prism quarter-point elements (Collapsed quarter-point elements) were comparatively better. Figure 6 shows a collapsed quarter-point element, where nodes 1, 8, and 4 are collapsed to move together as a single node. ABAQUS allows the user to use collapsed quarter-point elements for FEA, as shown in Figure 10. Furthermore, using numerical integration such as Gaussian integration rule to calculate the stiffness of special crack tip elements eliminates the stiffness singularity problem (Barsoum, 1976).

Although the usage of quarter-point elements to determine the SIF are widely known, there is an indirect energy method used to calculate the SIF. It is called the J-integral approach. Rice introduced the concept of J-integral (Rice, 1968). One advantage of using the J-integral approach is that it is path independent (Schreurs, 2012). It does not require refined meshes or usage of quarter-point elements around the crack region since it is dependent on the energy release rate. J-integral values are usually determined for elastic-plastic models, because of the dominant non-linear material behavior. For a linear material response, the SIF value can also be calculated from the J-integral value (Manual, 2006). For a plane strain condition, equation 15 can be used to calculate SIF from the obtained J-integral.

$$J = \frac{(1-\nu^2)}{E} K_I^2 \quad (15)$$

where ‘J’ is the J-integral, ‘K_I’ is the Mode-I SIF, ‘ν’ is the Poisson’s ratio, and ‘E’ is the Modulus of Elasticity of Steel.

Determination of J-integral and stress intensity factor using the commercial FE software ABAQUS in austenitic stainless steel (AISI 304) plates

Venkatachalam et.al., studied the variation of SIF, J-integral, and T-stress with respect to crack length, load, and specimen thickness. ‘T-stress’ is a fairly new term which is defined as a stress parallel to the crack plane (Venkatachalam, Harichandran et al., 2008). An edge cracked plate was analyzed for both linear-elastic and elastic-plastic models. Three dimensional FE models were developed using linear brick elements without reduced integration (C3D8).

It was observed that as the crack length was increased from 0.5 mm to 0.6mm, the SIF decreased significantly, approximately by $1000 \text{ MPa}\sqrt{\text{mm}}$. However, with further increase in

the crack length (0.6 mm to 0.9 mm) the decrease in the SIF was much less than before. Secondly, for both the linear-elastic and elastic-plastic models J-integral value decreased with the increase in load and there was a noticeable change in J-integral after the load crossed the elastic limit (300N). Lastly, the variation of T-stress with crack length, and specimen thickness was non-uniform (Venkatachalam, Harichandran et al., 2008).

Boundary Element Method (BEM)

In the past two decades, a new numerical technique called Boundary Element Method (BEM) was developed and introduced as an alternative to traditional analysis methods. Aliabadi in his book “The Boundary Element Method - Applications in Solids and Structures (Volume 2)”, describes BEM as one of the accurate and most efficient numerical technique for SIF calculation (Aliabadi, 2002). There have been a lot of developments in this field and the BEM has been applied by researchers to solve various 2-D, and 3-D problems.

Some of the important applications of the BEM includes the development of a fundamental solution or Green’s function which was limited to only 2-D problems. Next is the multi-region formulation which can be applied to solve symmetric and antisymmetric problems in both 2-D, and 3-D configurations by introducing artificial boundaries. Last of all, the Double Boundary Element Method (DBEM), where the problem is solved by applying displacement boundary integral equation and traction boundary integral equation to each one of the crack surfaces (Aliabadi, 2002).

2.3 Experimental and Analytical Research Studies on Fracture Mechanics

Fracture is one of the many structural failure modes which occurs with minimal to no warning and hence is very dangerous. Figure 11 shows that the stress required to cause member

fracture decreases as the crack length increase. SIFs also helps to evaluate the severity of an existing crack which could be a potential cause for fracture.

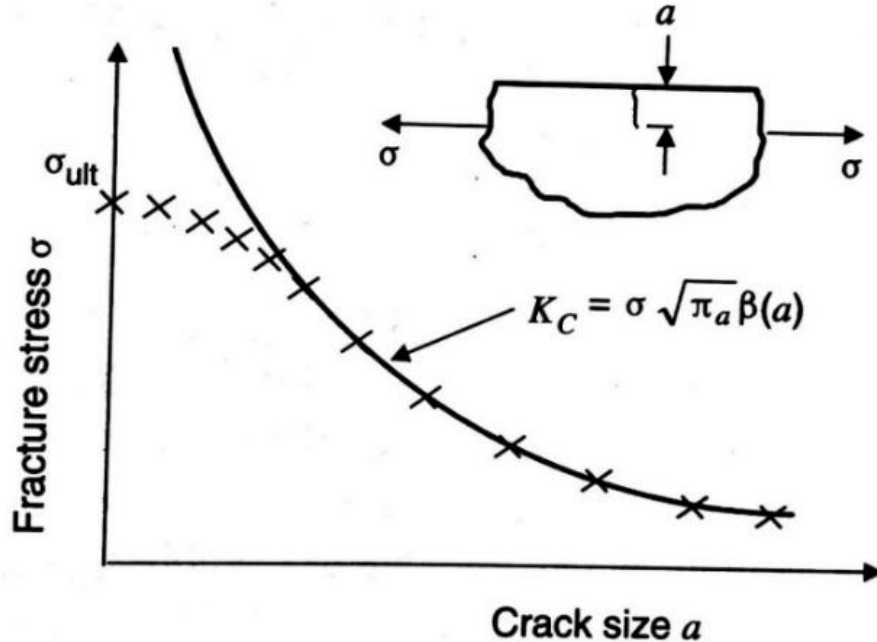


Figure 11: Relation between Fracture Stress and Crack Size (Grandt, 2004)

In bridge construction, I-beams and built-up sections are extensively used as super-structure members. Some literature is available which describes different methods of determining SIF for specifically cracked I-shaped member. Cracks usually originate at sudden cross-sectional change or weld toe details (Haddad El, Topper et al., 1979). With continuously acting fatigue stresses, these cracks can grow further and lead to member fracture.

Stress Intensity Factors for Structural Steel I-beams

A study conducted by Pedro et al., focused on developing a SIF equation for a “two-tip web crack” and a “symmetric three-tip crack” in an I-beam, as shown in Figure 12. Two-tip web crack is a crack with one front growing up the web and the other down the web. A

symmetric three-tip crack is a crack with two fronts growing symmetrically across the flange and the third up the web” (Pedro, Akhrawat et al., 2008).

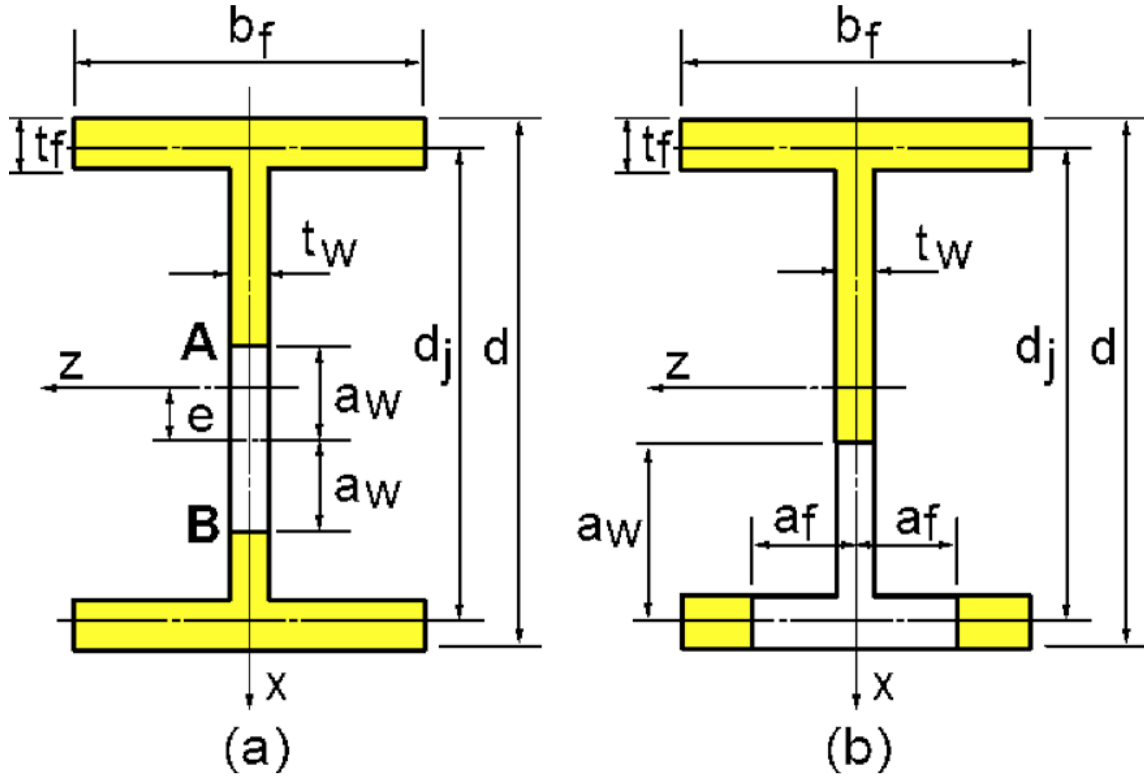


Figure 12: (a) Two-tip web crack (b) Symmetric three-tip crack (Pedro, Akhrawat et al., 2008)

As shown in Figure 12, the “two-tip cracks” are always eccentric. Hence, SIFs will be different. While, “three-tip cracks” are mostly symmetric, requiring two SIFs, one for the web crack tip and the other for the two flange crack tips. The following SIF equation was proposed by the author for a two-tip cracked I-beam subjected to tension or bending.

$$K^{A,B} = f^{A,B}(\lambda_w, \varepsilon, \beta) \sigma \sqrt{\pi a_w} \quad (16)$$

where, A and B represent upper crack tip and lower crack tip respectively, a_w = half web crack length, σ = axial and bending stress at the flange-to-web junction, $\varepsilon = e / (d_j / 2)$ (normalized

crack eccentricity), $\lambda_w = a_w / \left(\frac{d_j}{2} - e \right)$ (normalized web crack length). Refer to Figure 12 for the definition of variables.

For the three-tip cracked I-beam subjected to tension or bending SIF was given by equation 17.

$$K^{w,f} = f^{w,f} (\lambda_w, \lambda_f, \beta) \sigma \sqrt{\pi a_{w,f}} \quad (17)$$

Where, w and f represent the web crack tip and flange crack tip, a_w = web crack length, a_f = flange crack length, $\lambda_w = a_w / d_j$ (normalized web crack length), $\lambda_f = a_f / (b_f / 2)$ (normalized flange crack length).

The other two parameters included in the equation are $\beta = 2A_f / A_w$, flange-to-web area ratio and $\gamma = d_j / b_f$, depth-to-width ratio. ‘ f ’ is a correction factor used in the calculation of stress intensity. From the AISC manual, seven pairs of W shapes were considered which had the same ‘ β ’ value but different ‘ γ ’ value. These sections were further divided into two shapes. The deeper and narrower sections were categorized as shape 2 while remaining ones were categorized as shape 1, as shown in Figure 13.

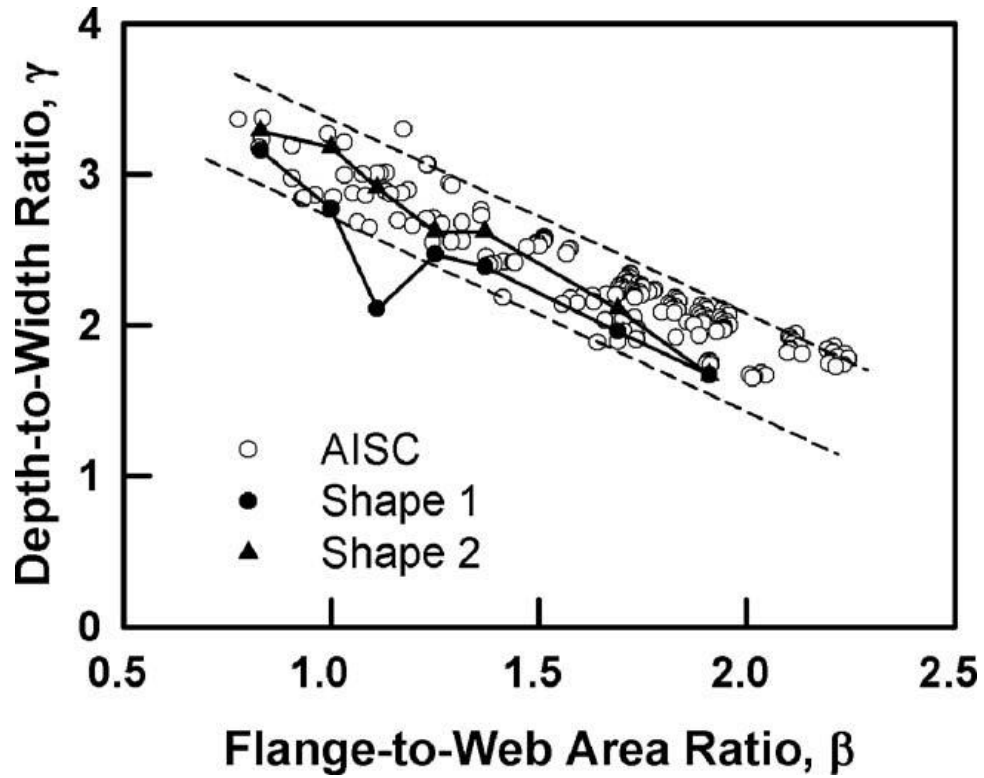


Figure 13: Shape Classification of the Specimens (Pedro, Akhrawat et al., 2008)

ABAQUS was used to develop the models and the J-integral method was used to calculate the SIF for Mode I (opening mode) type loading. The correction factor, 'f' was obtained by normalizing the calculated SIF value with applied stress and crack length (Pedro, Akhrawat et al., 2008). The parameter ' β ' was validated for central web cracks under tension and bending for both the crack configurations. The researchers concluded that the difference between SIF results between shape 1 and shape 2 was very small, which means ' γ ' does not influence the SIF calculation much. Hence, the parameter ' β ' can be used to characterize the SIF calculation of W shapes (Pedro, Akhrawat et al., 2008).

Stress Intensity for Cracked I-beams

Another study conducted by Dunn et.al. focused on determining the SIF for a cracked I-beam subjected to a pure bending moment, 'M'. The crack (a) was assumed to be extended to a part of the web from the flange of the I-beam, as shown in Figure 14.

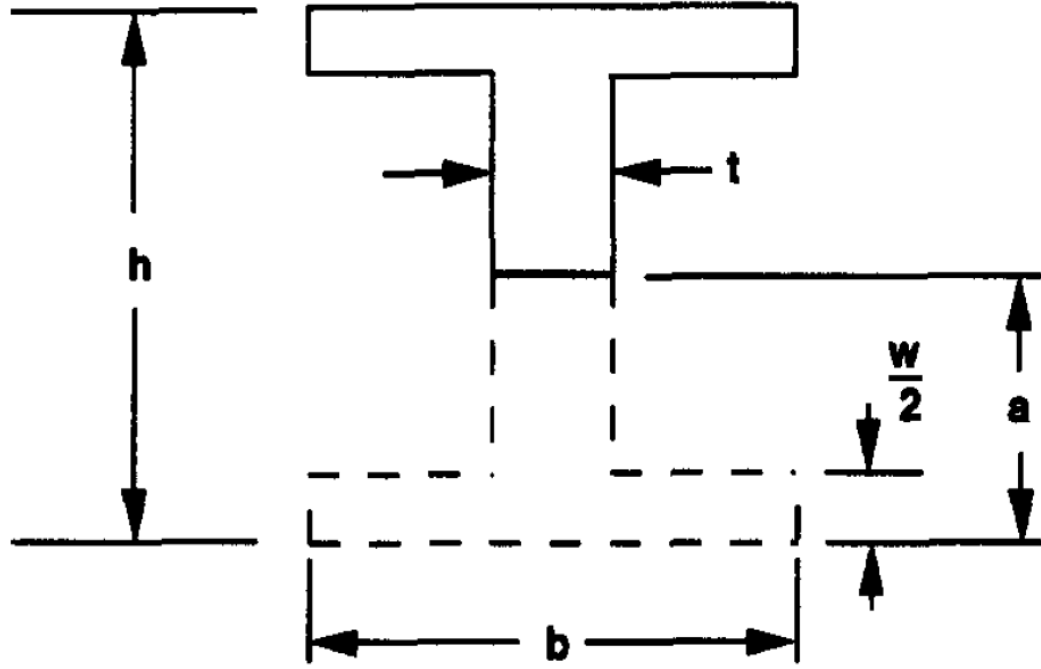


Figure 14: Cracked I-beam Geometry (Dunn, Suwito et al., 1997)

One of the objectives of the study was to find the non-dimensional parameter ' β ' for the geometry shown in Figure 14. In the past, researchers have used $\beta = 1$ for several engineering application. However, according to literature the parameter ' β ' depends on cross-sectional geometry and the crack length (Bazant, 1990). Detailed continuum finite element analysis was performed to develop a relationship for ' β ' in terms of three non-dimensional geometric

parameters ' ξ_1 ', ' ξ_2 ', ' ξ_3 ' defined as $\xi_1 = \frac{a}{h}$, $\xi_2 = \frac{t}{b}$, $\xi_3 = \frac{w}{h}$ (Figure 14).

Non-dimensional geometric parameter values were varied over a range and the data points obtained from the FEA were further fit (Figure 15) to obtain an equation for ' β '. From the analysis, it was found that the parameter ' ξ_1 ' had maximum influence on the parameter ' β '. Hence, equation 18 was determined for parameter ' β ' in terms of ' ξ_1 '.

$$\beta = 1.16 \xi_1^{-0.374} \quad (18)$$

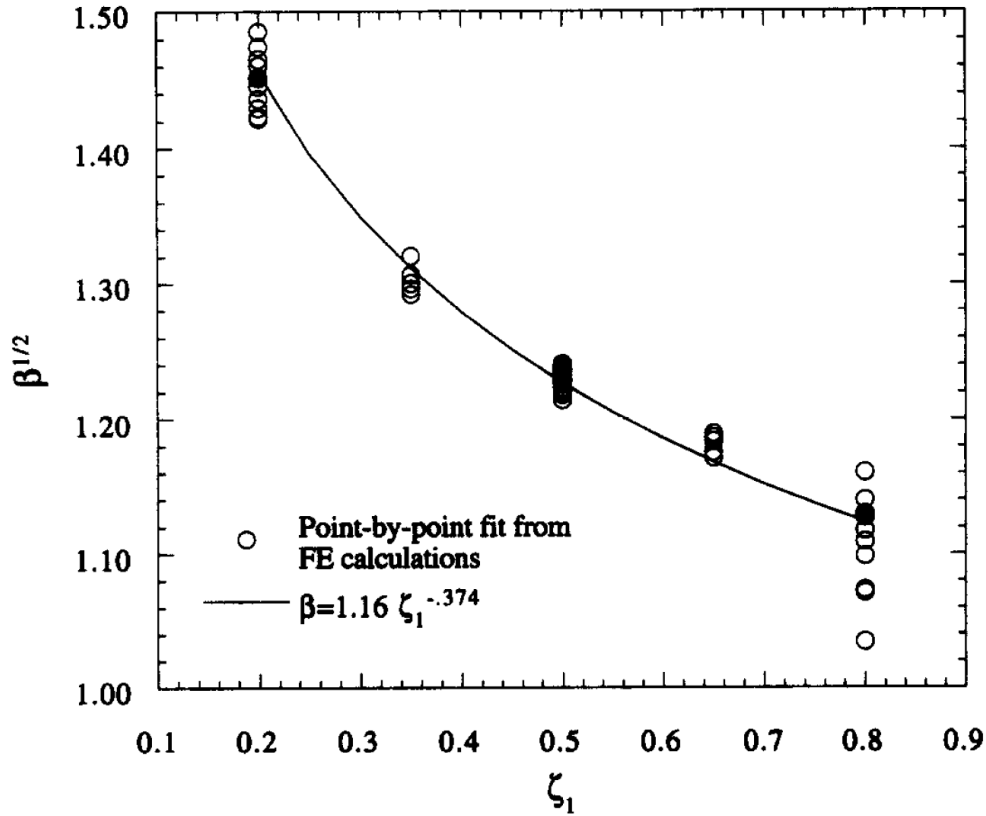


Figure 15: FE Data Points and Curve Fit (Dunn, Suwito et al., 1997)

For a range of ' ξ_1 ' between 0.2 and 0.8, the ' β ' decreased by about 40%. While there was a change of about 11% in the ' β ' with respect to the other two non-dimensional parameters ' ξ_2 ', ' ξ_3 ', which means their effect is less significant, and hence were neglected in further research (Dunn, Suwito et al., 1997). Dunn et.al. further conducted an experimental study to validate the numerical technique results. Twelve Polymethyl Methacrylate (PMMA) I-beams

specimens with the same crack profile were tested under four-point bending to determine the fracture load. The ' ξ_1 ' was varied between 0.37 and 0.7. The fracture loads were further used to calculate the fracture toughness (K_{Ic}). The author stated that the calculated K_{Ic} were in good agreement with the predicted results.

Standards to Control Fracture in Steel Bridges Through the Use of High-Toughness Steel and Rational Inspection

The two-year inspection interval and the Hands-on-inspection of FCMs have been useful in identifying the faults in bridge components, which could have been dangerous. But, these inspections are time-consuming, expensive and sometimes requires lane closures which interrupt the traffic. Hence, researchers are coming up with new methods to design and monitor the structures.

According to a study conducted by Sherman, an economical and safer bridge design can be achieved by incorporating the Fracture Control Plan (FCP) and Damage Tolerant Design (DTD). An FCP helps to treat fracture as another limit state and may also be used to form rational inspection intervals based on the type of bridge, as well as the likelihood of failure. Material toughness, design review, fabrication requirements, and welder certifications were considered to form the AASHTO FCP (Sherman, 2016).

The axial and bending specimens used in the experimental study conducted by Sherman were fabricated using two different grades of steel: grade 50 and grade 70. A total of 11 specimens (five axial and six bending) were used for the study. An angle grinder was used to create edge notches in the tension flange of the bending specimen, and in the plate as shown in Figure 16. After creating the crack, a load equal to 75% F_y was applied to test for fracture (AASHTO, 2011). The crack length was increased until the member fractured. Fracture load

and stress at the time of failure and the critical crack length were noted for all the specimens. From the study, it was found that the fracture toughness increased by almost 28.5% when grade 70 steel was used in comparison to grade 50 steel, because of the higher stress state related to the grade 70 steel (Sherman, 2016).

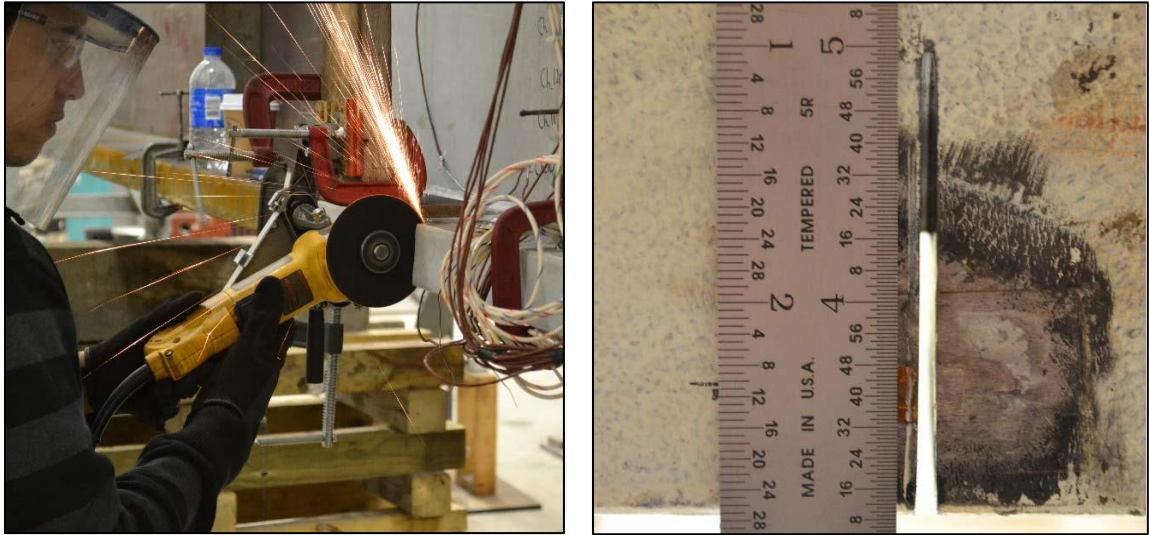


Figure 16: Creating V-notch in the Test Specimens (Sherman, 2016)

FE models of the experimental study specimens with the same crack profiles were developed to study the fracture toughness. In order to achieve good accuracy in the results, the area around the crack tip was meshed with very fine elements. Partition tool was used to divide the area around the crack line into two concentric circles and a rectangle. The circles were meshed to have ten elements of equal size, and the perimeter of the rectangle was meshed with local seed size of 0.125 inch. Figure 17 shows a generated structured mesh around the crack tip.

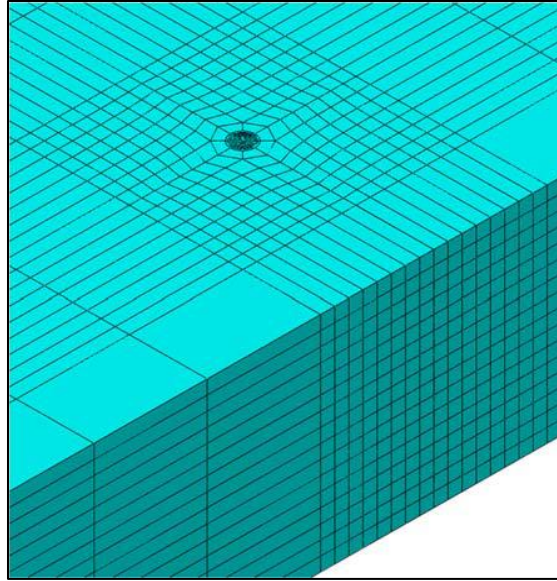


Figure 17: Refined Meshing at the Crack Tip (Sherman, 2016)

A parametric study was conducted where simplified beam and plate models were developed using ABAQUS software. A total of 32 specimens were analyzed for the edge crack profile. Based on the Probability of Detection (POD) study a crack length of 3inch was used in the study (Whitehead, 2015). Both linear-elastic and elastic-plastic analysis were carried. “The linear-elastic analysis provided the crack demand in terms of SIF while the elastic-plastic analysis provided the crack demand in terms of j-integral” (Sherman, 2016).

The bottom flange width, thickness, and web height were varied over a range of values in the parametric study of the simplified beam models. The fracture toughness demand decreased with the increase in tension flange thickness, and with the increase in tension flange width. However, the fracture toughness demand increased with the increase in the web height (Sherman, 2016). The researcher concluded that design and material properties are the two most important components in the integrated FCP which helps to reduce any structural failure due to brittle fracture (Sherman, 2016). Hence, it is important to keep in mind a few things for

the development of the integrated FCP which includes the type of loading, material properties, the existence of any defects, and both shop and in-service inspection methods.

2.4 Fracture Resilience and Redundancy

For the safety of the public, a bridge should be strong enough to tolerate damage and still have sufficient capacity to carry the load (Ghosn and Yang, 2014). One way to provide bridge safety is by making the structural components fracture resistant. A fracture resilience study conducted by Hebdon et.al. showed that the probability of a built-up steel member to experience brittle fracture is very scarce compared to experiencing failure due to fatigue crack growth over time and continuous load cycles (Hebdon, Bonachera Martin et al., 2017). The other ways to make the structure fracture resistant have been discussed in the above sections. For example, studying the crack growth behavior by determining the SIF, or J-integral.

Structural safety can also be achieved by providing redundancy. The NCHRP report 776 defines redundancy as “the capability of a bridge system to continue to carry the load after the failure of one of its main member” (Ghosn and Yang, 2014). There are three types of redundancy. NCHRP report 354 classifies them as follows, “member level redundancy; when the crack is restrained from propagating to the adjacent component from the failed component”. Second, “structural redundancy; an external static indeterminacy which occurs in continuous girders with more than two spans”. Third, “load-path redundancy; an internal static indeterminacy results from having redundant components or members” (Connor, Dexter et al., 2005).

Although AASHTO specifications classify the fracture critical bridges as non-redundant, some of the bridge failures in the past were prevented when the live load was carried by the

remaining intact members through alternative load paths. It is true that every bridge failure is unique and the level of redundancy in each case is different. The residual strength can be measured in terms of the redundancy ratio. Different methods of calculating the redundancy ratio have been discussed in the literature.

Load Redistribution and Remaining Fatigue Life of Steel Built-Up Members Subjected to Flexure Following a Component Failure

Hebdon et al. conducted a research study to find the remaining load carrying capacity of a partially failed built-up member and to calculate the remaining fatigue life after the failure of the first component. Both experimental and computational studies were conducted. The results of the experimental study were used to validate the FEA. A parametric study was conducted where FE models of girders with multiple cover plates varying from 1 to 4 were evaluated. The same number of cover plates were used in both tension and compression regions with 75% to 100% failure rate. The bending specimen with a single cover plate had nonsymmetrical stress greater than the symmetrical (100%) cover plate failure (Hebdon, Bonachera Martin et al., 2017).

After the failure of a component, the flexural strength of the remaining intact components of the built-up section was calculated using the standard bending equation ($\sigma = My/I_{net}$). Then, a plot between ‘ratio of FE stress-to-calculated stress’ and ‘number of cover plates’ was developed. With the increase in the number of the cover plates, the FE stress also increased. From the obtained relationship, an amplification factor ‘ β_{AF} ’ was determined which is given by equation 19. It is a function of the number of cover plates (N).

$$\beta_{AF} = 1 + 0.2 \left(1 + \frac{N}{4} \right) \quad (19)$$

This factor was useful in studying the stress distribution around the failure point in a built-up member. The amplification factor provides a method to approximate the stress in the adjacent component after the fracture. The localized stress increase can be determined by multiplying the calculated stress with the amplification factor (Hebdon, Bonachera Martin et al., 2017).

CHAPTER 3: Analytical Methods

3.1 Modeling

Two types of FE models were developed for analysis including flexural I-shaped member models, and axially loaded plate models. The flexural I-shaped member models with two different crack geometries were analyzed to determine the SIF (Figure 18). The first crack geometry was an edge crack located in the tension flange of the flexural member. The second crack geometry was a full-width crack located in the tension flange of the flexural member. The full-width crack was defined as a crack present along the entire width and partially through the thickness of the tension flange.

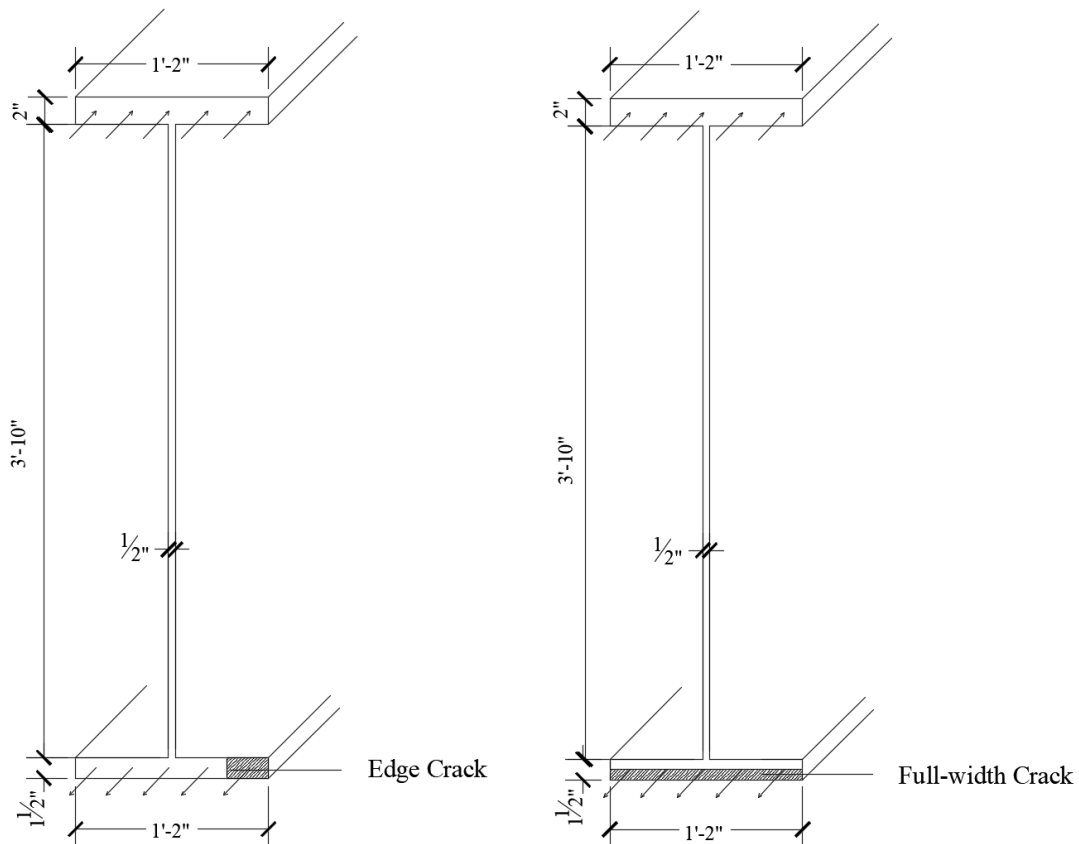


Figure 18: Flexural I-shaped Member with Edge Crack, and Full-width Crack Profile

After studying the flexural I-shaped member models, the tension flange was also separately evaluated as an axially loaded plate. This was done because the behavior of the tension flange of an I-shaped flexural member is similar to the axial plate under tension. The SIF solution for axial plates with an edge crack profile is available in the LEFM handbooks. A study was conducted where a comparison was made between the obtained SIF solution of the flexural I-shaped member model and the available handbook solution of the axially loaded plate with edge crack profile. Two comparison studies were made: the first one for the edge crack profile, and the second one for the full-width crack profile. This study was conducted to verify if the available handbook solution of the axially loaded plate with an edge crack profile can be used to find the SIF solution of the partially cracked flexural I-shaped member. The following section describes the ABAQUS modeling procedure used in the analysis of these models to determine SIF.

ABAQUS Modeling Procedure

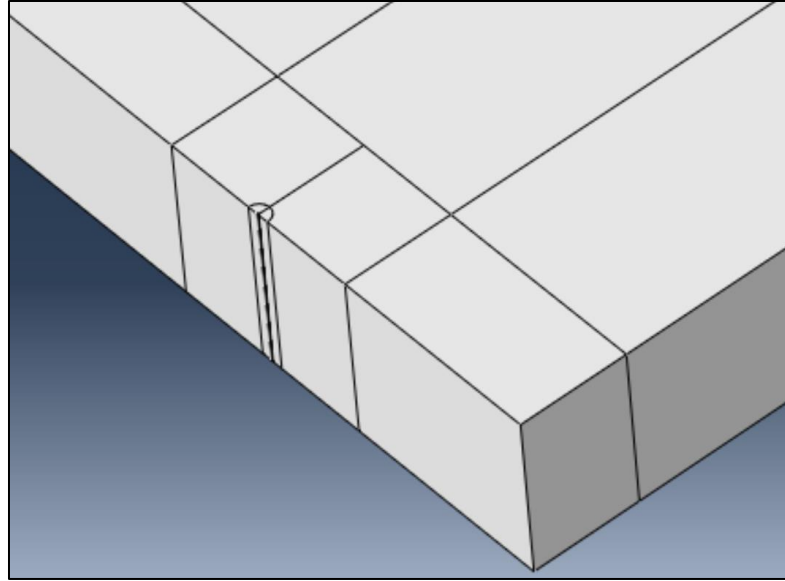
Finite Element Analysis software, ABAQUS CAE version 6.14 produced by Dassault System Simulia Corp. was used to develop all the models in this research study. Parts were extruded as three-dimensional solid deformable elements. Since LEFM analysis is the focus of this research study, material properties including a modulus of elasticity of 29,000 ksi, and a Poisson's ratio of 0.3 were used to achieve linear-elastic model behavior.

All models were meshed with linear three-dimensional hexahedral elements with reduced integration (C3D8R). The reduced integration did not make a difference in the results, and hence, was used for the analysis purpose. Five flexural I-shaped members with edge crack profile were modeled and were separately analyzed with (C3D8) and without reduced integration (C3D8R). It

was observed that there was a difference of less than 1% in the average SIF around the edge crack line. Hence, CED8R elements were used to mesh all the FE models.

In ABAQUS, a crack was created, assigned and edited using the ‘special’ tool under the ‘interaction’ module. A ‘contour integral’ type of crack was created, and the crack was allowed to open ‘normal to the crack plane’. To determine SIF from the FEA, the crack tip singularity property was incorporated in the model. As discussed in the literature review, the singularity tab under the crack edit option was used to simulate the strain singularity in the model (Figure 10). A mid-side node parameter of 0.25 was assigned and the nodes along the crack front were collapsed to move together as a single node.

In a cracked geometry, the stress field near the crack should be monitored closely, and the near crack stress field depends on the mesh around it (Kittur and Huston, 1990). Hence, an independent instance was created to mesh the part as per the preference. For this reason, a mesh refinement study was conducted for a rectangular beam model with an edge crack in the tension region. Rectangular beam model was used for benchmark study purposes. The structural mesh around the crack line was refined until there was minimal to no variation in the output. To achieve finely structured meshing around the crack tip, the partition tool was used to divide the region into two concentric circles and a rectangle. The two circles were centered on the crack tip and had a radius of 0.01 inch and 0.11 inch, respectively. The rectangular box had a dimension of 2 inch x 2 inch, as shown in Figure 19.



CL

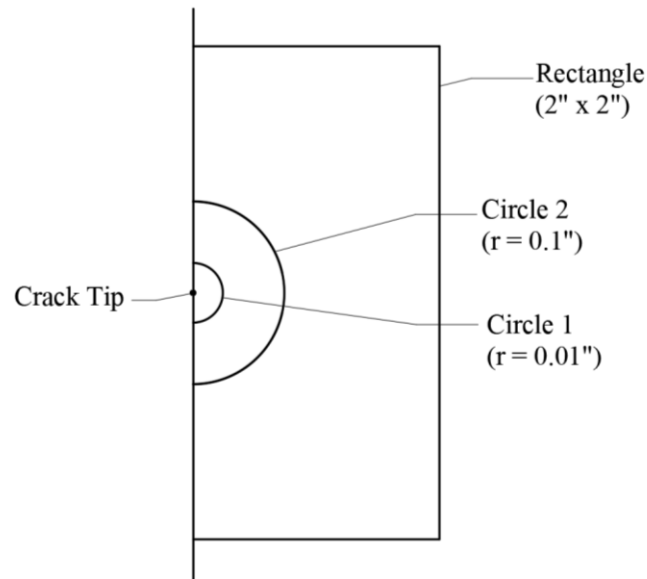


Figure 19: Partition around the Crack Line (Top), Schematic Diagram of Partition around the Crack tip (Bottom)

The area within the circles were meshed with ten elements to have a fine structured mesh in the region. The local seed size along the perimeter of the rectangle was refined until the difference in the output was negligible (Less than 1%). The element local seed size around the crack line was varied from 0.5 inch to 0.0625 inch in three increments. From each analysis

average SIF was obtained. It was observed that there was no difference (0%) in the SIF values between the local seed size of 0.125 inch and 0.0625 inch. Hence, a local seed size of 0.125 inch was chosen for modeling purposes. While a global seed size of 0.5 inch was used to mesh the remaining regions (outside the rectangular partition). Figure 20 shows a typically generated mesh with fine elements around the crack line and coarse elements in the remaining regions.

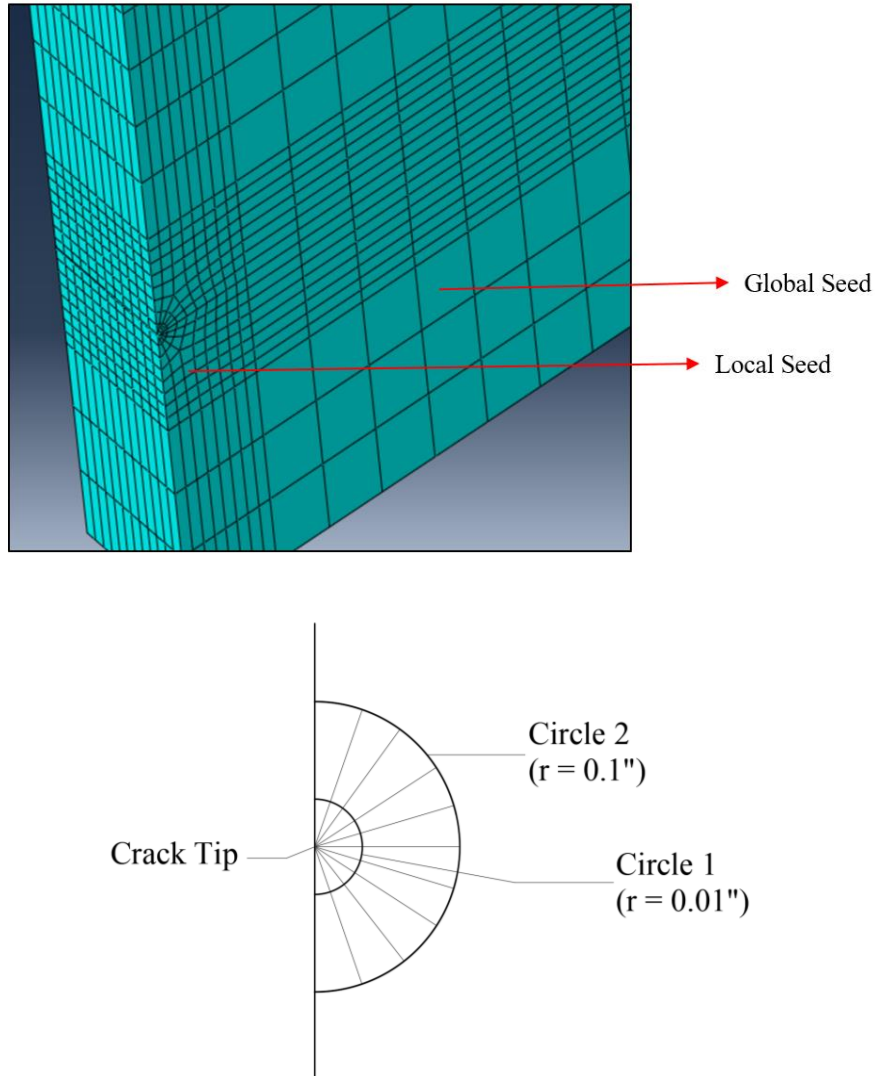


Figure 20: Typical Generated Mesh (top), Schematic Diagram of Circular Mesh (Bottom)

ABAQUS allows the user to calculate crack parameters in terms of SIF. Once the crack was created, a history output for SIF was requested for eight contours around the crack tip

using the history output tool (Figure 21). The requested output were calculated for a layer of elements around the crack line known as “Contours”. The ABAQUS manual defines a contour as a “ring of elements completely surrounding the crack tip or the nodes along the crack line from one crack face to the opposite crack face” (Manual, 2006). ABAQUS automatically selects the node-sets to form these element rings based on the generated mesh around the crack line.

Name: H-Output-1
Step: Step-1
Procedure: Static, General

Domain: Crack : Crack-1

Frequency: Every n increments n: 1

Timing: Output at exact times

Number of contours: 8

☐ Step for residual stress initialization values:

Type: ☐ J-integral
☐ Ct-integral
☐ T-stress
☒ Stress intensity factors

Crack initiation criterion: ☐ Maximum tangential stress
☒ Maximum energy release rate
☐ KII=0

Figure 21: History Output Request

Each contour will have a certain number of picked sets, which depends on the thickness of the member. For example, for a 1.5 inch thick plate and a seed size of 0.125 inch there will be 13 picked-sets (12 elements). Figure 22 below represents a typical picked-set for contours around the crack line. Each one of these picked-sets will have a corresponding history output. History output results for SIF were obtained using the results tool, (Figure 23). The localized stresses around the crack tip will cause plastic deformation, forming a plastic zone. So, the

results of the contours near the crack tip are less accurate. Hence, for the evaluation purpose, SIF values of all the picked-sets of eight contour were recorded.

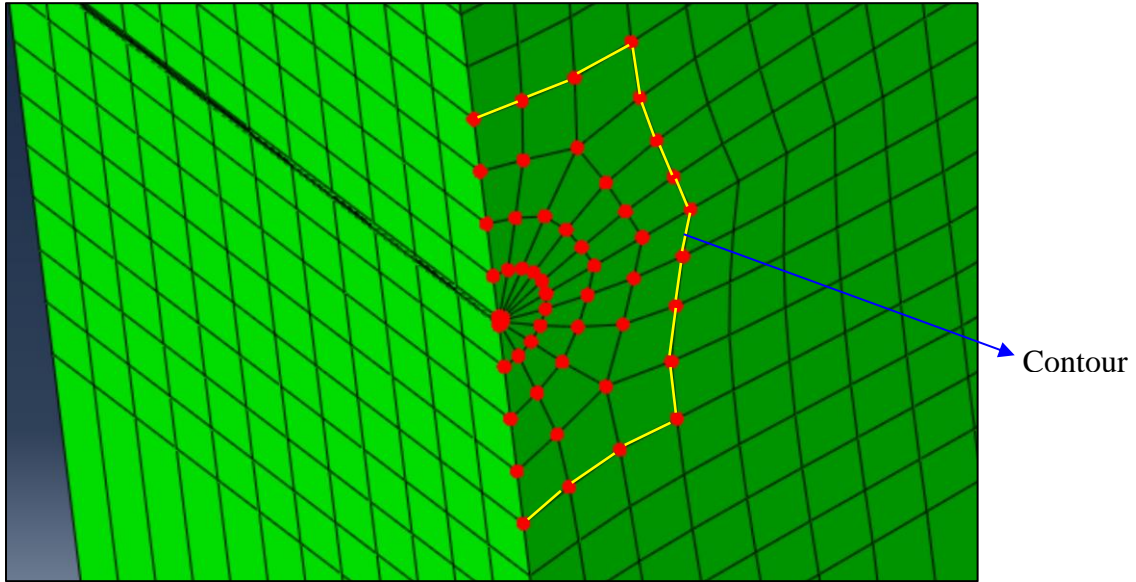


Figure 22: Typical Picked-set of a Contour

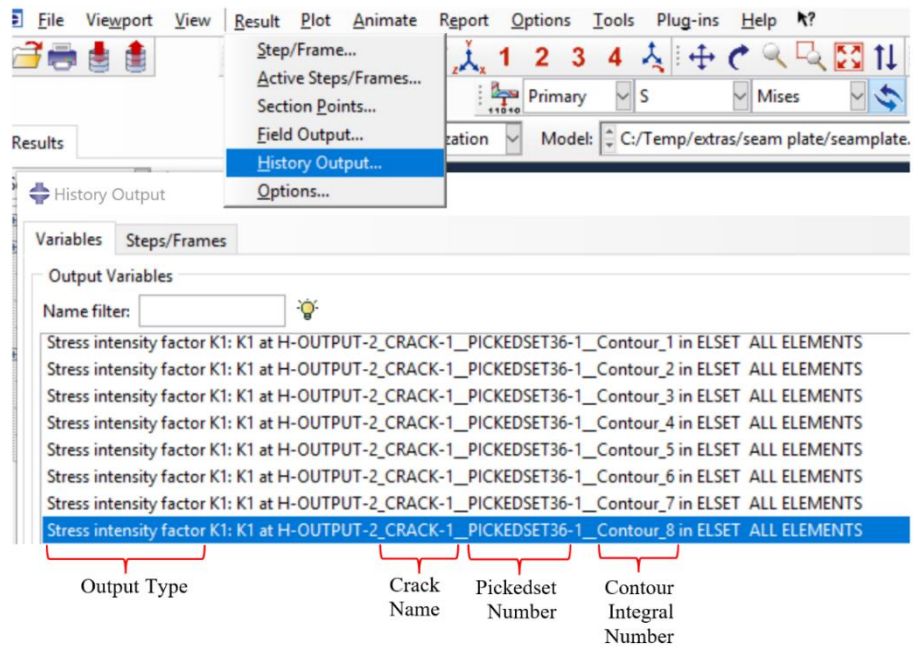


Figure 23: History Output

3.1.1 Benchmark Study

Axial Members

A benchmark study was performed to verify the ABAQUS modeling procedure used to calculate the SIF. The results obtained from the benchmark study were compared to the available handbook solutions to see the percentage difference in the output. In the benchmark study, axially loaded plates with different crack geometries were analyzed. The specimen dimensions were taken from the study conducted by Sherman 1 (Sherman, 2016). Two different plate geometries were considered. Plate 1 was 1.5 inch thick and 22 inch wide. Plate 2 was 2.5 inch thick and 14 inch wide. All the models were of same length equal to 120 inch.

A total of five axially loaded plate specimens were developed for the FEA. Models A1, A2, A3, & A4 had plate 1 geometry, while model A5 had plate 2 geometry. In each model, 50 ksi yield strength steel was used except in model A4 where 70 ksi yield strength steel was used to study the variation of SIF with the steel yield strength. Table 1 shows the specimen matrix of the axially loaded plates with their respective crack configuration.

Table 1: Axial Specimen Matrix

Model Name	Type of Crack	Plate Thickness (inch)	Plate Width (inch)	Grade of Steel (ksi)	Stress Applied (ksi)
A1	Edge	1.5	22	50	37.5
A2	Double-Edge	1.5	22	50	37.5
A3	Center	1.5	22	50	37.5
A4	Edge	1.5	22	70	52.5
A5	Edge	2.5	14	50	37.5

A half symmetry boundary condition was used to reduce the computation time. Figure 24 shows the half symmetric edge cracked plate model, with x-axis symmetry boundary condition

applied on the left end of the plate except at the crack plane. A crack length of 3 inch was used similar to the parametric study carried out at Purdue University(Sherman, 2016). Based on the Probability of Detection (POD) study a 3 inch crack length has a high detection rate of 65% (Whitehead, 2015). A uniform stress of 37.5 ksi (75% F_y) was applied over the cross-section of the plate. This was done to match the loading conditions used in the analysis of the axially loaded plate models by Sherman(Sherman, 2016).

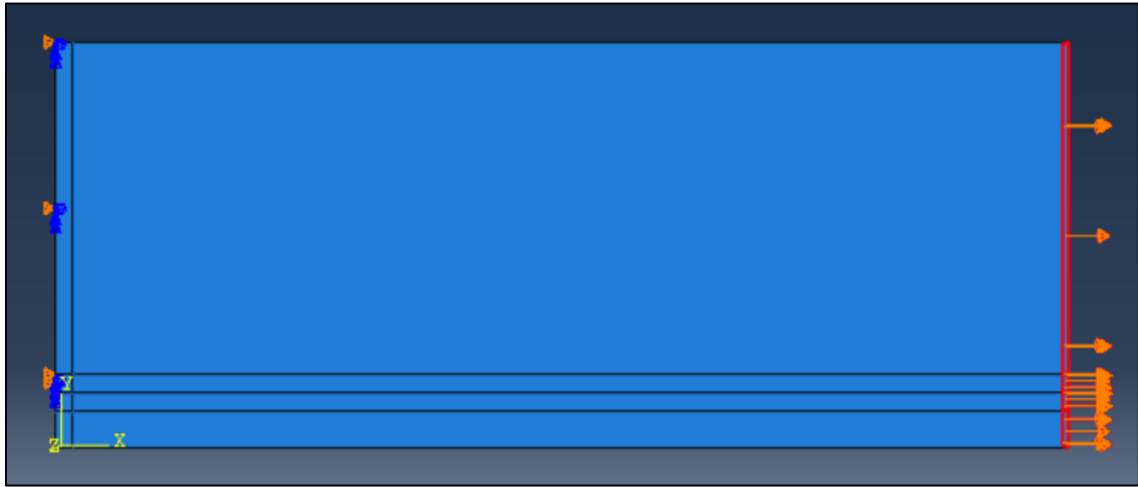


Figure 24: Half Symmetric Plate Model with Edge Crack Profile

Flexural Members

After evaluating the axial specimens, rectangular beam (flexural) models were studied under four-point loading. A flexural specimen 480 inch long, 12 inch wide, and 3 inch thick was selected for the study. A total of two beam models were developed (Table 2). Model B1, was a full-size beam model with no crack, while model B2 was a symmetric beam model with a 3 inch edge crack (Figure 25). A point load equal to 15 kips was applied at a $\frac{1}{3}^{\text{rd}}$ distance (160 inch) from both the supports. The cross-sectional stress profiles of both the models were compared to see the shift in the neutral axis due to the presence of the crack. Additionally, for Model B2, SIF was determined and was compared with the handbook solution.

Table 2: Bending Specimen Matrix

Model Name	Length of the Member (inch)	Type of Model	Type of Crack
B1	480	Full-Size Model	No Crack
B2	240	Symmetric Model	Edge Crack

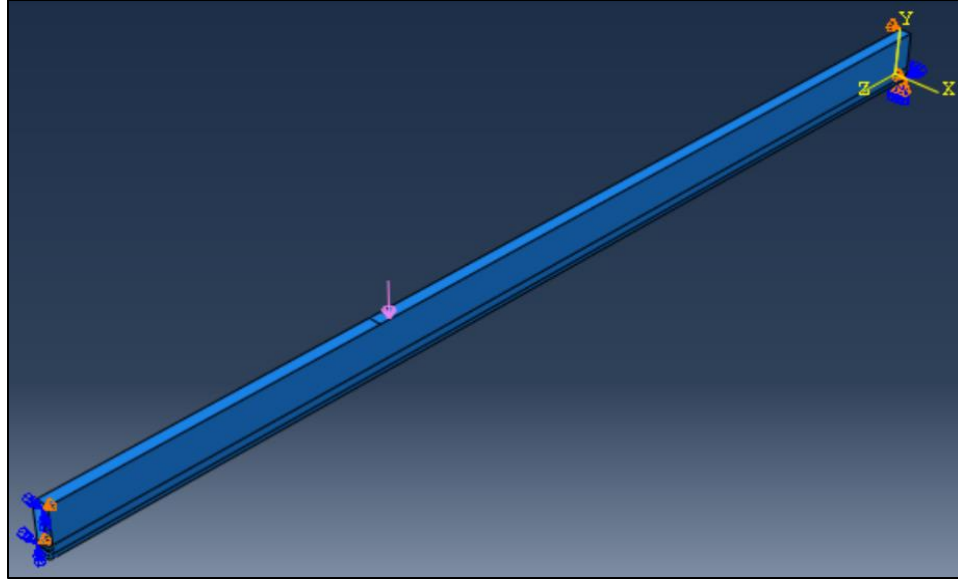


Figure 25: Specimen B2 Model

3.1.2 Model Types

After verifying the model development procedure in ABAQUS to calculate the SIF, FE models of the partially cracked flexural I-shaped members were developed for analysis following the same modeling procedure. Only the constant moment region of the flexural I-shaped member was modeled incorporating both the symmetry boundary condition and trapezoidal loading to save model development and analysis time. Afterward, parametric studies were conducted for each one of the crack configurations to determine an analytical equation for the geometric factor ' β '. The parameters evaluated in this study include: tension flange thickness, tension flange width, web height, and crack length. This geometric factor was

further used in the SIF solution of the partially cracked flexural I-shaped member to determine the SIF in the vicinity of the crack line.

Simplified Models of Flexural I-shaped member

For the analysis of a flexural specimen, a built-up member 46 feet long, made of steel plates and angles (Hebdon, 2015) was considered. The bottom flange of the member included an angle 6"x6"x $\frac{3}{4}$ " and a cover plate 14"x $\frac{3}{4}$ ", which were connected using rivets. The web was made of $\frac{1}{2}$ "x46" plate and the top flange was made of 14"x2" plate (Figure 26). Developing an FE model of the built-up member with fasteners was complex and time-consuming. Instead, a simplified I-shaped member model was developed with similar dimensions of the built-up member.

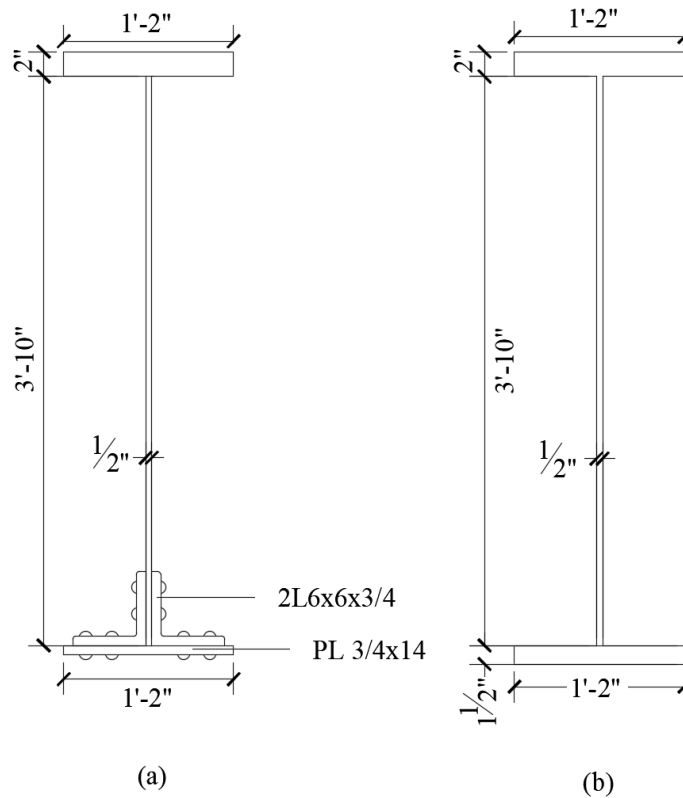


Figure 26: (a) Built-up Member, (b) I-shaped member

For the compression flange, the top flange dimensions 2"x14" were used. The web dimensions were kept equal to the dimensions of the web plate $\frac{1}{2}$ "x46". The tension flange width was equal to the width of the cover plate (14 inch). The thickness of the horizontal leg of the angle ($\frac{3}{4}$ inch) and the thickness of the bottom cover plate ($\frac{3}{4}$ inch) were added together and used as the thickness for the tension flange in the simplified I-shaped member model. Figure 26 shows the cross-sections of both the built-up member and the simplified I-shaped member.

A study was conducted to simplify the flexural I-shaped member model by using the symmetry boundary condition and trapezoidal loading. This simplification was necessary since nearly seventy I-shaped member models with or without cracks were developed for the analysis in parametric studies. For the study, flexural I-shaped member under four-point loading were studied, and the focus was the maximum moment region of the I-shaped member. For a beam under four-point loading, the region between the point loads have a constant moment value, and that region is called a "constant moment region".

A simplified I-shaped member model (184 inch long) representing only the constant moment region was developed. Trapezoidal loading in ABAQUS was used to apply the constant moment value on the member (Figure 27). An ASTM A709 Steel with a specified minimum yield strength of 50 ksi (ASTM International, 2005) was considered for the research purpose. An analytical expression field was used to define the equation for stress profile along the height (y-axis) of the girder. A target stress of 55% F_y (27.5 ksi) was applied at the extreme tension fiber of the flexural member. This was done to simulate the loading conditions used in the older structures to achieve full design load, and also to match the experimental testing done

at Purdue University (Hebdon, 2015). Global seed size of 0.5 inch was used to develop the structural mesh in the model.

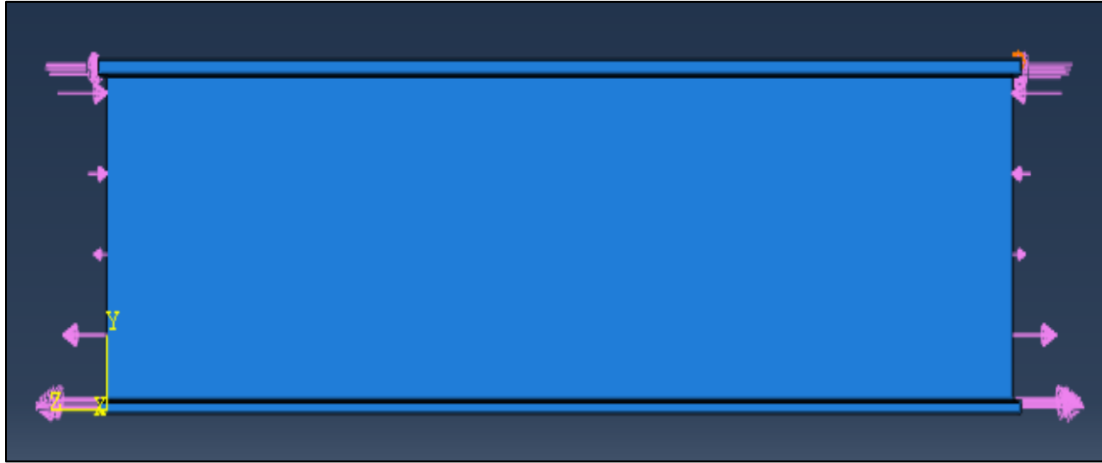


Figure 27: Trapezoidal Loading

To further simplify the above model, both the symmetry boundary condition and trapezoidal loading were used together. Therefore, only half of the constant moment region of the flexural I-shaped member was modeled. Figure 28 shows the 92 inch long simplified flexural I-shaped member model with trapezoidal loading on the right edge and the z-axis symmetry boundary condition on the left edge. Global seed size of 0.5 inch was used to generate the structured mesh in this model. The total time including the model development time and the analysis time was reduced significantly (50%) in comparison to the above flexural I-shaped member model.

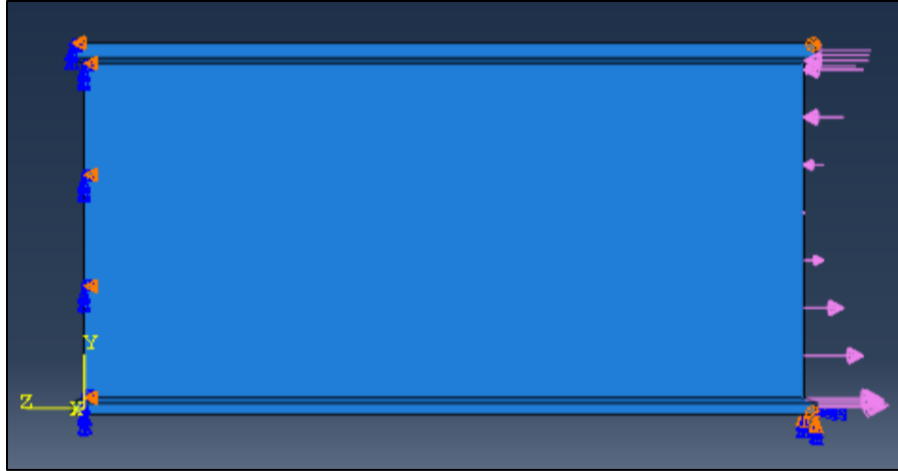


Figure 28: Symmetric Model with Trapezoidal Loading

Partially Cracked Flexural I-shaped Members

This research study mainly focused on analyzing two configurations of partially cracked flexural I-shaped members. The first flexural partially cracked I-shaped member geometry had an edge crack in the tension flange. The second flexural partially cracked I-shaped member geometry had a full-width crack in the tension flange. The same modeling procedure as described under ABAQUS modeling procedure in Section 3.1 was used to develop the partially cracked flexural I-shaped member models. Other details regarding the geometry and loading are described below.

Edge Crack Profile

Two FE models were developed to determine the SIF for an edge crack profile in a tension flange. An edge crack was selected because it has similar geometry to common edge cracked plates loaded in tension, and for such flaws, common practice is to treat the bottom flange as such. For flexural members, the tension flange represents the location with the largest tensile stress, and therefore the largest strain energy release rate. A crack will grow in size when the

strain energy release rate exceeds the energy required to form new crack surfaces(Griffith, 1921).

The first model was a flexural I-shaped member model (Figure 29), 92 inch long developed using both trapezoidal loading and symmetry boundary condition. The second model was an axially loaded plate, with plate dimensions matching the tension flange dimensions of the I-shaped member. The width and thickness of the plate were equal to the width and thickness of the tension flange (Figure 30). A symmetry boundary condition was used to develop the plate model, and it had the same edge crack configuration and loading as the I-shaped member tension flange. For the analysis of plate model, a uniform tensile stress of 27.5 ksi was applied to match the extreme tension fiber stress of the flexural I-shaped member.

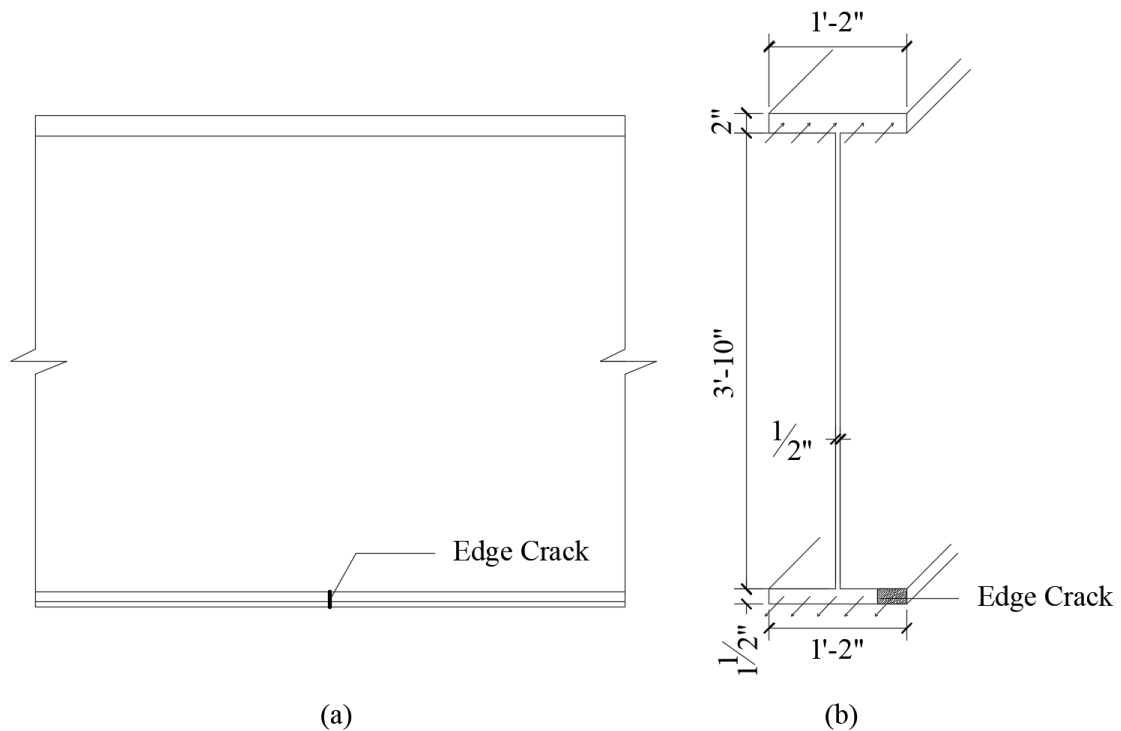


Figure 29: (a) Elevation and (b) Cross-sectional View of an Edge Crack Configuration in an I-shaped member

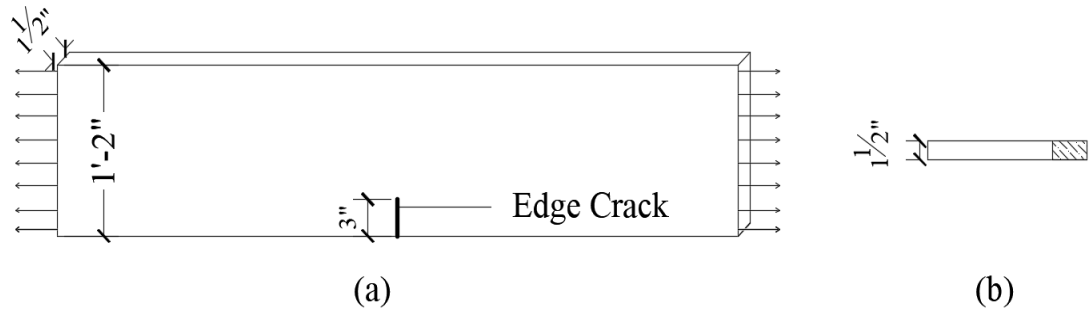


Figure 30: (a) Elevation and (b) Cross-sectional View of an Edge Crack Configuration in an Axially Loaded Plate

In both the models, a 3 inch long straight through thickness edge crack was created using the 'special' tool under the 'interaction' module (Figure 31). The stress field around the crack line was closely monitored by developing finely structured mesh. The same mesh generation procedure as described under ABAQUS modeling procedure (Section 3.1) was followed. Figure 32 shows the fine mesh around the edge crack in the tension flange of the I-shaped member.

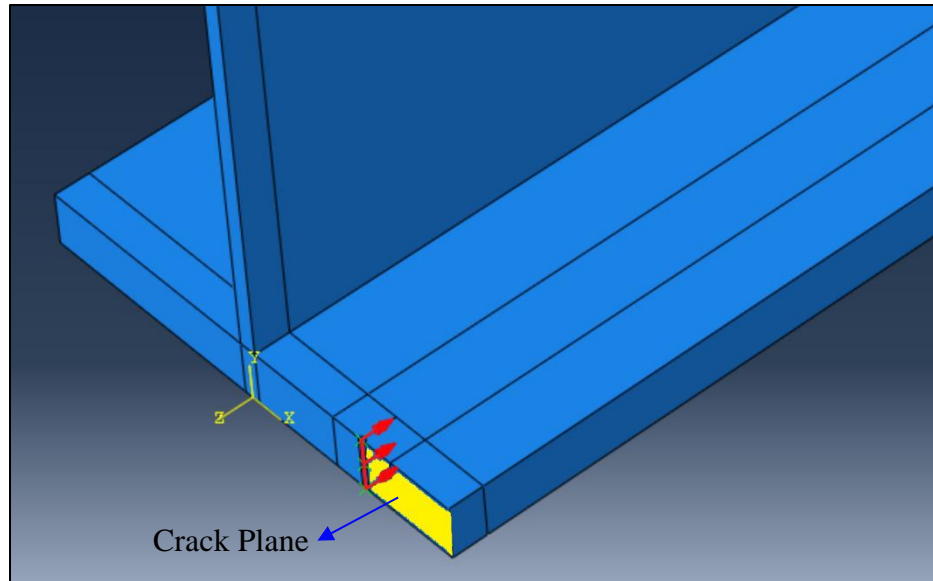


Figure 31: Edge Crack Plane in the Tension Flange

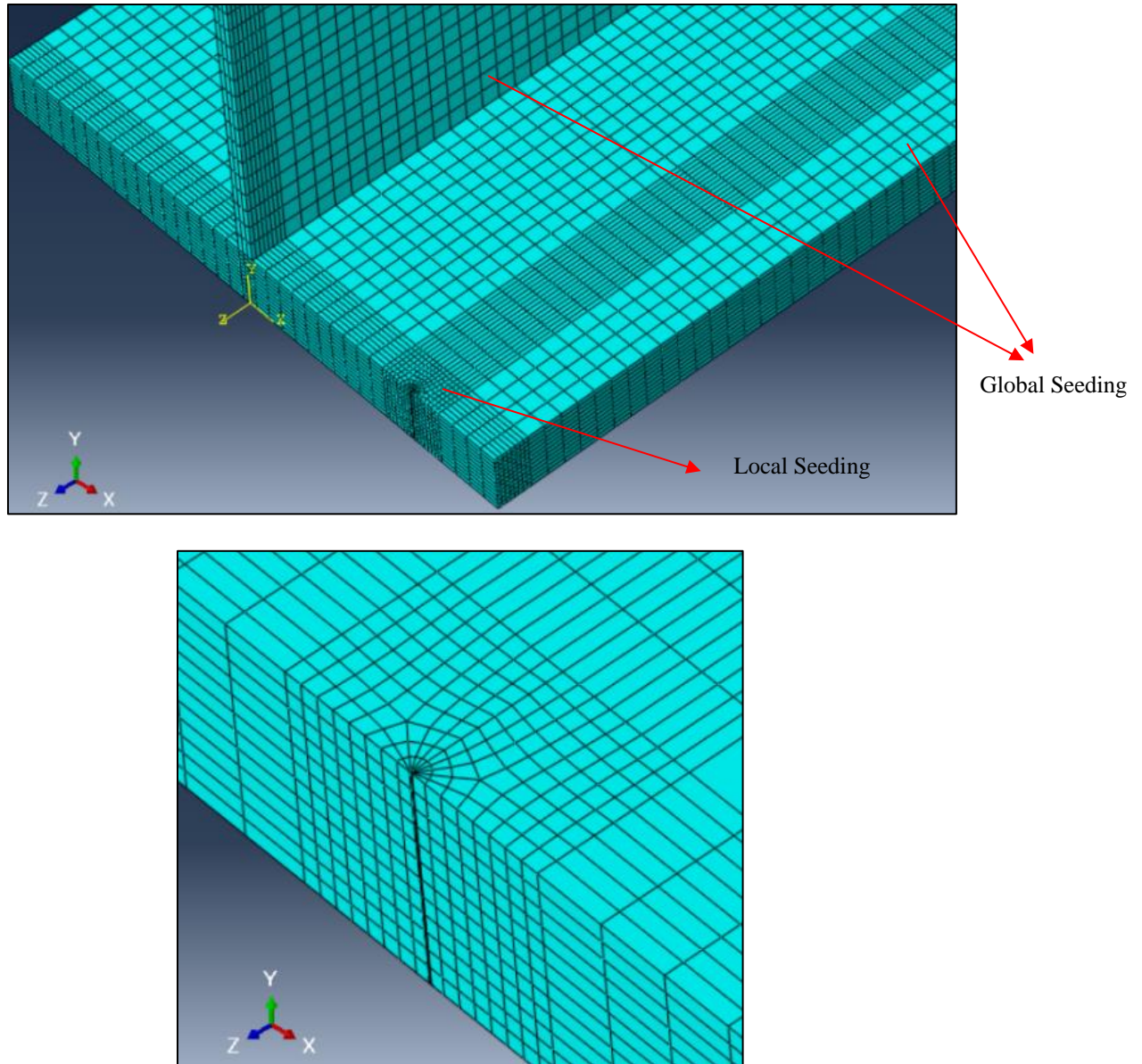


Figure 32: Fine Meshing around the Crack Line in the Tension Flange of the I-shaped member

Full-width Crack Profile

The second partially cracked flexural I-shaped member geometry had a full-width crack in the tension flange, as shown in Figure 33. A full-width crack is a crack which is all the way through the width and partially through the thickness of the component. This crack geometry

was selected to simulate the stress state resulting from a failure of a cover plate in the tension region of the built-up section (Hebdon, Bonachera Martin et al., 2017). Such a geometry was theorized to have the potential to describe the stress state for members with single component failure. For example, in order to represent a 0.75 inch thick cover plate failure, the full-width crack was assumed to be present throughout the width and up to 0.75 inch from the bottom of the tension flange.

Similar to the edge crack geometry, two FE models were developed to determine the SIF for the full-width crack profile. The first model was a flexural I-shaped member model, 92 inch long developed using both trapezoidal loading and symmetry boundary condition as described under Simplified Models of Flexural I-shaped member (Section 3.1.2). And, the second model was an axially loaded plate, with plate geometry matching the tension flange dimensions of the I-shaped member. Figure 34 shows the elevation and cross-sectional view of an axially loaded plate with the full-width crack profile.

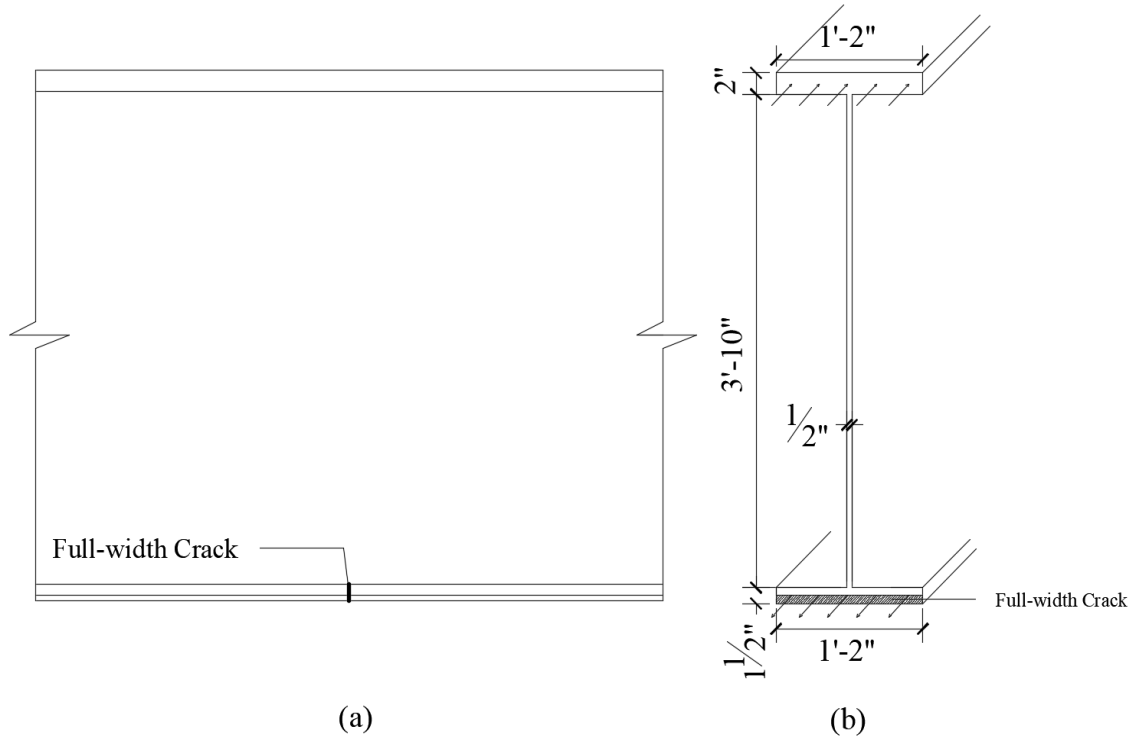


Figure 33: (a) Elevation and (b) Cross-sectional View of a Full-Width Crack Configuration in an I-shaped member

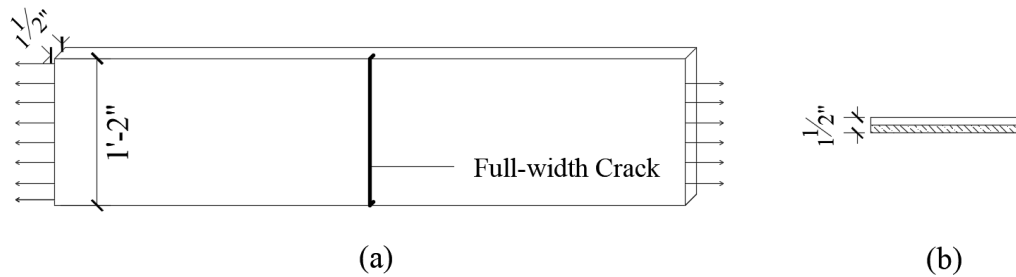


Figure 34: (a) Elevation and (b) Cross-sectional View of a Full-Width Crack Configuration in an Axially Loaded Plate

In both the models, a 0.75 inch full-width crack was created using the ‘special’ tool under the ‘interaction’ module (Figure 35). The stress field around the crack line was closely monitored by developing finely structured mesh. Figure 36 shows the fine structured mesh along the full-width crack line and coarse mesh in the remaining region of the I-shaped

member. The area between the circles were meshed to have ten elements and a local seed side of 0.125 inch was used along the perimeter of the rectangle. The remaining regions were meshed with global seed size of 0.5 inch. The same meshing procedure was used to develop all the remaining flexural I-shaped member models with a full-width crack profile.

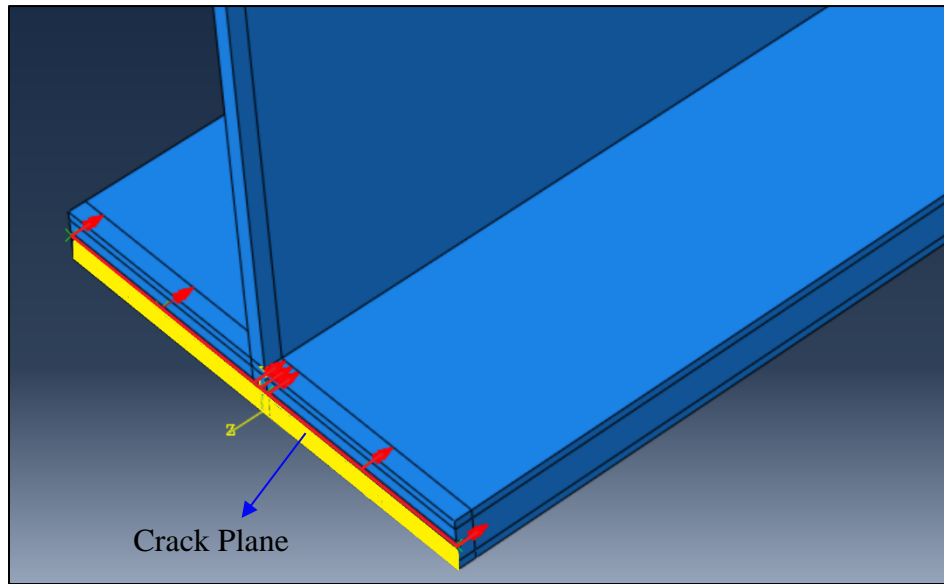


Figure 35: Full-width Crack Plane in the Tension Flange

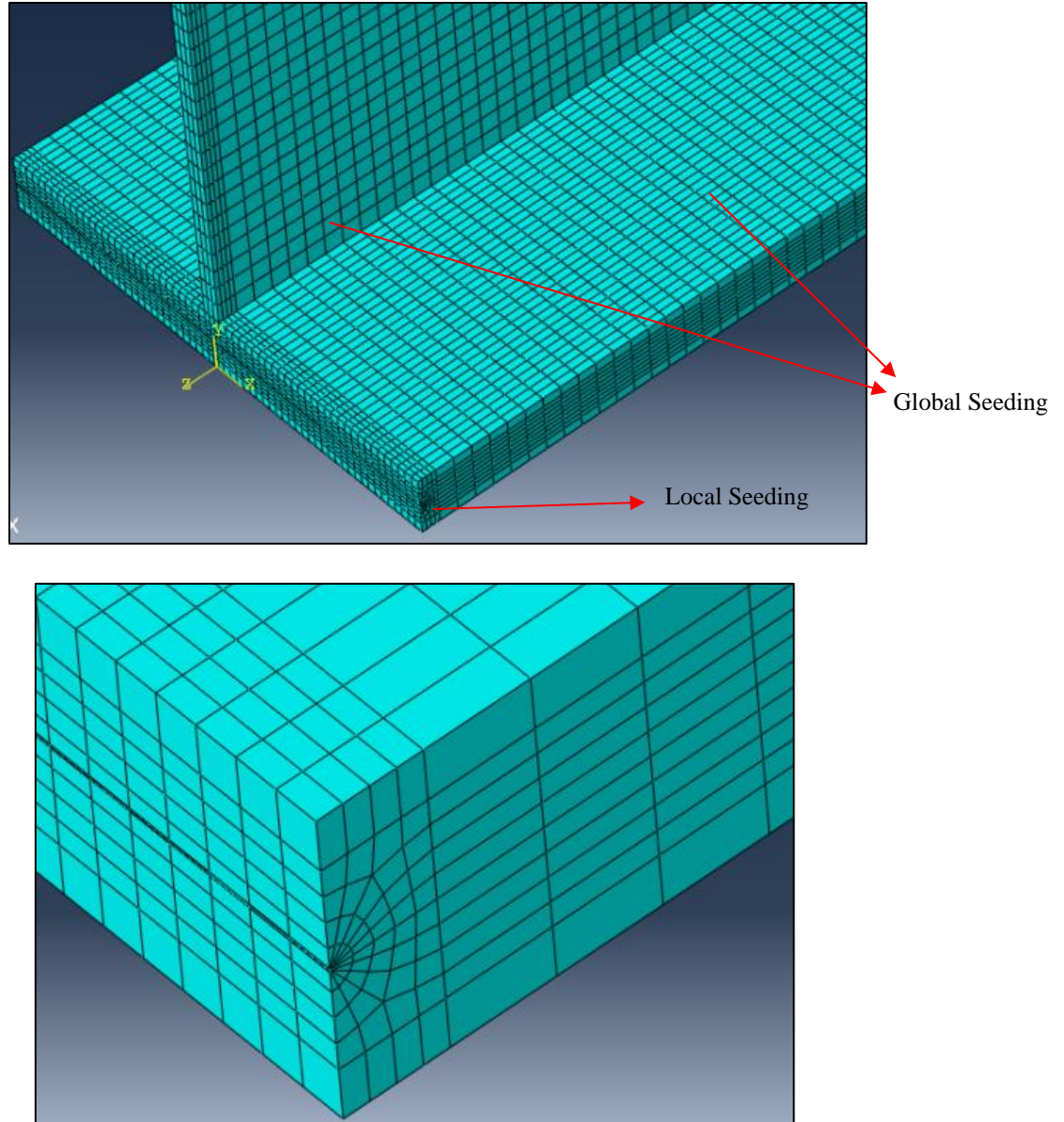


Figure 36: Structured Mesh in the Partially Cracked Flexural I-shaped Member (Top), Fine Mesh along the Full-width Crack Line in the Tension Flange (Bottom)

3.2 Parametric Study

One of the main objectives of the research study was to determine the SIF equation for both configurations of partially cracked I-shaped members. The fundamental SIF equation can be used to determine the SIF in the vicinity of a crack of any arbitrary geometry with a unique geometry factor ' β ', which means a different geometry factor will be used for every geometry.

The SIF equation given by equation 20 includes three important terms: crack length ‘a’, the far-field stress ‘ σ ’, and the geometry factor ‘ β ’.

$$K = \beta \sigma \sqrt{\pi a} \quad (20)$$

The geometry factor ‘ β ’ varies for different cracked orientations relative to the member and direction of loading. It is known that, for a cracked geometry, the ‘ β ’ generally depends on the crack length and cross-sectional dimensions of the member. For example, the ‘ β ’ for an edge cracked plate is a function of the ratio of crack length ‘a’ to plate width ‘W’ (Figure 37), and one of the handbook solutions is given by equation 21 (Grandt, 2004).

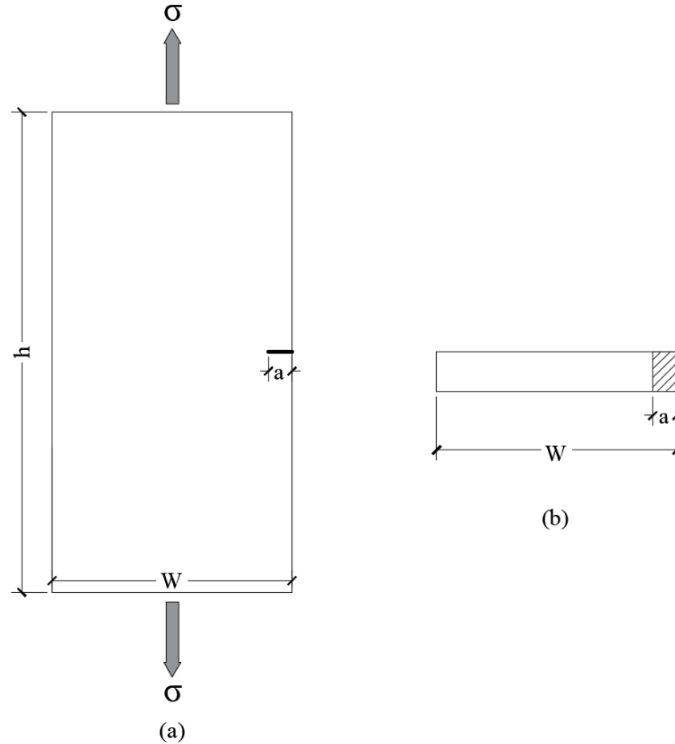


Figure 37: Edge Cracked Plate: (a) Elevation View (b) Cross-sectional View

$$\beta\left(\frac{a}{W}\right) = 1.12 - 0.231\left(\frac{a}{W}\right) + 10.55\left(\frac{a}{W}\right)^2 - 21.73\left(\frac{a}{W}\right)^3 + 30.29\left(\frac{a}{W}\right)^4 \quad (21)$$

The focus of the research study is partially cracked flexural I-shaped members. Hence, in the parametric study, the parameters tested to see their influence on the SIF included tension

flange thickness (t_f), tension flange width (b_f), web height (h_w), and crack length (a). Figure 38 shows the cross-sections of the partially cracked flexural I-shaped members.

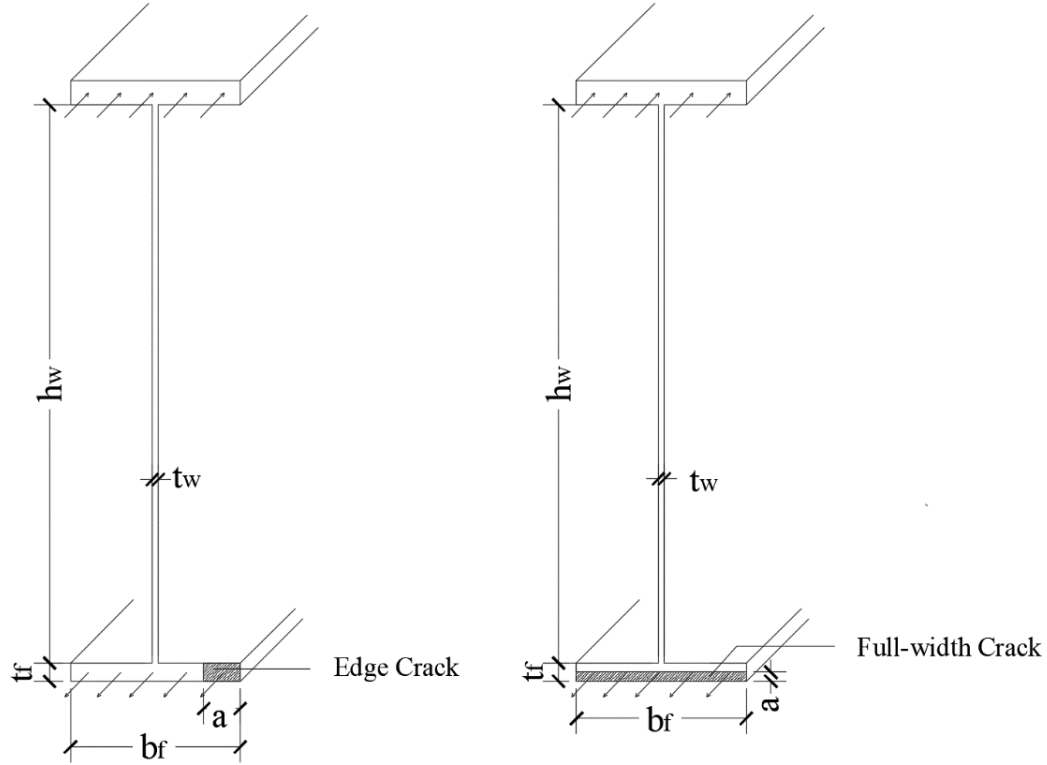


Figure 38: Partially Cracked Flexural Member Cross-sections

3.2.1 Edge Crack Geometries

The first parametric study was performed for the I-shaped member geometry with an edge crack in the tension flange. The SIF variation was studied for four parameters which were understood to influence the SIF directly. The study parameters included tension flange thickness, web height, tension flange width, and edge crack length.

Tension Flange Thickness (t_f)

The first parameter considered in the parametric study was the tension flange thickness. A total of 5 flexural I-shaped member models were developed. The thickness of the tension flange was varied between 1 inch and 2 inch in increments of 0.25 inch (Table 3). In all the models,

a constant edge crack length of 3 inch and a constant tension flange width of 14 inch was used. All the remaining parameters such as web dimensions and top flange dimensions were kept unaltered.

Table 3: Flange Thickness Variation for Edge Crack Profile

Group No.,	Model Name	Tension Flange Thickness, t_f (inch)	Tension Flange Width, b_f (inch)	Web height, h_w (inch)	Crack Length, a (inch)
A	A1	1	14	46	3
	A2	1.25	14	46	3
	A3	1.5	14	46	3
	A4	1.75	14	46	3
	A5	2	14	46	3

Web Height (h_w)

The second parameter considered in the parametric study was the web-height. A total of 5 flexural I-shaped member models were analyzed. The web-height was varied between 34 inch and 58 inch, with an increment of 6 inch with a constant web thickness of 0.5 inch (Table 4). All the other parameters like crack length and tension flange dimensions were kept constant so that the effect of web height could be analyzed separately.

Table 4: Web Height Variation for Edge Crack Profile

Group No.,	Model Name	Web height, h_w (inch)	Tension Flange Width, b_f (inch)	Tension Flange Thickness, t_f (inch)	Crack Length, a (inch)
B	B1	34	14	1.5	3
	B2	40	14	1.5	3
	B3	46	14	1.5	3
	B4	52	14	1.5	3
	B5	58	14	1.5	3

Tension Flange Width (b_f)

The third parameter considered in the parametric study was the tension flange width. A total of 6 flexural I-shaped member models were analyzed. In these models, the flange width was varied between 13 inch and 26 inch with a constant flange thickness of 1.5 inch, as shown in All the other parameters like crack length and web dimensions were kept constant so that the effect of tension flange width could be analyzed separately.

Table 5. All the other parameters like crack length and web dimensions were kept constant so that the effect of tension flange width could be analyzed separately.

Table 5: Tension Flange Width Variation for Edge Crack Profile

Group No.,	Model Name	Tension Flange Width, b_f (inch)	Tension Flange Thickness, t_f (inch)	Web height, h_w (inch)	Crack Length, a (inch)
C	C1	13	1.5	46	3
	C2	14	1.5	46	3
	C3	15	1.5	46	3
	C4	18	1.5	46	3
	C5	22	1.5	46	3
	C6	26	1.5	46	3

Edge Crack Length (a)

The last parameter considered in the parametric study was the edge crack length. From the SIF equation (Equation 20), the crack length is directly proportional to SIF. A total of 5 flexural I-shaped member models were developed with an edge crack length varying from 1 inch to 5 inch, as shown in Table 6. In all the models, the cross-sectional dimensions were kept constant.

Table 6: Edge Crack Length Variation for Edge Crack Profile

Group No.,	Model Name	Crack Length, a (inch)	Tension Flange Width, b_f (inch)	Tension Flange Thickness, t_f (inch)	Web height, h_w (inch)
D	D1	1	14	1.5	46
	D2	2	14	1.5	46
	D3	3	14	1.5	46
	D4	4	14	1.5	46
	D5	5	14	1.5	46

In each of the simplified I-shaped member models, the trapezoidal loading expression was changed with respect to the specimen dimensions. For flexural I-shaped member models, stress equal to 55% F_y (27.5 ksi) was applied at the extreme tension fiber of the member. The modeling procedure as described in the sections above was followed to develop all the models.

3.2.2 Full-width Crack Geometries

The second parametric study performed was for the I-shaped member geometry with a full-width crack in the tension flange. The same parameters evaluated in the parametric study of the edge crack profile were studied to observe the variation in the SIF of the full-width crack profile. When the influence of a single parameter on the SIF was studied, the remaining parameters were kept unaltered, as shown in the tables above.

Tension Flange Width (b_f)

The variation in SIF was studied for three different tension flange widths 14 inch, 20 inch and 26 inch for a constant tension flange thickness of 1.5 inch (Table 7). In all the models, a

crack length of 0.75 inch, and a web height of 36 inch was used. All the parameters except the tension flange width were kept constant so that the effect of tension flange width could be analyzed separately.

Table 7: Tension Flange Width Variation for Full-width Crack Profile

Group No.,	Model Name	Tension Flange Width, b_f (inch)	Tension Flange Thickness, t_f (inch)	Web height, h_w (inch)	Crack Length, a (inch)
E	E1	14	1.5	46	0.75
	E2	20	1.5	46	0.75
	E3	26	1.5	46	0.75

Web Height (h_w)

The web height was varied between 34 inch and 58 inch in increments of 12 inch, for a constant web thickness of 0.5 inch. Tension and compression flange dimensions were kept unaltered, as shown in Table 8. In all the models a full-width crack length of 0.75 inch was used.

Table 8: Web Height Variation for Full-width Crack Profile

Group No.,	Model Name	Web height, h_w (inch)	Tension Flange Width, b_f (inch)	Tension Flange Thickness, t_f (inch)	Crack Length, a (inch)
F	F1	34	14	1.5	0.75
	F2	46	14	1.5	0.75
	F3	58	14	1.5	0.75

Tension Flange Thickness (t_f)

The tension flange thickness was varied between 1.5 inch and 2.25 inch in increments of 0.25 inch (Table 9). In all the models, a crack length of 0.75 inch and a tension flange width

of 14 inch was used. All the other parameters except tension flange thickness were kept constant to study the variation of SIF with tension flange thickness.

Table 9: Tension Flange Thickness Variation for Full-width Crack Profile

Group No.,	Model Name	Tension Flange Thickness, t_f (inch)	Tension Flange Width, b_f (inch)	Web height, h_w (inch)	Crack Length, a (inch)
G	G1	1.5	14	46	0.75
	G2	1.75	14	46	0.75
	G3	2	14	46	0.75
	G4	2.25	14	46	0.75

Full-width Crack Length (a)

The variation in SIF was studied for two different crack lengths of 0.75 inch and 1.125 inch, as shown in Table 10. All the parameters except crack length was kept constant. In both the models, tension flange width of 14 inch, a tension flange thickness of 2.25 inch, and web height of 46 inch was used.

Table 10: Full-width Crack Profile Variation for Full-width Crack Profile

Group No.,	Model Name	Crack Length, a (inch)	Tension Flange Width, b_f (inch)	Tension Flange Thickness, t_f (inch)	Web height, h_w (inch)
H	H1	0.75	14	2.25	46
	H2	1.125	14	2.25	46

CHAPTER 4: Results and Discussion

4.1 Benchmark Study

This subsection consists of the FE results of the benchmark study specimens. The benchmark study included analysis of axially loaded plate models and rectangular beam models.

Axial Members

The analysis of axially loaded plates with different crack configurations included three types of crack configurations: edge cracked, double-edge cracked, and center cracked. The FE models were analyzed to determine the crack parameters in terms of SIF for each crack profile, and the obtained FE results were further compared with available handbook solutions. SIF solutions for common crack geometries are available in linear-elastic fracture mechanics handbooks. In the current study, “*Fundamentals of Structural Integrity*” (Grandt, 2004) was used to calculate the closed-form solutions of the cracked geometries considered in the benchmark study.

The benchmark study results were compared with the handbook solutions to verify the accuracy of the modeling procedure followed in ABAQUS to calculate the SIFs. For the purpose of analysis, SIF values from the eight contour were determined for each model. Each contour included thirteen picked-sets, and each picked-set had a corresponding SIF value. From the recorded SIF values, maximum, minimum, and average SIF values were obtained. Then, a comparison was made between the average SIF and the closed form solution, as shown in Table 11. The calculation of closed-form solutions for all the axial plate benchmark study specimens is shown in Appendix B.1.

Table 11: Benchmark Study Results

Model Name	Stress Intensity Factor (SIF) ($ksi\sqrt{in}$)				
	Maximum	Minimum	Average	Closed form solution	% Difference
A1	151.1	140.9	148.9	143	4
A2	92.7	89.5	94	91.3	3
A3	86.3	82.4	85.4	83.3	3
A4	220.8	205.7	216.5	209.4	3
A5	170.2	156.1	167.6	162	3

The FE results showed a good correlation with the closed form solution. An average difference of about 3% was observed between the FE results and the closed form solution. The dimensions and the material grade used in these models can be found in Table 1. Additionally, for an edge crack profile, it was observed that a 2.5 inch thick plate (Model A5) had higher stress intensity factor as compared to a 1.5 inch plate (Model A1). Thicker material offers higher constraint to the crack growth limiting the plastic deformation around the crack tip (Francesco M. Russo, 2016). Model A4 with a yield strength of 70 ksi had higher SIF in comparison to Model A1 with a yield strength of 50 ksi.

Flexural Members

Two rectangular beam models, B1 and B2 (Table 2) under four-point loading with and without an edge crack respectively were analyzed. For a point load of 15 kips, the calculated stress value ($\sigma = Mc/y$) at the extreme fibers due to bending was found to be 33.3 ksi. The presence of 3 inch edge crack in the tension flange at the mid-span reduced the cross-sectional net area which in turn increased the net-section stress. Also, the neutral axis shifted upwards

by approximately 0.7 inch due to the presence of edge crack. Comparison between the cross-sectional stress profiles of both the models is shown in Figure 39.

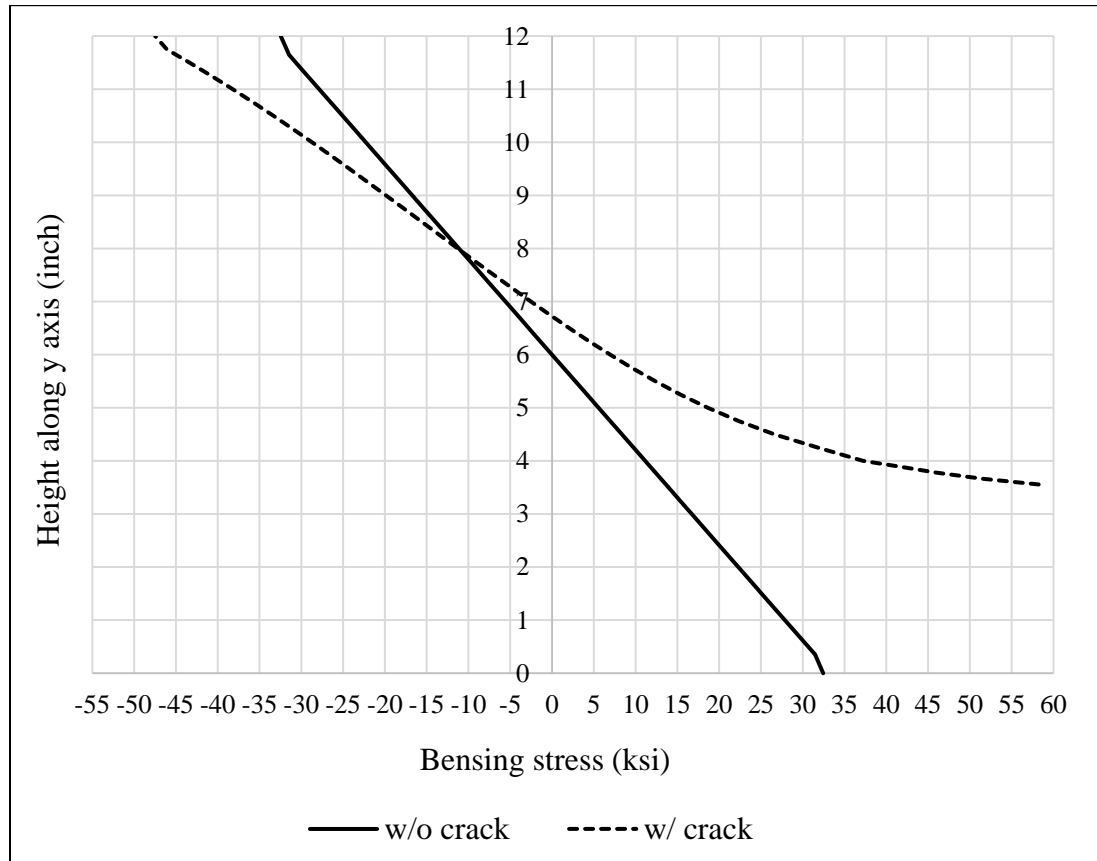


Figure 39: Cross-Sectional Stress Profiles of Rectangular Beam Models

For model B1, the cross-sectional stress profile was linear with a stress value of approximately 32.5 ksi at the extreme tension and compression fiber. While in the edge cracked beam model (B2), a theoretical stress increase of up to approximately 1500 ksi was observed in the tension region near the edge crack line. This is because of the stress concentration near the crack tip, and the linear elastic member material behavior.

The SIF in the vicinity of the edge crack was obtained for model B2. A maximum SIF value of $58.7 \text{ ksi}\sqrt{\text{in}}$, minimum SIF of $52.4 \text{ ksi}\sqrt{\text{in}}$, and an average SIF of $53.3 \text{ ksi}\sqrt{\text{in}}$ were recorded from the FEA. Using the handbook solution, a SIF of $58.2 \text{ ksi}\sqrt{\text{in}}$ was calculated

which is about 8% higher than the FE solution. The calculation of closed-form solutions for specimen B2 is shown in Appendix B.1.

The results of both axial and bending models used in the benchmark study were in close approximation with the available closed-form handbook solutions. Hence, the modeling procedure followed for the benchmark study in ABAQUS was further employed to determine the SIFs of partially cracked flexural I-shaped cross-sections.

4.2 Model Types

Simplified Models of Flexural Members

Two simplified models of the flexural I-shaped member were analyzed. The first I-shaped member model represented the constant moment region, where trapezoidal loading was used to apply the constant moment on the section. The second model was the simplified version of the first model in which both the symmetric boundary conditions and trapezoidal loading were used together. A load causing stress equal to 55% F_y (27.5 ksi) at the extreme tension fiber was applied in both the models.

The cross-sectional stress profiles of both the I-shaped member models were compared and studied. (Figure 40). There was minimal difference in the results between the two models. From the FEA, stress equal to 27.3 ksi was recorded at the extreme tension fiber, which was 0.7% less than the applied stress 27.5 ksi. In addition, the model development and analysis time were reduced significantly. Therefore, a simplified version of the beam model (92 inch long) with both trapezoidal loading and symmetric boundary condition was used in modeling all the flexural specimens.

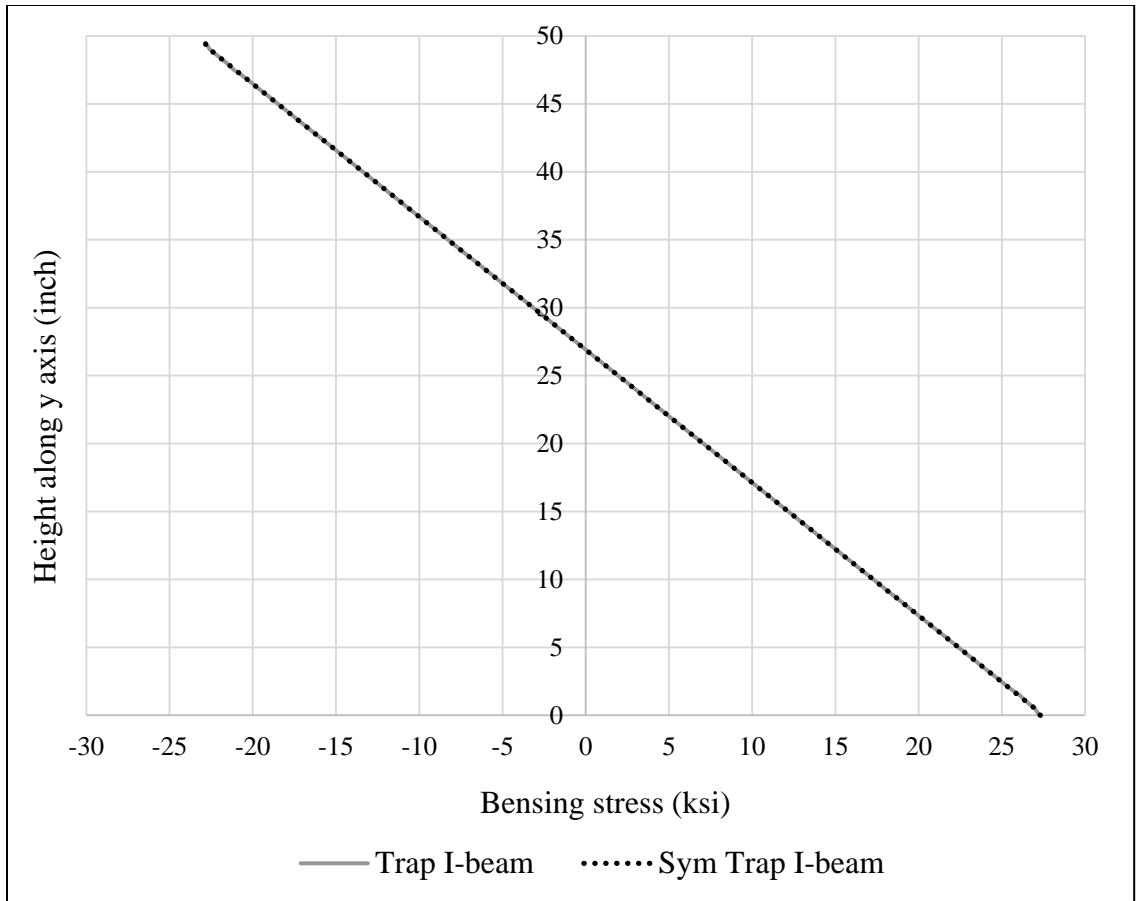


Figure 40: Cross-sectional Stress Profiles of the I-shaped member

Partially Cracked Flexural I-shaped Members

Edge Crack Profile

The first partially cracked I-shaped member geometry had an edge crack in the tension flange. A simplified model of the I-shaped member with an edge crack was developed and analyzed to find the SIF in the vicinity of the edge crack. Figure 41 shows the stress contours in the constant moment region of the edge cracked I-shaped member, and Figure 42 shows a close-up view of the localized stress concentration around the edge crack.

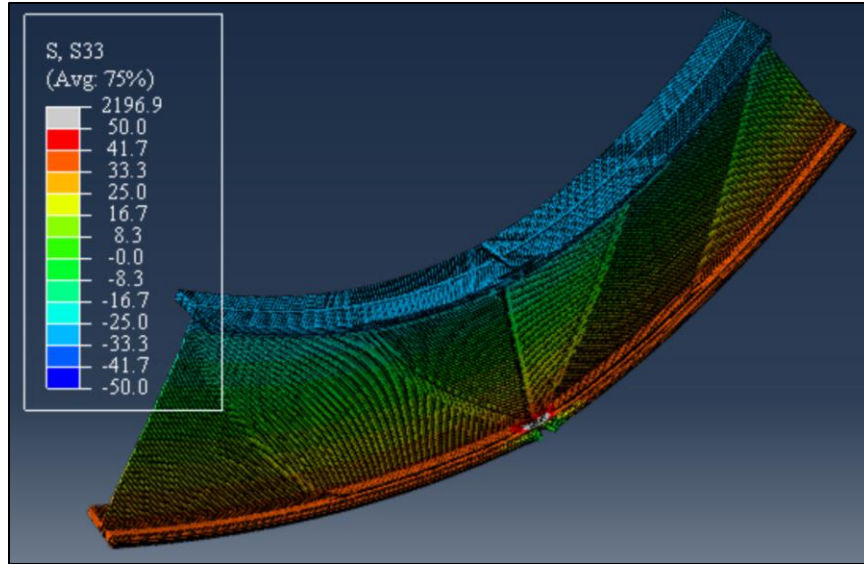


Figure 41: Partially Cracked I-shaped member with an Edge Crack

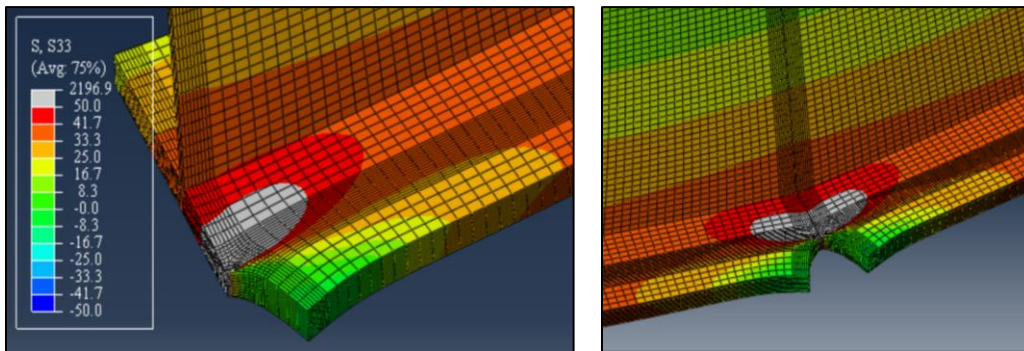


Figure 42: Local Stress Concentration around the 3 inch Edge Crack in an I-shaped member

There was a significant stress increase in the tension flange and part of the web around the crack line, while the stress in the crack plane was almost zero. From the FEA, an average SIF of $116.7 \text{ ksi}\sqrt{\text{in}}$ was obtained at the eighth contour from the crack tip. After analyzing the flexural I-shaped member model, the tension flange of the I-shaped member was separately simulated as an axially loaded plate. Figure 43 shows the localized stress concentration around the edge crack in the axial plate. From the FEA, an average SIF of $122.6 \text{ ksi}\sqrt{\text{in}}$ was obtained at the eighth contour from the crack tip.

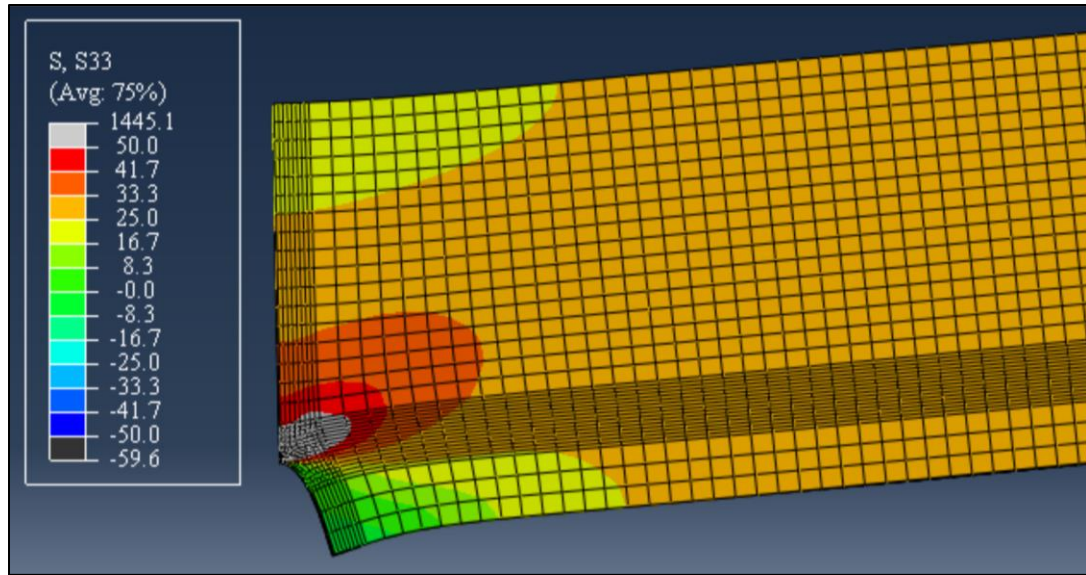


Figure 43: Stress Concentration in a 3 inch Edge Crack Axial Member

Using the handbook solution for an edge cracked plate, a SIF of $118.8 \text{ ksi}\sqrt{\text{in}}$ was obtained, which was approximately 3% lower than the FE result. Next, a comparison between the axial plate and flexural I-shaped member SIFs were made, and it was observed that the SIF value of the flexural beam model was approximately 5% less than the SIF value of the plate model. The reason for getting a lower SIF value in the flexural beam model was because of the constraint provided by the web to the edge crack opening.

Full-width Crack Profile

The second partially cracked flexural I-shaped member geometry had a full-width crack in the tension flange. Similar to the first crack geometry, two FEAs were performed. The first model was a flexural I-shaped member model, while the second model was an axially loaded plate model. The same crack profile and the similar loading conditions were used for analysis in both models.

FE output in terms of SIF was obtained for both the models. Figure 44 shows the partially cracked flexural I-shaped member with a full-width crack, and Figure 45 shows the close-up view of the localized stress concentration around the full-width crack. There was a significant stress increase in the remaining portion of the tension flange above the full-width crack line. For the partially cracked flexural I-shaped member, an average SIF of $76.5 \text{ ksi}\sqrt{\text{in}}$ was obtained at the eighth contour from the crack tip.

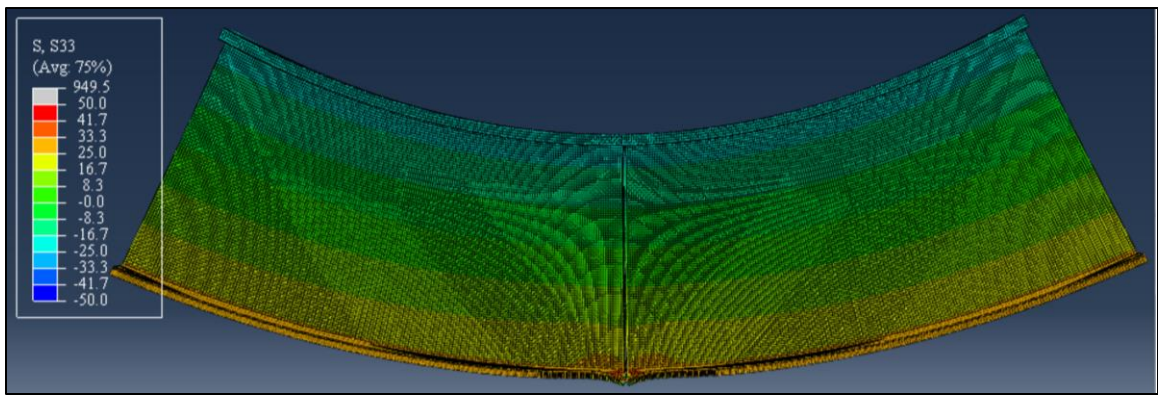


Figure 44: Stress Contours in a Partially Cracked flexural I-shaped member with a Full-width Crack

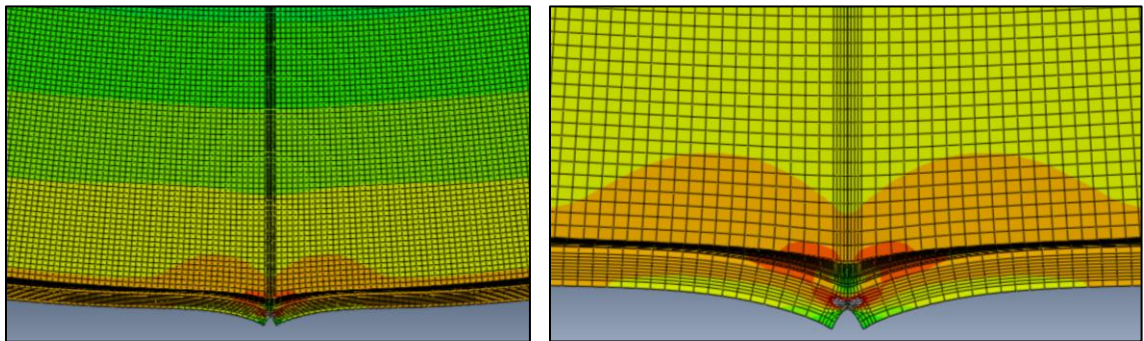


Figure 45: Localized Stress near the Full-width Crack in a flexural I-shaped member

From the analysis of an axially loaded plate, an average SIF of $119.3 \text{ ksi}\sqrt{\text{in}}$ was obtained, which was almost the same as the calculated closed form solution ($119.4 \text{ ksi}\sqrt{\text{in}}$). However, there was a large difference between the SIF of the flexural I-shaped member and plate models.

The SIF of the axial plate with a full-width crack was approximately 56% more than the SIF of the flexural I-shaped member with a full-width crack in the tension flange. The web of the flexural I-shaped member gives some constraining effects, limiting the full-width crack from opening. While the axially loaded plate had no such constraints.

4.3 Parametric Study – Edge Crack Geometry

The following section discusses the parametric study results of the specimens with an edge crack profile. Parameters including the tension flange thickness, tension flange width, web height, and edge crack length were studied for their influence on the SIF. The main focus was to find an analytical equation for the geometry factor ‘ β ’ which can be used to calculate the SIF of a partially cracked flexural I-shaped member with an edge crack configuration.

For each model, the FE results in terms of SIF were calculated from the ABAQUS output file, and the average SIF at the 8th contour was recorded. The SIF value directly depends on the crack length, and hence it is not correct to study the variation of SIF with the above-mentioned parameters. Therefore, from each analysis, the ‘ β ’ was calculated (Equation 22) using the obtained SIF, and the respective crack length ‘ a ’.

$$\beta = \frac{K_I}{\sigma\sqrt{\pi a}} \quad (22)$$

where ‘ K_I ’ is the average SIF obtained from FEA, ‘ a ’ is the crack length, and ‘ σ ’ is the far-field stress. Next, the percentage difference in the ‘ β ’ value for each of the parameters was recorded and studied. The results from the parametric studies are shown below.

Tension Flange Thickness (t_f)

Ten FEA models were conducted to see the influence of tension flange thickness (t_f) on the SIF. Table 12 shows the variation of ‘SIF’ and ‘ β ’ for five different flange thickness values. It was observed that as the flange thickness was increased from 1 inch to 2 inch, there was a slight decrease (1%) in the SIF value. A negligible percentage difference of about 1.5 % was calculated between the ‘ β ’ values of specimen A1 & A5. The results indicated that the tension flange thickness had an insignificant influence on the geometry factor ‘ β ’. Hence was not included in the finite element data fit (analytical equation) of the geometry factor ‘ β ’.

Table 12: Variation of SIF with the Tension Flange Thickness

Group No.,	Model Name	Tension Flange Thickness, t_f (inch)	Tension Flange Width, b_f (inch)	Web height, h_w (inch)	Crack Length, a (inch)	Avg SIF ($ksi\sqrt{in}$)	Geometry Factor ‘ β ’
A	A1	1	14	46	3	117.3	1.39
	A2	1.25	14	46	3	117.2	1.39
	A3	1.5	14	46	3	116.9	1.38
	A4	1.75	14	46	3	116.5	1.38
	A5	2	14	46	3	116	1.37

Web Height (h_w)

The second parameter evaluated in the parametric study was the web height (h_w) of the partially cracked flexural I-shaped member. Table 13 shows the parametric study results for different web height values and their respective ‘SIF’ and ‘ β ’ values. The results show that as the web height was increased from 34 inch to 58 inch, the SIF values also increased. However, the increase in the SIF value was insignificant. A percentage difference of about 1.5% was observed between specimen B1 & B5. The results indicated that the web height had an

insignificant influence on the geometry factor ' β '. Hence was not included in the finite element data fit (analytical equation) of the geometry factor ' β '.

Table 13: Variation of SIF with the Web Height

Group No.,	Model Name	Web height, h_w (inch)	Flange Width, b_f (inch)	Tension Flange Thickness, t_f (inch)	Crack Length, a (inch)	Avg SIF ($ksi\sqrt{in}$)	Geometry Factor ' β '
B	B1	34	14	1.5	3	115.7	1.37
	B2	40	14	1.5	3	116.2	1.38
	B3	46	14	1.5	3	116.6	1.38
	B4	52	14	1.5	3	116.9	1.39
	B5	58	14	1.5	3	117.2	1.39

Tension Flange Width (b_f)

The third parameter in the parametric study was the tension flange width (b_f). Six FEA were performed where the flange width was varied between 13 inch and 26 inch, and it was observed that the SIF decreased significantly with the increase in flange width (Table 14). It was also observed that there was a difference of about 15% between the ' β ' values of specimen C1 & C6. The results indicated that the tension flange width had a significant influence on the geometry factor ' β '. Hence was used in the finite element data fit for the determination of the analytical equation for geometry factor ' β '.

Table 14: Variation of SIF with Tension Flange Width

Group No.,	Model Name	Tension Flange Width, b_f (inch)	Tension Flange Thickness, t_f (inch)	Web height, h_w (inch)	Crack Length, a (inch)	Avg SIF ($ksi\sqrt{in}$)	Geometry Factor ' β '
C	C1	13	1.5	46	3	119.6	1.42
	C2	14	1.5	46	3	116.9	1.38
	C3	15	1.5	46	3	114.4	1.35
	C4	18	1.5	46	3	108.9	1.29
	C5	22	1.5	46	3	104.5	1.24
	C6	26	1.5	46	3	101.8	1.21

Crack Length (a)

Flexural I-shaped member models with varying crack lengths were analyzed to study the localized stress increase around the crack tip and the shift in the neutral axis. For all the models, in-plane bending stress along the longitudinal direction (z-axis) of the member were recorded. Due to the presence of a crack, the stress at the crack tip was found to be very high compared to the applied or the far field stress, and these high stresses resulted in plastic deformation around the crack. This region of stress concentration around the crack is also called the plastic zone.

Figure 46 shows the localized stress in the flexural I-shaped members with an edge crack varying from 1 inch to 5 inch, in increasing order of the crack length. Grey coloured region which is outside the selected stress range of 50 ksi to -50 ksi shows the plastic deformation near the crack line. As the crack length was increased the localized stress region also increased, resulting in a larger crack tip plastic zone. It was observed that the maximum influence of edge crack is on the tension flange, and as the crack length was increased there was some plastic deformation in the web region near the flange-web joint.

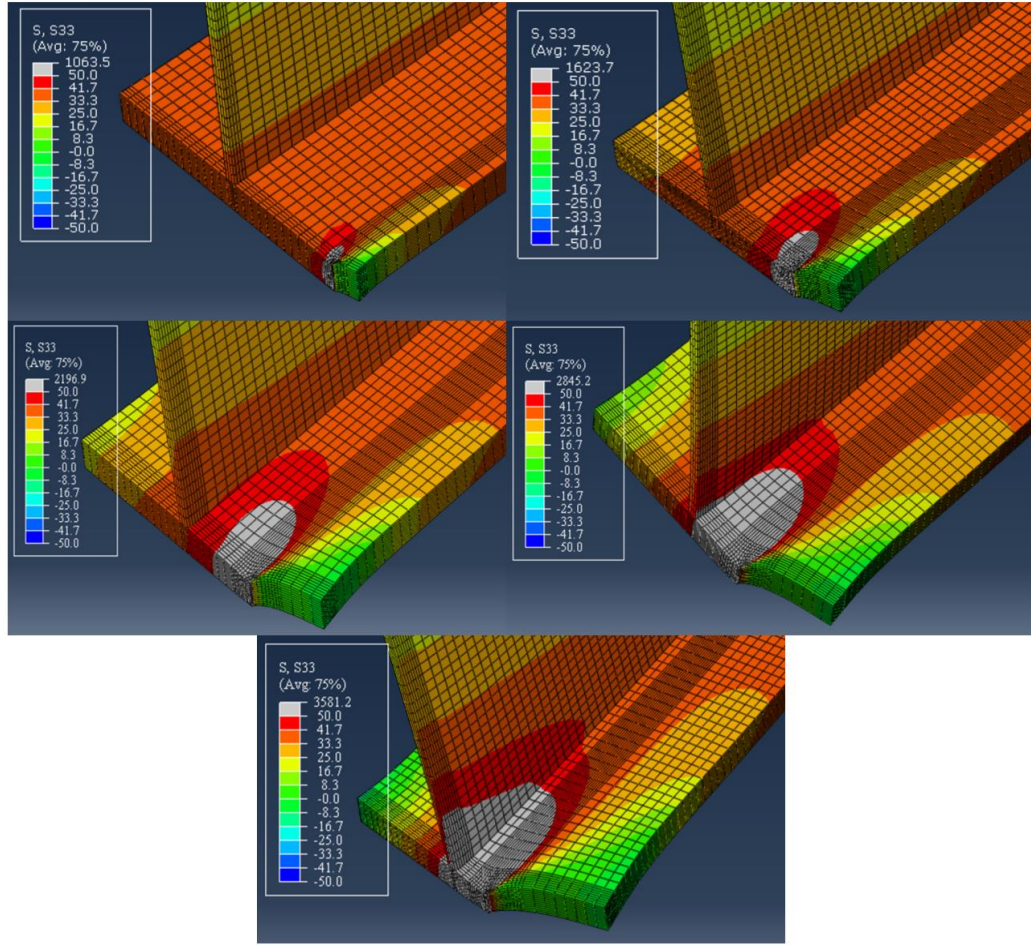


Figure 46: Stress Concentration in Flexural Member with Crack Growth

The effect of the edge crack was also studied at each of the cross-sectional stress profiles. Figure 47 shows the cross-sectional stress profiles along the centerline of the partially cracked flexural I-shaped members with different edge crack profiles, and Figure 48 shows the close-up view of the shift in neutral-axis as the edge crack length is increased from 1 inch to 5 inch.

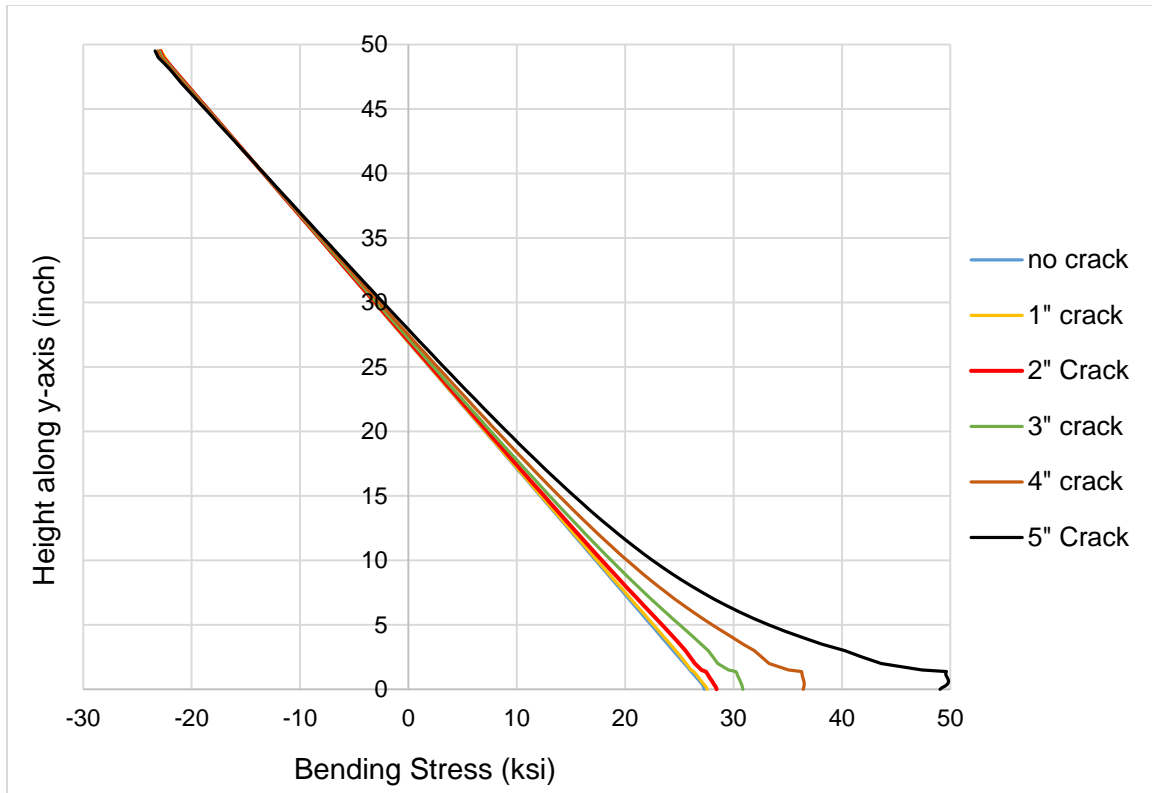


Figure 47: Cross-Sectional Stress Profiles of Flexural Member with Different Crack Lengths

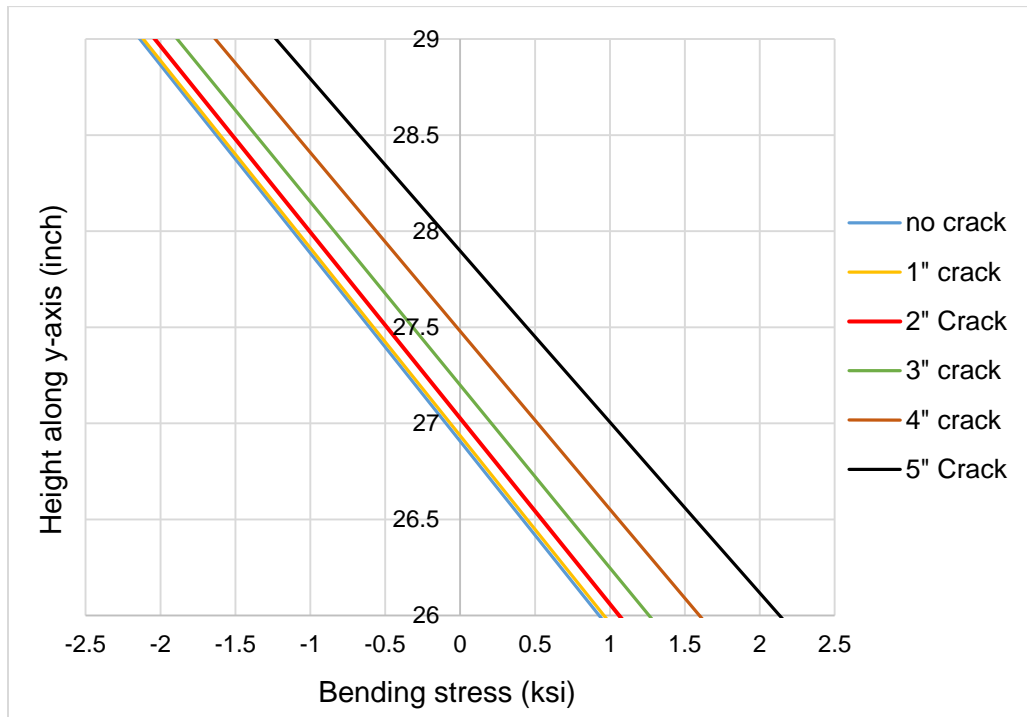


Figure 48: Shift in Neutral-Axis of Flexural Member with Increasing Crack Length

It was observed that as the crack length was increased, the stress in the extreme tension fiber increased by up to 20 ksi, and the stress in the extreme compression fiber was increased by about 0.5 ksi. In addition, with the increase in crack length the neutral axis shifted upwards by approximately an inch. Additionally, the influence of the edge crack length on the SIF was studied. It was observed that as the crack length was increased, there was an increase in the SIF values as shown in Table 15. It was observed that as the crack length was increased from 1 inch to 5 inch, there was an increase of about 50 % in the ‘ β ’ value.

Table 15: Variation of SIF with Edge Crack Length

Group No.,	Model Name	Crack Length, a (inch)	Tension Flange Width, b_f (inch)	Tension Flange Thickness, t_f (inch)	Web height, h_w (inch)	Avg SIF ($ksi\sqrt{in}$)	Geometry Factor ‘ β ’
D	D1	1	14	1.5	46	55.7	1.14
	D2	2	14	1.5	46	86.2	1.25
	D3	3	14	1.5	46	116.7	1.38
	D4	4	14	1.5	46	151.1	1.55
	D5	5	14	1.5	46	190	1.74

Geometry Factor – Edge Crack Geometry

Based on the parametric study results, the parameters which had the most significance or highest influence on the SIF were used to develop an analytical equation for the geometry factor ‘ β ’. For the edge crack profile, the edge crack length (a), and tension flange width (b_f) had the most significant influence on the SIF, while the influence of tension flange thickness (t_f), and web height (h_w) was insignificant and hence were neglected.

An analytical equation for the geometric factor as a function of crack length (a), and flange width (b_f) was developed by curve fitting the FE data points. A total of twenty-one FE models

of different partially cracked flexural I-shaped member geometries were developed for analysis. After evaluating the flexural I-shaped member models, the tension flange of the member was separately studied as an axially loaded plate. Similar to the flexural members, twenty-one FE models of the axially loaded plates were analyzed. The geometry of the plate was similar to the tension flange geometry including the crack profile and loading conditions. The crack length (a) was varied between 1 inch and 12.5 inch, and the flange width (b_f) was varied between 14 inch and 26 inch. In order to match the fracture mechanics terminology, the tension flange width (b_f) was denoted by 'W'. Table 16 shows the specimen matrix in increasing order of the ratio of the crack length (a)-to-flange width (W).

Table 16: Specimen Matrix for Edge Crack Profile

Crack Length, a (inch)	Tension Flange Width, W (inch)	a/W	Avg SIF ($ksi\sqrt{in}$)		Geometry Factor 'β'	
			Plate	Beam	Plate	Beam
1	26	0.038	55.8	54.1	1.14	1.11
1	22	0.045	56.1	54.5	1.15	1.12
1	18	0.056	56.5	54.9	1.16	1.13
1	14	0.071	57.3	55.7	1.18	1.14
2	26	0.077	82.9	80	1.2	1.16
2	22	0.091	84	81.2	1.22	1.18
2	18	0.111	86	83	1.25	1.2
3	26	0.115	105.9	101.8	1.25	1.21
3	22	0.136	108.7	104.5	1.29	1.24
2	14	0.143	89.4	86.2	1.3	1.25
3	18	0.167	113.4	108.8	1.34	1.29
3	15	0.2	119.6	114.4	1.42	1.36
5.5	26	0.212	165.3	157.2	1.45	1.38
3	14	0.214	122.6	116.9	1.45	1.38
3	13	0.231	126.3	119.6	1.5	1.42
3.5	14	0.25	142	133.3	1.56	1.46
4	14	0.286	162.6	151.1	1.67	1.55
5.4	18	0.3	195.7	180.2	1.73	1.59
5	14	0.357	213.9	190.1	1.96	1.74
8.8	22	0.4	318.1	273.1	2.2	1.89
8.1	18	0.45	350.6	274.2	2.53	1.98
12.5	26	0.481	459.1	350.2	2.66	2.03

At first, FEA of flexural I-shaped member models was performed. Then, from each analysis, the average SIF value from the eighth contour was used to calculate the respective 'β' of the specimen. Table 16 shows the SIF obtained from the FEA, and the calculated geometry factor 'β'. Next, a plot between the 'β' and 'a/W' was generated using all the obtained flexural I-shaped member specimen data points. An analytical equation for the geometry factor 'β' as a function of the ratio of crack length (a)-to-flange width (W) was determined by curve fitting the data points as a second-degree polynomial function, as shown in Figure 49.

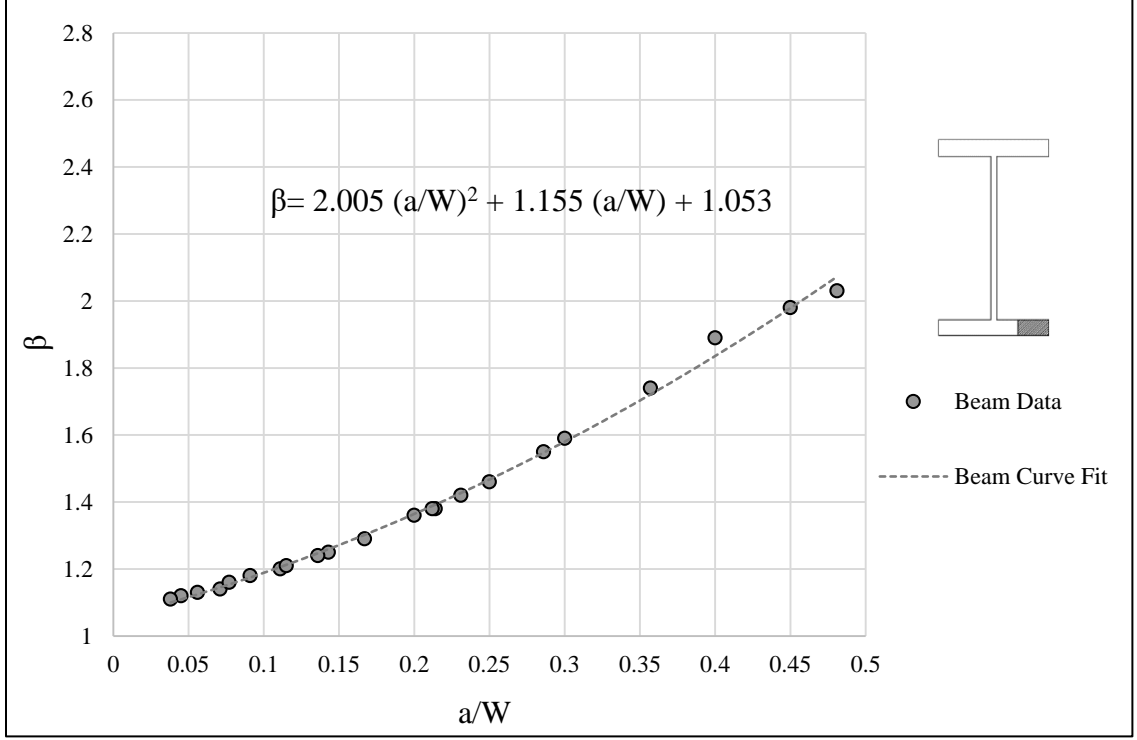


Figure 49: Geometry Factor ‘β’ for a flexural I-shaped member with an Edge Crack Profile

The following equation 23 is the determined analytical equation for the geometry factor ‘β’. This obtained geometry factor can further be used in the SIF equation to calculate the SIF in the vicinity of the edge crack in a flexural I-shaped member.

$$\beta\left(\frac{a}{W}\right) = 1.053 + 1.155\left(\frac{a}{W}\right) + 2.005\left(\frac{a}{W}\right)^2 \quad (23)$$

where, ‘a’ is the crack length, ‘W’ is the tension flange width.

After evaluating the flexural I-shaped member models, the tension flange of the member was separately studied as an axially loaded plate. A similar procedure was followed and the ‘β’ for each specimen was calculated using the SIF obtained from FEA (Table 16). Then, a plot between ‘β’ and ‘a/W’ was developed and the data points were further used to develop an equation to represent the geometry factor ‘β’ as a function of ‘a/W’ for an edge cracked plate (Figure 50).

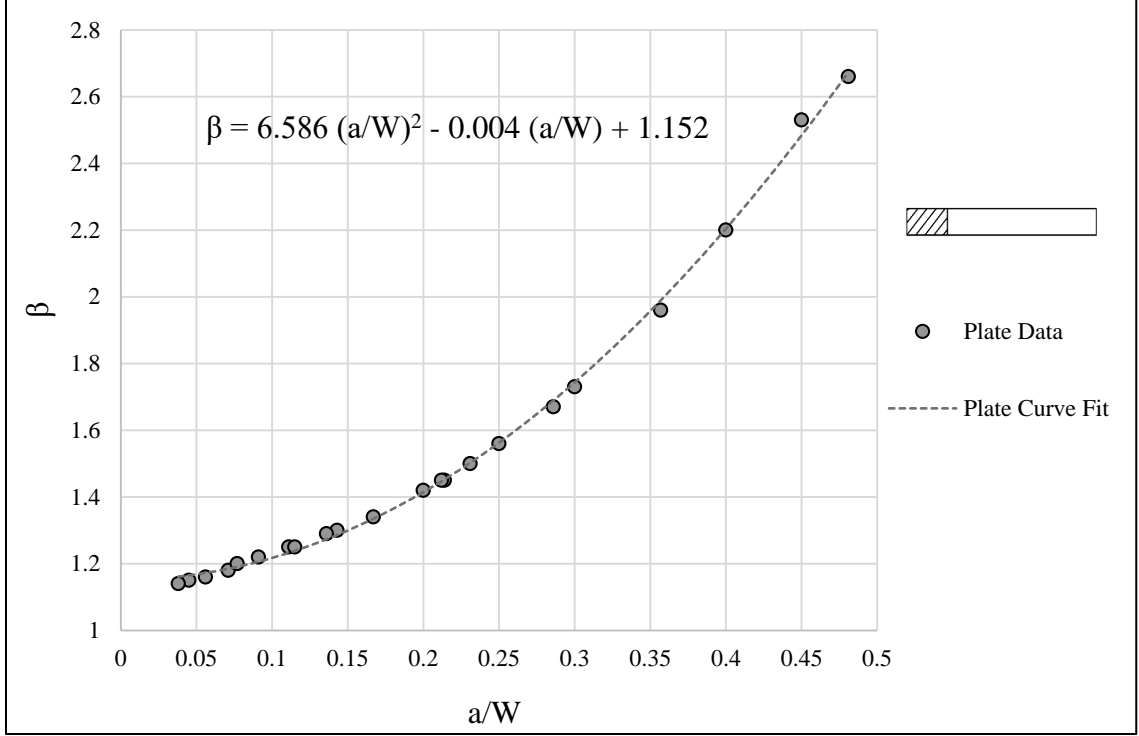


Figure 50: Geometry Factor ‘β’ for an Axially Loaded Plate with an Edge Crack Profile

The following equation 24 is the determined analytical equation for the geometry factor ‘β’. This obtained geometry factor can be used in the SIF equation to calculate the SIF in the vicinity of the edge crack in an axially loaded plate.

$$\beta\left(\frac{a}{W}\right) = 1.152 - 0.004\left(\frac{a}{W}\right) + 6.586\left(\frac{a}{W}\right)^2 \quad (24)$$

where, ‘a’ is the crack length, ‘W’ is the tension flange width.

Furthermore, a plot (Figure 51) between ‘β’ vs ‘a/W’ was developed for comparison of the three solutions: obtained beam solution (Equation 23), obtained plate solution (Equation 24) and the available handbook solution (Equation 21). The plate solution for edge crack profile was further compared with the available handbook solution. It was observed that the obtained plate solution for the geometry factor ‘β’ was in close approximation with the available

handbook solution. However, the determined plate and beam geometry factor solutions were in a good agreement up to a/W ratio of approximately 0.20 and deviated beyond that.

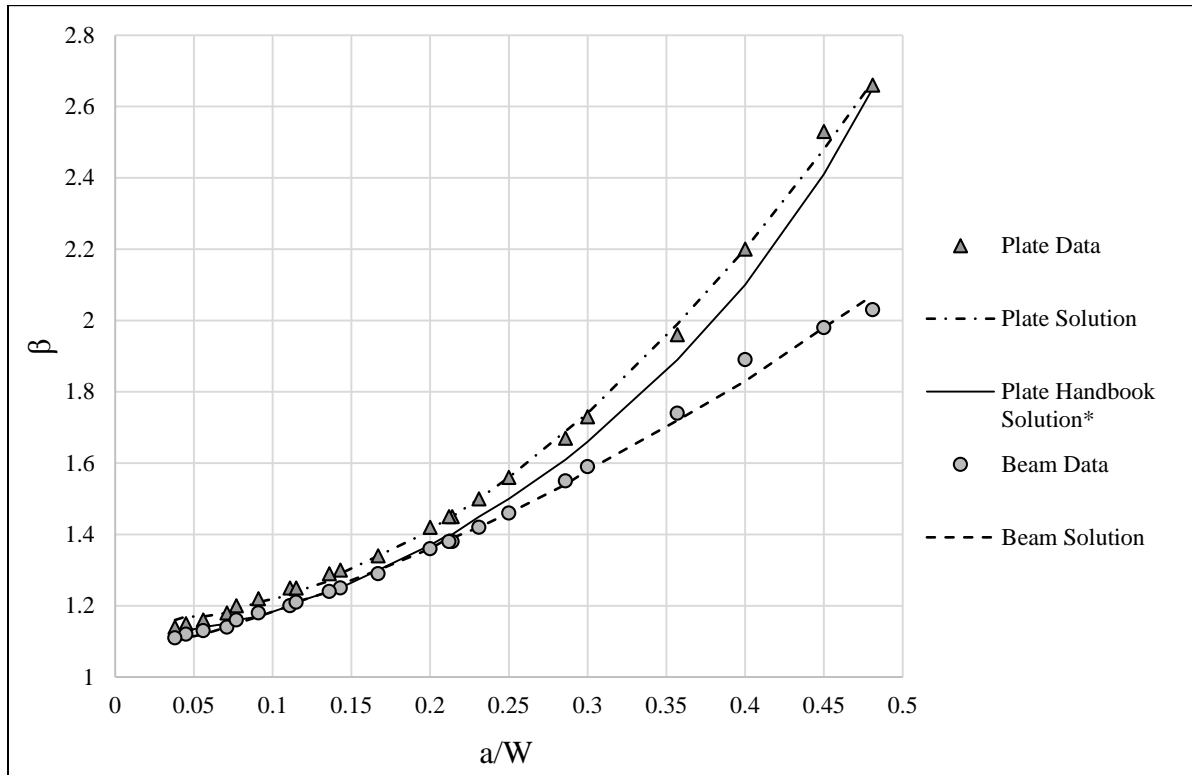


Figure 51: Geometry Factor ' β ' for an Edge Crack Profile

4.4 Parametric Study – Full-Width Crack Geometry

Similar to the edge crack profile, the variation of SIF was studied for parameters including tension flange thickness, tension flange width, web height, and full-width crack length.

Tension Flange Width (b_f)

Table 17 shows the FE results in terms of SIF for three different flange width values. The geometry factor ' β ' was calculated using the obtained SIF value. It was observed that there was an increase in the SIF with the increase in the flange width. There was a difference of about 10% between the ' β ' values of specimen E1 & E3.

Table 17: Variation of SIF with Tension Flange Width

Group No.,	Model Name	Tension Flange Width, b_f (inch)	Tension Flange Thickness, t_f (inch)	Web height, h_w (inch)	Crack Length, a (inch)	Avg SIF ($ksi\sqrt{in}$)	Geometry Factor ' β '
E	E1	14	1.5	46	0.75	76.5	1.81
	E2	20	1.5	46	0.75	80.7	1.91
	E3	26	1.5	46	0.75	83.9	1.99

Web Height (h_w)

Web height was the second parameter studied in the parametric study. As shown in Table 18, there was no difference (0%) in the ' β ' value as the web height was increased from 34 inch to 58 inch. The results indicated that the geometry factor ' β ' of the flexural I-shaped member with full-width crack profile does not depend on the web height. Hence, it was not considered in the determination of analytical for geometry factor ' β '.

Table 18: Variation of SIF with the Web Height

Group No.,	Model Name	Web height, h_w (inch)	Tension Flange Width, b_f (inch)	Tension Flange Thickness, t_f (inch)	Crack Length, a (inch)	Avg SIF ($ksi\sqrt{in}$)	Geometry Factor ' β '
F	F1	34	14	1.5	0.75	76.3	1.81
	F2	46	14	1.5	0.75	76.5	1.81
	F3	58	14	1.5	0.75	76.6	1.81

Tension Flange Thickness (t_f)

In Table 19, the variation of SIF with the tension flange thickness (t_f) was recorded. It was observed that when the thickness was increased from 1.5 inch to 2.25 inch, there was about a 20% decrease in the ' β ' value. The results indicated that the tension flange thickness had a significant influence on the geometry factor ' β '. Hence was used in the finite element data fit for the determination of the analytical equation for geometry factor ' β '.

Table 19: Variation of SIF with the Tension Flange Thickness

Group No.,	Model Name	Tension Flange Thickness, t_f (inch)	Tension Flange Width, b_f (inch)	Web height, h_w (inch)	Crack Length, a (inch)	Avg SIF ($ksi\sqrt{in}$)	Geometry Factor ' β '
G	G1	1.5	14	46	0.75	76.5	1.81
	G2	1.75	14	46	0.75	69.2	1.64
	G3	2	14	46	0.75	64.1	1.52
	G4	2.25	14	46	0.75	60.6	1.44

Full-width Crack Length (a)

The crack length has a direct influence on the SIF value. As shown in Table 20, there was a significant increase in the SIF by about $30 \text{ ksi}\sqrt{in}$ when the crack length was increased from 0.75 inch to 1.125 inch. And, there was a 21.5% increase between in the ' β ' values of specimen H1 & H2. The results indicated that the crack length had a significant influence on the geometry factor ' β '. Hence was used in the finite element data fit for the determination of the analytical equation for geometry factor ' β '.

Table 20: Average SIF values for a Specific Crack Length

Group No.,	Model Name	Crack Length, a (inch)	Tension Flange Width, b _f (inch)	Tension Flange Thickness, t _f (inch)	Web height, h _w (inch)	Avg SIF (ksi√in)	Geometry Factor 'β'
H	H1	0.75	14	2.25	46	60.6	1.44
	H2	1.125	14	2.25	46	90.7	1.75

Geometric Factor – Full-width Crack Geometry

The geometry factor depends on the cross-sectional dimension of the member and the crack dimension. Although all the parameters except the web height influenced the geometry factor, only the parameters with the most significant or highest influence on the SIF were used to develop the analytical equation. From the parametric study conducted on the full-width crack configuration, it was observed that tension flange thickness and the full-width crack length had the highest influence on the SIF, of about 20%, and 21.5% respectively. Other than that, there was a variation of about 10% in the SIF with the tension flange width variation, and there was no variation in the SIF with the web height. Considering the amount of influence of these parameters on the SIF, tension flange thickness, and full-width crack lengths were used to determine an analytical equation for geometry factor 'β' of the partially cracked flexural I-shaped member with a full-width crack.

A total of thirteen FE models of different configurations of partially cracked flexural I-shaped member s were developed for the analysis. Following the analysis of flexural I-shaped member models, axially loaded plate models were analyzed. Thirteen FE models of axially loaded plate were developed and analyzed to determine an analytical equation for the geometry factor 'β'. The same crack configuration and loading conditions were used for the analysis. All the FE models had a full-width crack in them. The crack length (a) along the component

thickness was varied between 0.45 inch and 1.35 inch, while the tension flange thickness (t_f) was varied between 1.5 inch and 2.25 inch. In order to match the fracture mechanics terminology, the flange thickness was denoted by ‘W’. Table 21 shows the specimen matrix in terms of increasing order of ‘a/W’.

Table 21: Specimen Matrix for Full-width Crack Profile

Crack Length, a (inch)	Flange Thickness, W (inch)	a/W	Avg SIF ($ksi\sqrt{in}$)		Geometry Factor ‘ β ’	
			Beam	Plate	Beam	Plate
0.45	1.5	0.3	46.4	1.42	55.2	1.69
0.75	2.25	0.33	60.6	1.44	75.9	1.8
0.7	2	0.35	60.2	1.48	76.3	1.87
0.75	2	0.38	64.1	1.52	83.8	1.99
0.6	1.5	0.4	60.3	1.6	80.7	2.14
0.75	1.75	0.43	69.2	1.64	99.8	2.36
1	2.25	0.44	79.7	1.64	116.3	2.39
0.9	2	0.45	77.2	1.67	115.2	2.49
0.75	1.5	0.5	76.5	1.81	119.3	2.83
1	2	0.5	86.2	1.77	140.2	2.88
1.125	2.25	0.5	90.7	1.75	154.9	3
1.125	2	0.56	98.3	1.9	180.9	3.5
1	1.75	0.57	95	1.95	174.9	3.59
1.35	2.25	0.6	111.9	1.98	230.8	4.08

From each analysis, the average SIF from the eighth contour were recorded. Next, using the obtained SIF, the geometry factor ‘ β ’ for each crack length was back-calculated using the SIF equation (Equation 22). Then, for the partially cracked flexural I-shaped member models, a plot between ‘ β ’ and ‘a/W’ was developed, and the data points were fit as a second-degree polynomial equation, as shown in Figure 52.

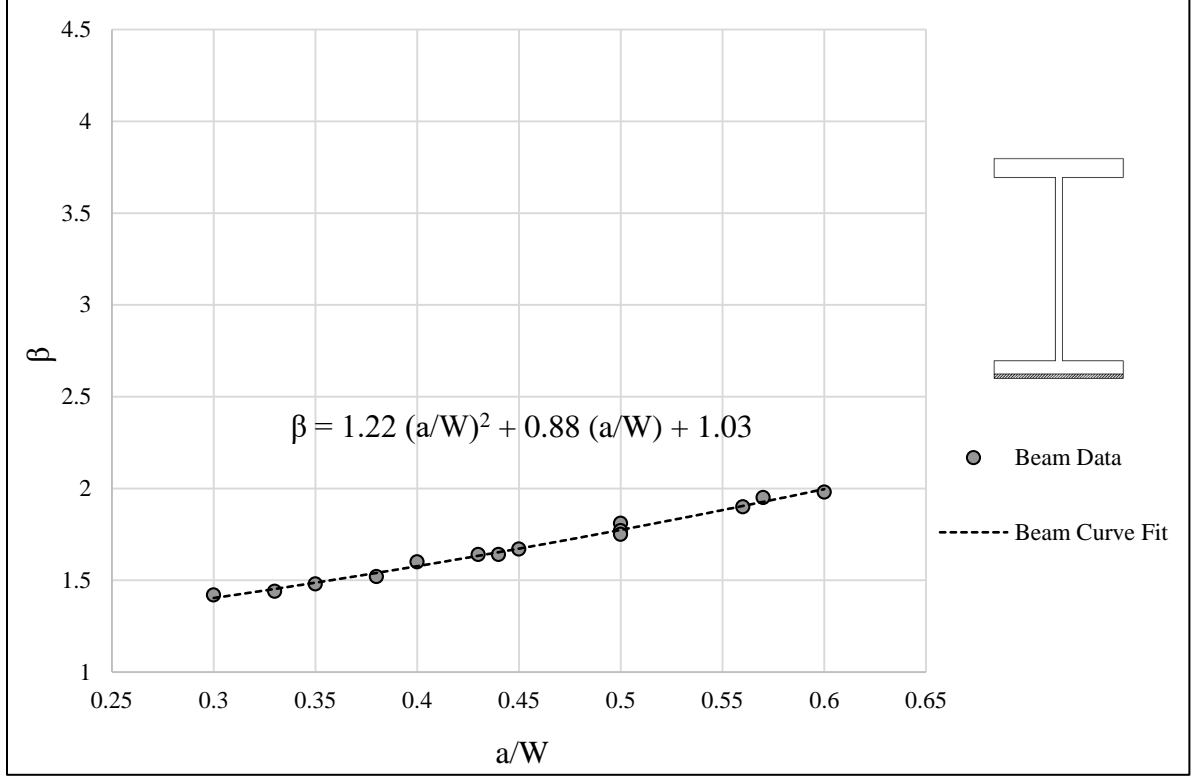


Figure 52: Geometry Factor 'β' for a flexural I-shaped member with a Full-width Crack Profile

An analytical equation was determined for the geometry factor 'β' in terms of 'a/W'. The following 26 is the determined analytical equation for the geometry factor of a partially failed flexural I-shaped member with a full-width crack.

$$\beta\left(\frac{a}{W}\right) = 1.03 + 0.88\left(\frac{a}{W}\right) + 1.22\left(\frac{a}{W}\right)^2 \quad (25)$$

where, 'a' is the crack length, 'W' is the tension flange thickness.

Similar FE modeling and analysis procedure was followed to determine an analytical equation for 'β' of plate models with a full-width crack profile. Average SIF was obtained from the FE output file of each analysis. Figure 53 shows the polynomial curve fit of the FE data points, and equation 26 is the determined second-degree polynomial equation for geometry factor 'β' of the plate models with a full-width crack profile.

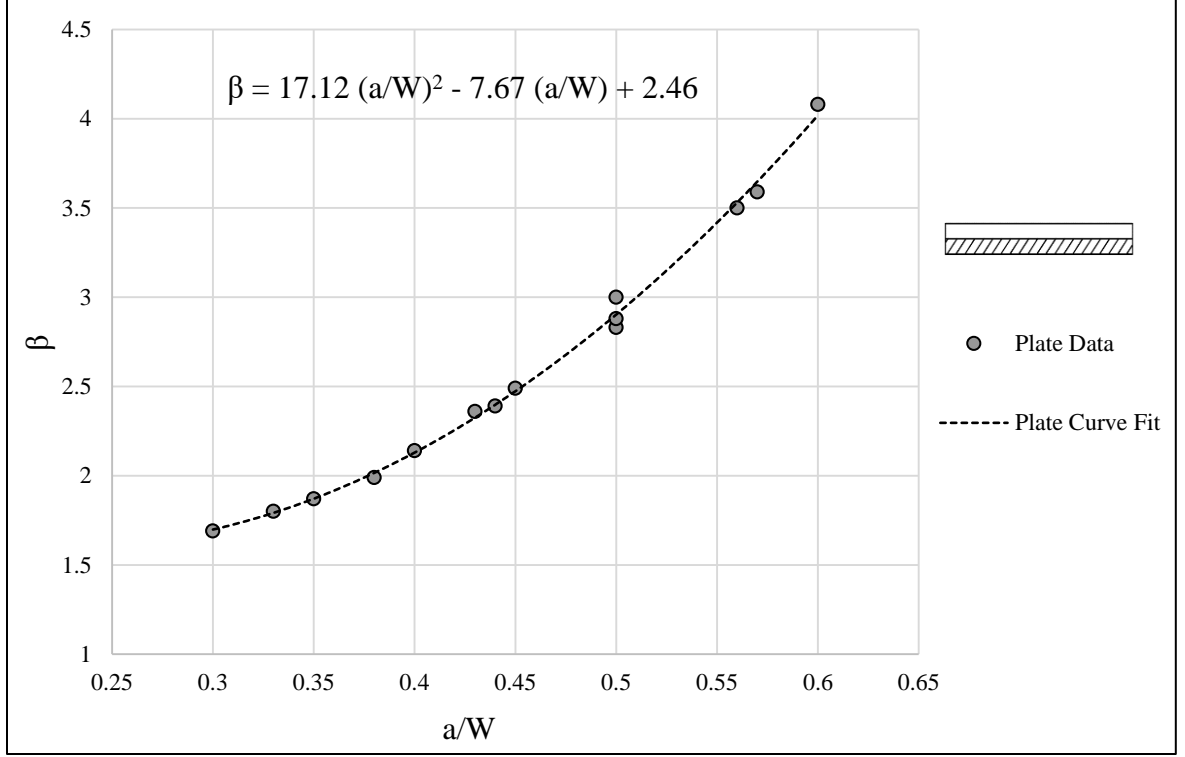


Figure 53: Geometry Factor ‘β’ for an Axially Loaded Plate with a Full-width Crack Profile

$$\beta\left(\frac{a}{W}\right) = 2.46 - 7.67\left(\frac{a}{W}\right) + 17.12\left(\frac{a}{W}\right)^2 \quad (26)$$

where, ‘a’ is the crack length, ‘W’ is the tension flange width.

Figure 54 shows a combined plot comprising the obtained beam solution, plate solution, and the available handbook solution. The obtained plate solution was further compared to available handbook solution for an edge crack profile (Equation 21). The results show that there was a good approximation between the obtained plate solution and the available handbook solution. However, the difference between the obtained plate and flexural I-shaped member solutions increased with the increase in the ‘a/W’ ratio. This indicates that the plate solutions were conservative compared to the determined flexural I-shaped member solution, especially with larger a/W ratios.

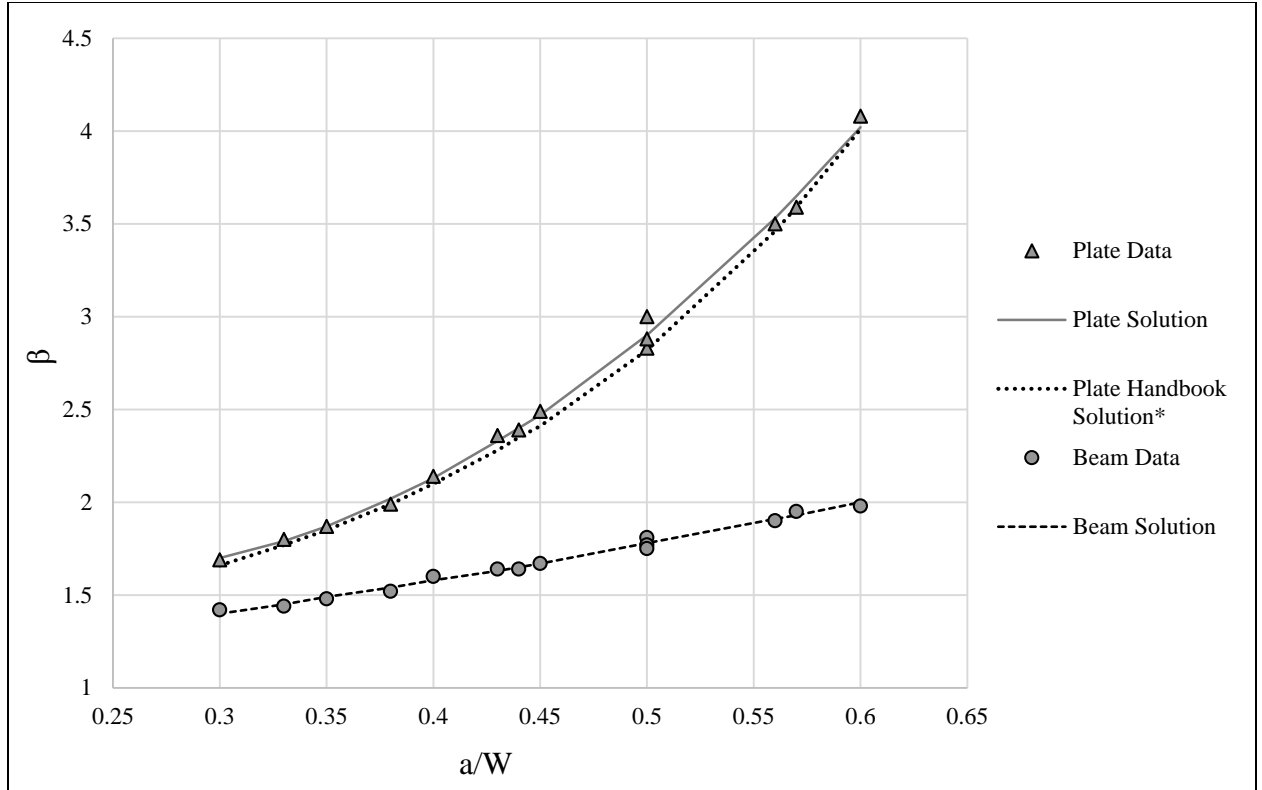


Figure 54: Geometry Factor 'β' for Full-width Crack Profile

4.5 Fracture Behavior of Edge Cracked Specimens

The determined geometry factor 'β' for the partially cracked flexural I-shaped member was further used to study the fracture behavior of the edge cracked members. The fracture behavior of both flexural and axial specimens with an edge crack was studied under the applied loading condition (55% F_y). In this study, the stability of the crack as a function of stress, crack size, and fracture toughness was studied. Additionally, the fatigue crack growth behavior under the applied load condition was studied.

At first, the fracture toughness which is a measure of resistance offered by a specimen to the crack growth was determined. One of the most widely used methods to calculate fracture toughness is by using the Charpy V-notch test notch toughness value. From a previous

research, a two-stage CVN- K_{Id} - K_c correlation was found (Barsom and Rolfe, 1999). ' K_{Id} ' is the dynamic SIF and is given by Equation 27.

$$K_{Id} = \sqrt{5(CVN)E} \quad (27)$$

where 'CVN' is the notch toughness value, 'E' is the modulus of elasticity. ' K_{Ic} ' is the static SIF, and the difference between ' K_{Id} ' & ' K_{Ic} ' is given by temperature shift, denoted as ' T_{shift} ' (Figure 55). Temperature shift is a function of yield strength ' σ_{ys} ', and is given by Equation 28.

$$T_{shift} = 215 - 1.5\sigma_{ys} \quad (28)$$

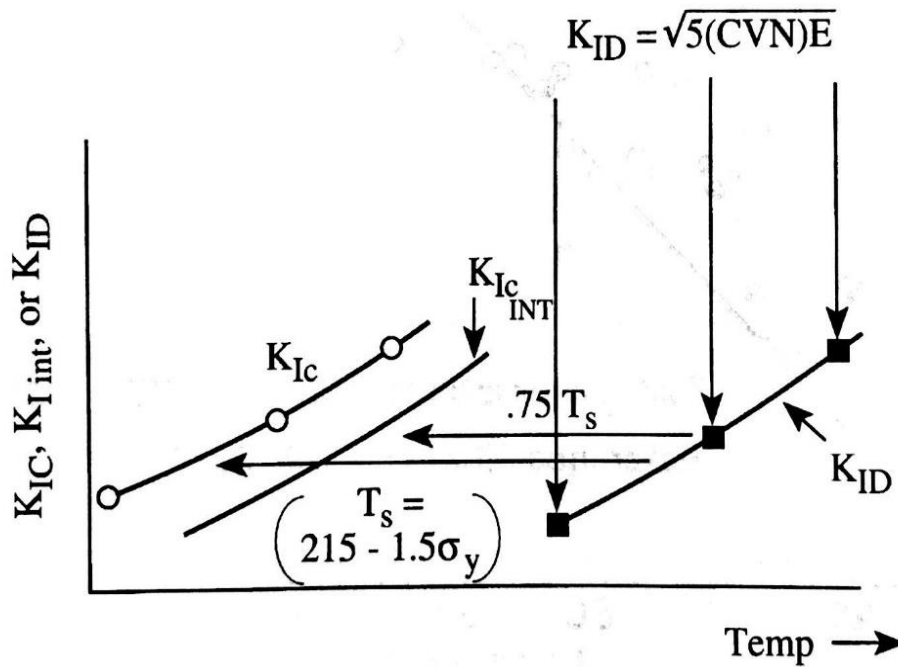


Figure 55: Temperature Shift between ' K_{Id} ' & ' K_{Ic} ' (Barsom and Rolfe, 1999).

The minimum specified CVN values for bridge steels are given in AASHTO LRFD Bridge Design Specifications. AASHTO specifies a CVN value of 30 ft-lb @ 10 °F for A709 Grade 50 steel under Zone III (Wright, 2015). Using the following two-stage CVN- K_{Id} - K_c correlation

(Equation 27 & 28) (Barsom and Rolfe, 1999) the fracture toughness (K_{Ic}) value for this specified CVN was calculated.

For steel with a yield strength of 50 ksi, modulus elasticity of 29,000 ksi, and CVN value of 30 ft-lb @ 10 °F, a fracture toughness (K_{Ic}) of $228.5 \text{ ksi}\sqrt{\text{in}}$ @ -130 °F was obtained. Alternatively, using the Roberts-Newton lower-bound CVN- K_{Ic} relation (Equation 29) (Barsom and Rolfe, 1999) a fracture toughness of $80 \text{ ksi}\sqrt{\text{in}}$ was calculated for this same CVN value.

$$K_c = 9.35(CVN)^{0.63} \quad (29)$$

The calculated material fracture toughness was further used to find the fracture stress values for the corresponding edge crack length. The calculations were performed for both the plate and flexural I-shaped member models. Fracture toughness is the critical SIF which causes the member fracture. The obtained fracture toughness was further used to calculate the anticipated critical stress at member fracture (Equation 30).

$$\sigma_c = \frac{K_{Ic}}{\beta\sqrt{\pi a}} \quad (30)$$

where ' K_{Ic} ' is the fracture toughness, ' σ ' is the fracture stress, ' a ' is the edge crack length, and ' β ' is the determined geometry factor for the edge crack profile.

Both the plate and flexural I-shaped member models with an edge crack profile were analyzed to find the anticipated fracture stress values. The edge crack length was varied from 1 inch to 5 inch in increments of 1 inch. I-shaped flexural member models were analyzed and the fracture stress was determined for each corresponding edge crack length using Equation 30. For the calculations, a fracture toughness (K_{Ic}) of $228.5 \text{ ksi}\sqrt{\text{in}}$ was used.

The same calculations were repeated for five values of the edge crack. Following the flexural I-shaped member models, axially loaded plate models were analyzed to find the fracture stress values for the same material fracture toughness (K_{Ic}). Then, a comparison between the results of flexural I-shaped member and plate models were made to see the variation in the output by using different geometric configurations. Table 22 below shows the calculated fracture stress values for five different edge crack values for both the flexural I-shaped member and plate models.

Table 22: Fracture Stress Values for Higher Fracture Toughness Value ($228.5 \text{ ksi}\sqrt{\text{in}}$)

Crack Length (a), in	a/W	Geometry Factor (β)		Fracture Stress (σ), ksi		% Difference
		Beam	Plate	Beam	Plate	
1	0.071	1.14	1.18	113.1	109.3	3%
2	0.143	1.26	1.29	72.3	70.7	2%
3	0.214	1.39	1.45	53.5	51.3	4%
4	0.286	1.54	1.69	41.9	38.1	9%
5	0.357	1.72	1.99	33.5	29	13%
8.8	0.4	1.83	2.2	23.7	19.8	16%
12.5	0.481	2.07	2.67	17.6	13.7	22%

Afterward, the fracture behavior of the same flexural I-shaped member and plate models were studied for a lower-bound fracture toughness (K_{Ic}) of $80 \text{ ksi}\sqrt{\text{in}}$. Table 23 shows the calculated fracture stress values for five different edge crack lengths for both the flexural I-shaped member and plate models. Figure 56 shows the plot for fracture stress vs crack length for both the plate and flexural I-shaped member models for both a lower-bound and a higher fracture toughness value.

Table 23: Fracture Stress Values for Lower-bound Fracture Toughness Value ($80 \text{ ksi}\sqrt{\text{in}}$)

Crack Length (a), in	a/W	Geometry Factor (β)		Fracture Stress (σ), ksi		% Difference
		Beam	Plate	Beam	Plate	
1	0.071	1.14	1.18	39.6	38.3	3%
2	0.143	1.26	1.29	25.3	24.7	2%
3	0.214	1.39	1.45	18.7	18	4%
4	0.286	1.54	1.69	14.7	13.4	9%
5	0.357	1.72	1.99	11.7	10.1	14%
8.8	0.4	1.83	2.2	8.3	6.9	17%
12.5	0.481	2.07	2.67	6.2	4.8	23%

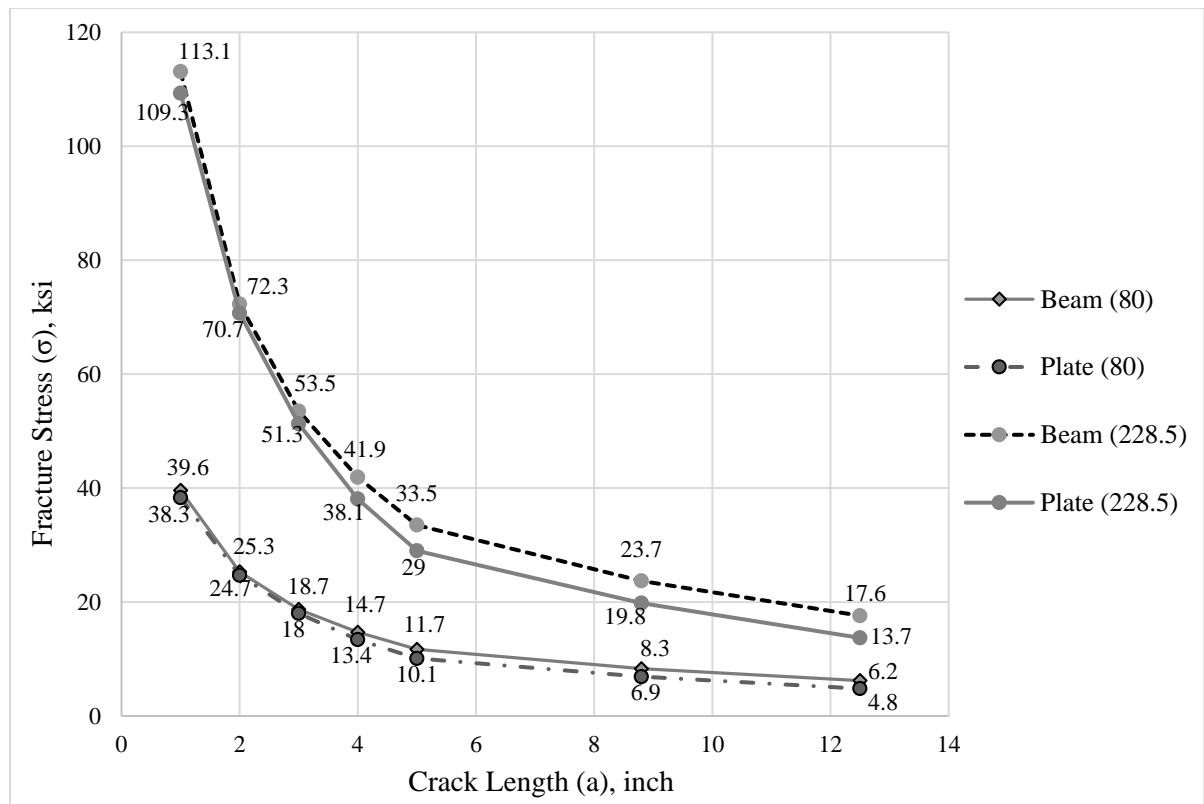


Figure 56: Fracture Stress vs Crack Length Relation for Higher ($228.5 \text{ ksi}\sqrt{\text{in}}$), and Lower-bound Fracture Toughness ($80 \text{ ksi}\sqrt{\text{in}}$)

Fracture stress and the crack length are inversely proportional to each other. As the crack length increases, the stress required to cause the member fracture decreases, and vice-versa.

The results indicated that the difference in fracture stress outputs between the flexural I-shaped member and plate models increased with the increase in the crack length for higher fracture toughness, as shown in Table 22 & Table 23.

This relation between the fracture stress and crack length helps to characterize the crack as critical or sub-critical. For example, if we consider the fracture stress vs crack length relation curve for a fracture toughness $80 \text{ ksi}\sqrt{\text{in}}$ (lower-bound curve), for a 4 inch long edge crack the stress required to cause the flexural I-shaped member fracture is 14.7 ksi, while for the same edge crack length, the stress required to cause the plate fracture is 13.4 ksi. The result from the plate model were approximately 9% less than the flexural I-shaped member model, which means that the results obtained from the plate models were conservative. Also, the plate models result in a shorter calculated fatigue life to get to the critical crack length when compared to the flexural I-shaped member models.

Another application of these results is to study the fatigue life of the rolled steel girder: by using the relationship between Stress Cycles and Crack Length (Figure 2). The crack may grow slowly with continuous live load cycles and may cause member fracture when it becomes critical. Another way to interpret these results is. For example, for a stress of 10 ksi, using the lower-bound fracture toughness ($80 \text{ ksi}\sqrt{\text{in}}$), the results from the plate model indicated that the member fracture will occur when the crack reaches approximately 7.5 inch in length. While the flexural I-shaped member model results indicate that the member fracture will occur when the crack reaches approximately 5.3 inch in length. This difference in the crack length indicates that the flexural I-shaped member model will take several more fatigue live load cycles in comparison to the plate model before experiencing a fracture.

4.6 Stress Redistribution in a Partially Cracked Flexural I-shaped Member

The following section discusses the stress distribution in a partially cracked flexural I-shaped member with a full-width crack. A comparison was made between the stress distribution of a flexural I-shaped member with a full-width crack and a built-up section with a failed cover plate.

A study conducted by Hebdon et.al. focused on determining the load distribution in a steel built-up member composed of angles and cover plates. The researchers concluded that after the failure of the first component (cover plate), the stress mostly distributes to the adjacent component (cover plate or angles). From the analysis, an amplification factor as a function of the number of cover plates was determined (Equation 19). For a built-up section, after the failure of a component, the stress increase in the adjacent component can be calculated by multiplying the net section stress with the amplification factor. The net-section stress of the remaining intact-components can also be calculated using the mechanics-of-materials equation $(\sigma = My/I)$.

In the present study, the full-width crack in a flexural I-shaped member was assumed to represent the 100% failure of a cover plate in a built-up section. So, a comparison was made between the current study and the results obtained by Hebdon et.al. The cross-sectional dimensions of both the flexural I-shaped member and the built-up section are the same as shown in Figure 57. The same boundary conditions and loading (55% F_y) were used for the analysis of both the models.

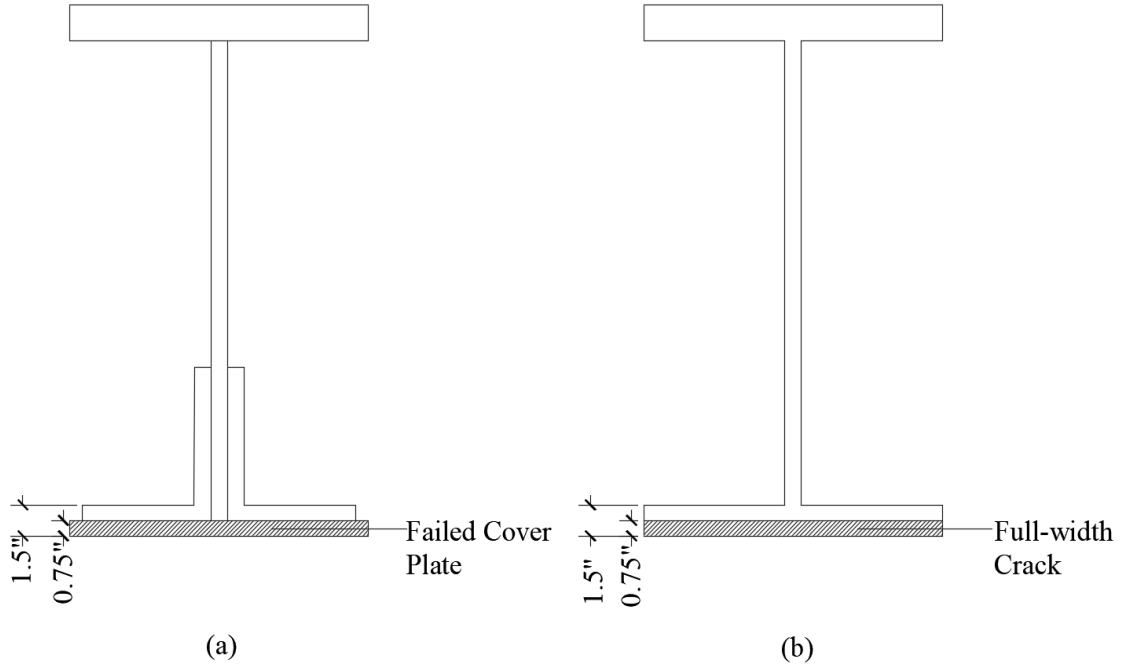


Figure 57: (a) Built-up Member (b) Partially Cracked flexural I-shaped member

For the study, a partially cracked flexural I-shaped member with a full-width crack located in the tension flange was considered. The tension flange was 1.5 inch thick and 14 inch wide. The depth of the full-width crack was 0.75 inch from the bottom of the flange which was equal to the thickness of the cover plate (Figure 57). The a/W ratio was 0.5. In the FE model of the flexural I-shaped member, the region around the full-width crack line was finely meshed following the same meshing procedure as explained in the previous chapters. The tension flange was meshed into 16 elements of different size along the cross-section of the member, as shown in Figure 58. The detailed view of the elements above the full-width crack line with element number and size is shown in Figure 59.

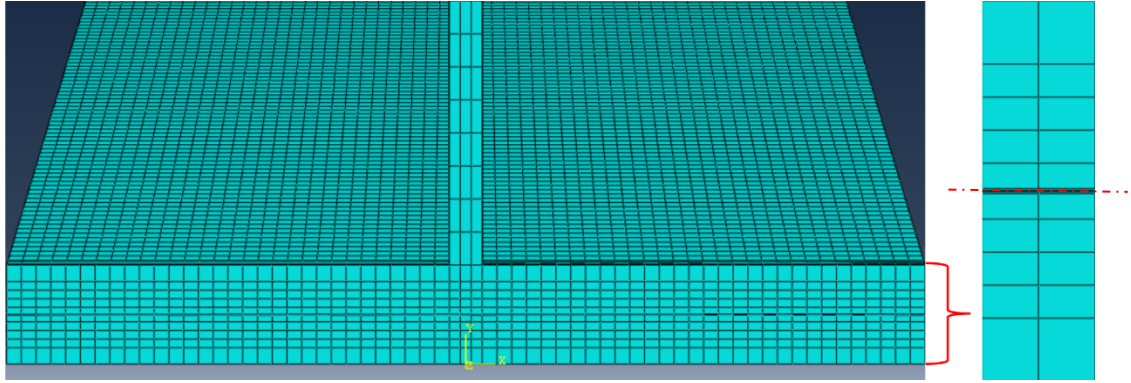


Figure 58: Structured Mesh along the Cross-section of the Tension Flange

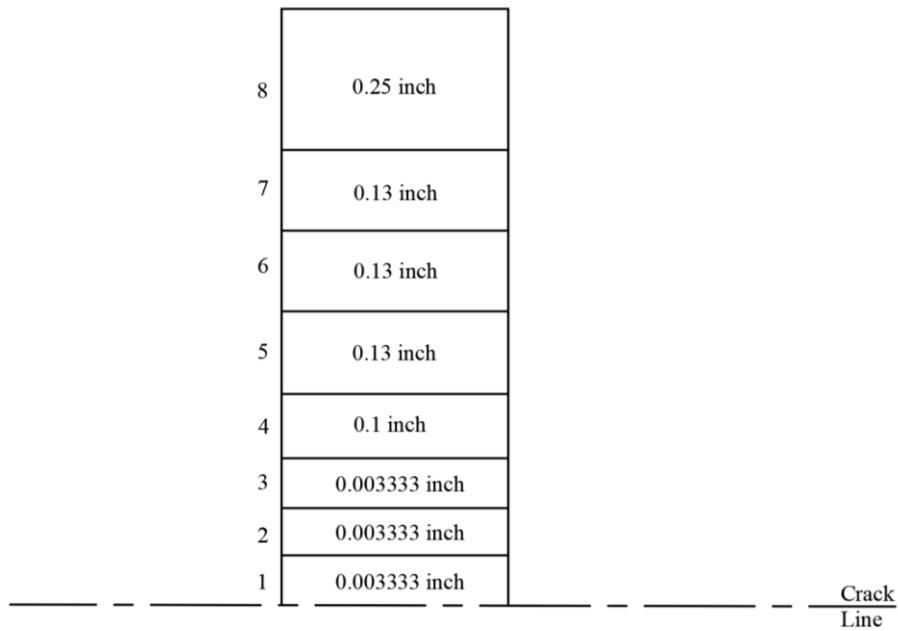


Figure 59: Detailed View of the Elements above the Full-width Crack Line

Due to a reduction in the net-sectional area, the cross-sectional stress increases, especially in the remaining tension flange region (0.75 inch x 14 inch). Hence, a cross-sectional stress profile (Figure 60) for the partially cracked flexural I-shaped member was obtained to calculate the resultant stress in the remaining portion of the tension flange. It was seen that there was a steep increase in the stress near the crack line in the tension flange. Also, it was observed that there was significant stress increase in the remaining portion of the tension flange above the

crack line. The neutral axis shifted upwards by about 0.6 inch due to the presence of 0.75inch full-width crack.

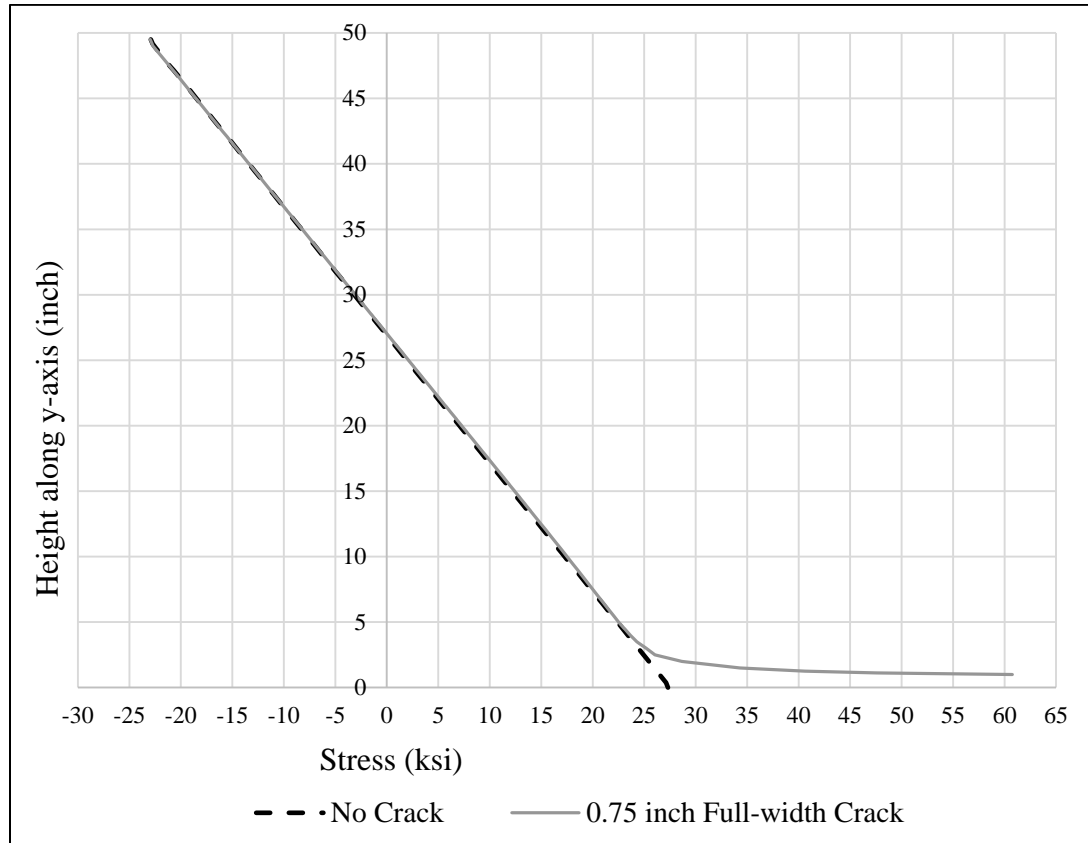


Figure 60: Cross-sectional Stress Profile of the Partially Cracked flexural I-shaped member with a Full-width Crack

The full-width crack was present along the entire width of the flange and hence will affect the cross-sectional stress throughout the flange width. Therefore trapezoidal rule was used to calculate the stress increase in the remaining tension flange region. The remaining tension region (0.75 inch x 14 inch) had eight elements of different size along the cross-section. At each node location, a horizontal path was created and the stress values at a hundred equal intervals along the flange width were recorded. Figure 61 shows the selected horizontal paths (top), and the detailed view of the element number and size (bottom).

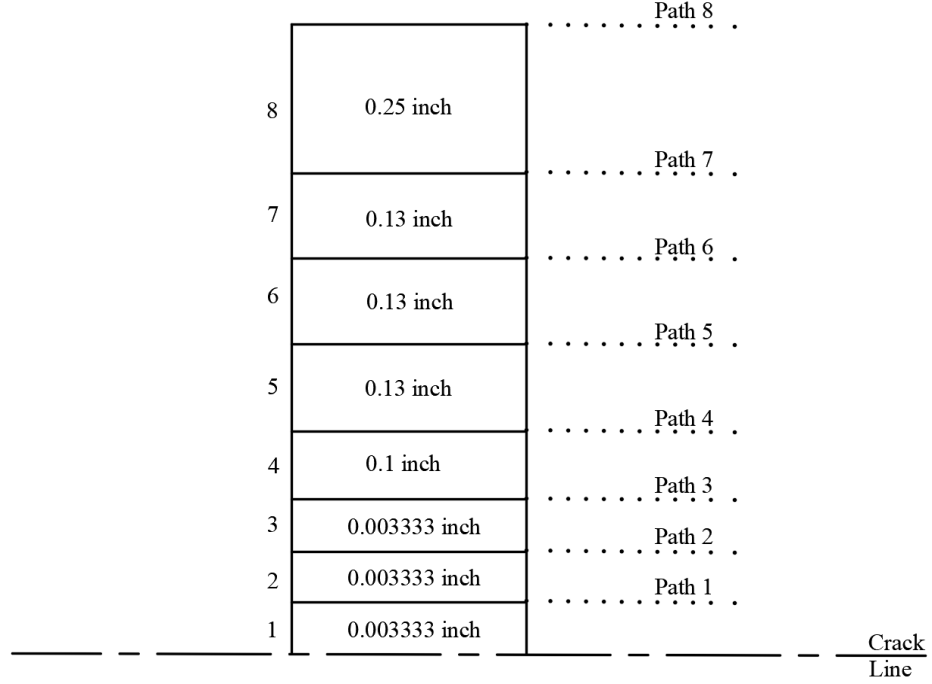
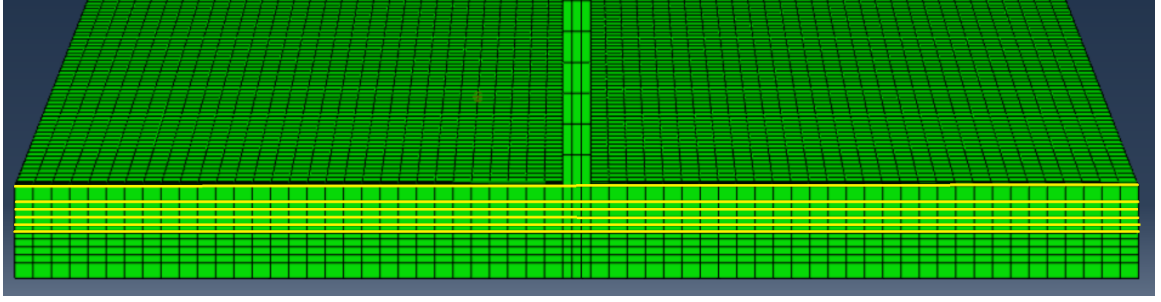


Figure 61: Paths along the Flange Width (Top), Detailed View of the Elements (Bottom)

Next, for each path, net-stress was calculated using the trapezoidal rule (Equation 31).

$$\sigma_{path} = \frac{1}{b_f} \sum \left\{ \frac{(\sigma_i + \sigma_j)}{2} (x_j - x_i) \right\} \quad (31)$$

where ‘ σ_{path} ’ is the equivalent cross-sectional stress along each specified path along the flange width, ‘ σ_i ’ & ‘ σ_j ’ are stresses calculated at integration points for node 1 & 2 respectively, ‘ x_i ’ & ‘ x_j ’ is the distance between node 1 & 2 from the origin respectively, ‘ b_f ’ is the tension flange width.

Table 24 shows the resultant stress calculation along all the eight paths. Next, the resultant flange stress was calculated using the cross-sectional stress at each path. Further, the trapezoidal rule (Equation 32) was used to find the resulting cross-sectional stress along the height in the remaining tension flange region.

$$\sigma_{cs} = \frac{1}{t_f} \sum \left\{ \frac{(\sigma_i + \sigma_j)}{2} (y_j - y_i) \right\} \quad (32)$$

where, ‘ σ_{cs} ’ is the resulting cross-sectional stress along the height of the tension flange, and ‘ t_f ’ is the tension flange thickness excluding the full-width crack.

A resulting net-section stress of 65.4 ksi was obtained from the calculations as shown in Table 24. The results indicate that there was a stress increase of 138% in the tension flange of the flexural I-shaped member due to the presence of the full-width crack.

Table 24: FE Stress Calculations

Path Number	Cross-sectional Stress (ksi)	Element size	Net Element Stress
1	895.5	0.0033	2.92
2	514.6	0.0033	2.35
3	300.5	0.0033	1.36
4	95.15	0.10	19.8
5	56.87	0.13	9.88
6	38.14	0.13	6.18
7	18.24	0.13	3.66
8	5.16	0.25	2.93
Net-section Stress			65.4ksi

Following the analysis of flexural I-shaped member, a built-up steel member composed of a single cover plate and angles in the tension region having the same cross-sectional dimensions as that of flexural I-shaped member was considered for analysis using equations

proposed by Hebdon (Equation 19). First, the moment capacity of the built-up section including all the components was calculated using the bending stress equation, for stress of 27.5 ksi (55% F_y) in the extreme tension fiber. The calculations are shown in equation 33.

$$M = \sigma \times \frac{I_{net}}{y_{net}} = 27.5ksi \times \frac{31625.4in^4}{26.9inch} = 32330.8kip-in \quad (33)$$

Next, for the same moment capacity, the stress in the extreme tension fiber of the built-up section with a completely failed cover plate was calculated using equation 34. There was a stress increase of about 16.2 ksi in the extreme tension region due to the reduced cross-sectional area.

$$\sigma_{cr} = M \times \frac{y_{cr}}{I_{cr}} = 32330.8kip-in \times \frac{30.7inch}{22972in^4} = 43.2ksi \quad (34)$$

Using equation 19 an amplification factor of 1.25 was calculated for a built-up section with one cover plate. The calculations are shown below (Equation 35).

$$\beta_{AF} = 1 + 0.2 \left(1 + \frac{N}{4} \right) = 1 + 0.2 \left(1 + \frac{1}{4} \right) = 1.25 \quad (35)$$

The calculated stress (σ_{cr}) was further multiplied by the amplification factor (β_{AF}) to find out the stress increase in the adjacent angle (Equation 36) due to the failed cover plate.

$$\sigma_{angle} = \beta_{AF} \times \sigma_{cr} = 1.25 \times 43.2ksi = 54ksi \quad (36)$$

The obtained FE net-section stress for the flexural I-shaped member with a full-width crack was almost 21% higher than the calculated stress for the built-up section with a single cover failure. The reason for achieving a higher net-section for the flexural I-shaped member with a full-width crack is because of the stress concentration around the crack line. This indicates that evaluating the built-up member with a failed cover plate as a flexural I-shaped member with a full-width crack in the tension region yielded conservative results.

Furthermore, similar calculations were performed on a built-up section having two cover plates and an angle in the tension region. The bottommost cover plate was failed (Figure 62) and the stress increase in the adjacent cover plate was calculated by multiplying the amplification with the net-section stress of the remaining intact components. The amplification factor is a function of number of cover plates (Equation 19), and for two cover plates, an amplification factor of 1.3 was calculated. Using the amplification factor, stress of 48.35 ksi was calculated in the second cover plate due to the failure of a first cover plate.

The calculated stress was further compared with the FE cross-sectional stress of the flexural I-shaped member with a full-width crack. The cross-sectional dimensions of the flexural I-shaped member were same as that of the build-up section (Figure 62). The tension flange was 2.25 inch thick and the full-width crack was 0.75 inch from the bottom of the flange, with an a/W ratio was 0.33. The full-width crack geometry was equal to the failed cover plate geometry.

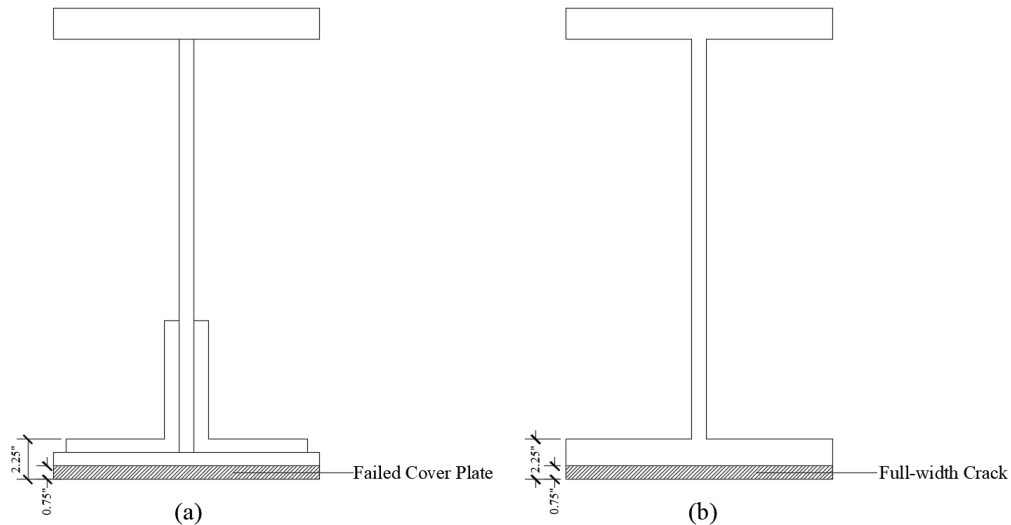


Figure 62: (a) Built-up Section (b) flexural I-shaped member with Full-width Crack

The same procedure as explained above was used to calculate the stress in the remaining portion of the tension flange (0.75 inch x 14 inch) above the full-width crack line. Eight horizontal paths were created to calculate the average stress along the flange width. Then, the trapezoidal rule (Equation 32) was used to calculate the net-section stress in the tension flange of the flexural I-shaped member, as shown in Table 25.

Table 25: FE Stress Calculation

Path Number	Cross-sectional Stress (ksi)	Element size	Resulting Element Stress
1	387	0.0033	1.74
2	228.28	0.0034	1.03
3	77.42	0.1	15.3
4	50.94	0.13	8.22
5	41.65	0.13	5.93
6	35.92	0.13	4.97
7	31.85	0.13	4.34
8	26.1	0.13	3.71
Total			60.3ksi

For a load of 55% F_y , and due to a 0.75 inch full-width crack, net-section stress of 60.3 ksi was calculated. The results indicate that there was a stress increase of about 119% in the remaining tension flange region. Also, a difference of about 25% was observed between the FE stress and the calculated stress values. The stress concentration around the full-width crack line is the reason for obtaining higher stress in the remaining tension flange region of the flexural I-shaped member. It was observed that near the full-width crack line there was a steep increase in the cross-sectional stress of the flexural I-shaped member. While in the built-up section there is no such local stress concentration due to the failed cover plate.

CHAPTER 5: Conclusions and Summary

5.1 Conclusions

1. There are no available SIF solutions for the partially cracked flexural I-shaped member with edge crack or with a full-width crack profile.

Edge Crack Profile

2. It was concluded that varying the tension flange thickness (t_f) and the web height (h_w) had a negligible influence on the geometry factor ' β ' of the partially cracked flexural I-shaped member with an edge crack profile.
3. The geometry factor ' β ' of the partially cracked flexural I-shaped member with an edge crack profile was found to depend on the tension flange width (b_f). The geometry factor ' β ' was found to decrease with an increase in the tension flange width (b_f). There was a difference of about 15% between the specimens having flange width (b_f) 13 inch and 26 inch.
4. The edge crack length (a) had the most profound influence on the geometry factor ' β ' of the partially cracked flexural I-shaped member with an edge crack profile. There was a 50% increase in the ' β ' values when the edge crack length was varied between 1 inch and 5 inch.
5. It was observed that there was a redistribution of stresses in the tension flange and part of the web near the crack line in partially cracked flexural I-shaped member with edge crack. Additionally, the neutral axis shifted upwards by about an inch between the flexural I-shaped member models with no edge crack and a 5 inch edge crack.

6. For both the partially cracked flexural I-shaped member, and an axially loaded plate with an edge crack profile, the geometry factor ' β ' was determined and was found to be a function of the ratio of crack length-to-flange width (a/W). The determined SIF solution (β factor) for the flexural I-shaped member was only in good agreement with the plate solution (or handbook solution) up to a/W ratio of 0.2 (within 5%), and the solutions deviated at larger a/W ratios.
7. For the partially cracked flexural I-shaped member with an edge crack profile, the relationship between the fracture stress and crack length can be further used to analyze the flaw criticality (i.e. the number of fatigue cycles before the member fracture can be calculated).

Full-width Crack Profile

8. The tension flange thickness (t_f) and the crack length (a) had the most significant influence on the geometry factor ' β ' of the partially cracked flexural I-shaped member with a full-width crack profile. There was a difference of about 20% in the geometry factor ' β ' between the specimens having flange thickness (t_f) 1.5 inch and 2.25 inch. Also, a 21.5% increase in the geometry factor ' β ' of the flexural I-shaped member was recorded as the full-width crack was varied from 0.75 inch to 1.125 inch.
9. For both the partially cracked flexural I-shaped member, and an axially loaded plate with a full-width crack profile, the geometry factor ' β ' was determined as a function of the ratio of crack length-to-flange thickness (a/W). There was a difference of about 19% between the obtained flexural I-shaped member and the plate SIF solution for an a/W ratio of 0.3, and the solution deviated beyond that. For an a/W ratio of 2.25, the difference in the SIF solutions was as high as 106%.

10. The local stress concentration was seen in the majority portion of the tension flange and part of the web around the full-width crack line. The region of the plastic zone was larger in the case of the edge crack profile in comparison to a full-width crack profile.
11. The cross-sectional stress profiles under a loading of 55% F_y (27.5 ksi) were studied to analyze the effect of stress redistribution. Flexural I-shaped member models with two different a/W ratio were analyzed: 0.5 and 0.33. The results show that the higher a/W (0.5) was the worst case, and there was a stress increase of about 138% in the tension flange due to the presence of a full-width crack.
12. A built-up section with a failed cover plate was simulated using a simplified partially cracked flexural I-shaped member with full-width crack and the stress redistribution was studied. The stress increase in the tension flange due to full-width crack was calculated and compared to previous research results of built-up sections with a failed cover plate. There was a difference of approximately 23% between both the results. The stress in the tension flange of the flexural I-shaped member was higher than the stress in the adjacent angle of the built-up section due to the localized stress concentration around the full-width crack.

5.2 Future Work and Recommendation

Geometry Factor ' β ' of the flexural I-shaped member with a full-width crack profile

From the parametric study of the partially cracked flexural I-shaped member with a full-width crack profile, it was observed that in addition to the tension flange thickness (t_f) and full-width crack length (a), the tension flange width (b_f) had some influence on the geometry factor (SIF). So, additional FEA models should be performed to include the effect of tension flange width (b_f) in the SIF solution. A more sophisticated (accurate) solution for geometry factor as

a function of all the three parameters- tension flange thickness (t_f), full-width crack length (a), tension flange width (b_f) can then be determined.

Elastic-Plastic Fracture Mechanics (EPFM)

This research had focused on LEFM of partially cracked flexural I-shaped members. The plastic zone around the crack line/crack tip limits the application of LEFM. Also, the plastic deformation around the crack tip is not captured in the LEFM. Hence, EPFM analysis can be performed to quantify the stress in the vicinity of the crack line, especially when the nonlinear material behavior is dominant in the member. The crack parameter in terms of the J-integral can be obtained instead of SIF which is a common practice for linear-elastic models.

Internal cracks

In structural steel girders, it is more likely to observe internal cracks. A similar study could be conducted to determine a SIF solution for the flexural I-shaped member with different types of internal cracks. The Penny shaped cracks are one of the most types of internal cracks seen in flexural I-shaped members. Structural members with high tensile stresses are prone to crack formation such as the tension flange of the I-shaped member. Therefore, similar research can be performed to analyze the penny-shaped cracks, and a parametric study can be conducted to determine an analytical equation for the geometry factor ' β '.

Failure Assessment Diagram (FAD)

A Failure Assessment Diagram (FAD) helps to study the nature of crack: acceptable, critical or unacceptable. Considering the loading condition, material property, and member geometry, a FAD curve can be developed. FAD gives a relation between the brittle fracture and plastic collapse. Figure 63 shows the schematic representation of FAD(Sharma, Ghosh et

al., 2014), where the x-axis is plastic collapse ratio (L_r), and the y-axis is the brittle fracture ratio (K_r). The FAD helps to analyze the nature of crack, and the chances of structural failure due to the presence of a crack. In this research study, the SIF solution was determined for partially cracked flexural I-shaped cross-sections. Also, the fracture toughness value was determined using the CVN notch toughness value. These parameters can be used to develop a FAD for partially cracked flexural I-shaped cross-sections, and study the nature of crack for the potential chances of structural failure. Next, for a specific crack length, a FAD point can be calculated. Then, using the FAD curve and the calculated FAD point, a crack can be classified as critical or sub-critical. If the FAD point is within the area of the curve then the crack is stable. Further, using that information, the remaining fatigue life of the structure can also be calculated.

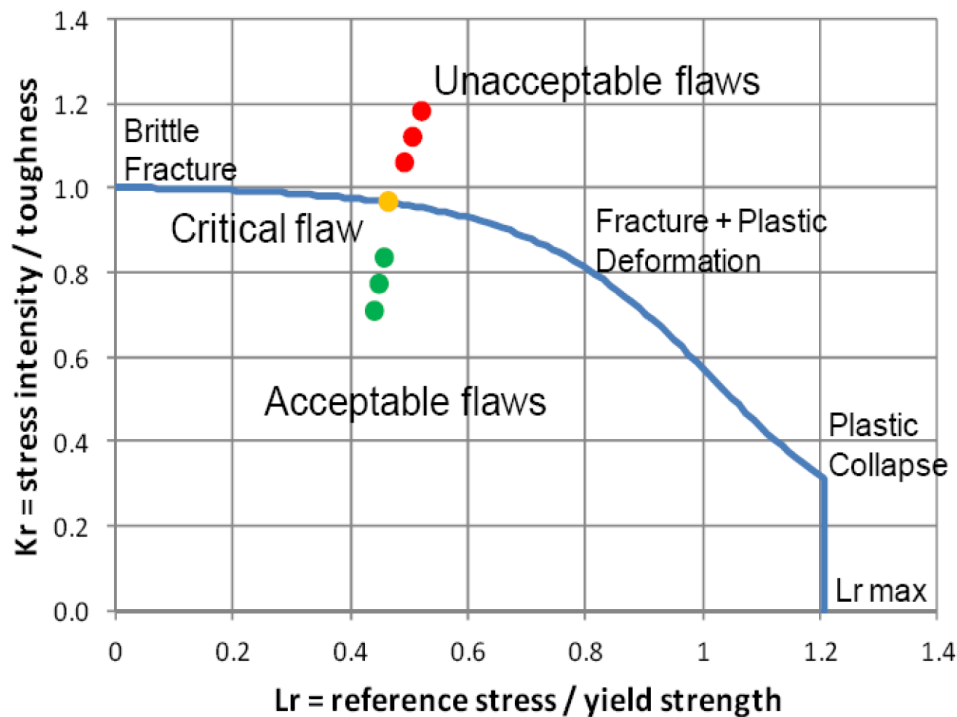


Figure 63: Typical Failure Assessment Diagram (Sharma, Ghosh et al., 2014)

References

- AASHTO. (2011). *The Manual For Bridge Evaluation (2nd ed.)*. Washinton DC: American Association of State Highway and Transportation Officials.
- ABAQUS 6.14 Documentation. (2014). *Simulia*. Waltham, MA.
- ABAQUS Analysis User's Manual. (2006). *DS Simulia*. Retrieved from <https://classes.engineering.wustl.edu/2009/spring/mase5513/abaqus/docs/v6.6/books/usb/default.htm?startat=pt04ch11s04aus56.html#usb-anl-acontintegral-singularity>
- Aliabadi, M. (2002). *The Boundary Element Method - Volume 2 Applications in Solids and Structures*. John Wiley & Sons, Ltd.
- ASTM International. (2005). *Standard Specification for Structural Steel for Bridges*. West Conshohocken, PA: ASTM International.
- Barnby, J. (1971). An Introduction to Fracture Mechanics. *Non-destructive testing*.
- Barsom, J. M., & Rolfe, S. T. (1999). *Fracture and Fatigue Control in Structures - Application of Fracture Mechanics*. Philadelphia, PA: ASTM.
- Barsoum, R. S. (1976). On the use of isoparametric finite elements in linear fracture mechanics. *International journal for numerical methods in engineering*, 25-37.
- Bazant, Z. (1990). Justification and improvement of Kienzler and Herrmann's estimate of stress intensity factors of cracked beams. *Engineering Fracture Mechanics*, 523-525.
- Connor, R. J., Dexter, R., & Mahmoud, H. (2005). *Inspection and Management of Bridges with Fracture-Critical Details*. Washington DC: Transportation research board.
- Courtin, S., Gardin, C., Bezine, G., & Hamouda, B. (2005). Advantages of the J-integral approach for calculating stress intensity factor when using the commercial finite element software ABAQUS. *Engineering Fracture Mechanics*, 2174-2185.
- Dunn, M. L., Suwito, W., & Hunter, B. (1997). Stress Intensity for Cracked I-beams. *Engineering Fracture Mechanics, Vol 57*, 609-615.

- Ghosn, M., & Yang, J. (2014). *Bridge System Safety and Redundancy*. Transportation Research Board.
- Grandt, A. (2004). *Fundamentals of Structural Integrity*. John Wiley & Sons, Inc.
- Griffith, A. (1921). The Phenomena of rupture and flow in solids. *Philosophical transactions of the royal society of London, Series A*, pp. 163-198.
- Haddad El, M., Topper, T., & Smith, K. (1979). Prediction of Non Propagating Cracks. *Engineering Fracture Mechanics*, 573-584.
- Hebdon, M. H. (2015). *Member-Level Redundancy of Built-up Steel Girders*. West Lafayette: Purdue University .
- Hebdon, M., Bonachera Martin, F. J., Korkmaz, C., & Connor, R. J. (2017). Fracture resilience of Steel Built-up members subjected to flexure. *Journal of Bridge Engineering*.
- Hebdon, M., Bonachera Martin, F. J., Korkmaz, C., & Connor, R. J. (2017). *Load Redistribution and Remaining Fatigue Life of Steel Built-Up Members Subjected to Flexure Following a Component Failure*. ASCE.
- Huizer, C. (2017). *Modelling a crack using Abaqus*. Retrieved from info.simuleon.com: <https://info.simuleon.com/blog/modelling-a-crack-using-abaqus>
- Irwin, G. (1957). Analysis of stresses and strains near the end of a crack traversing a plate. *Journal of Applied Mechanics*, 361-364.
- Kittur, M., & Huston, R. (1990). Finite Element Mesh Refinement Criteria For Stress Analysis. *Computer and Structures, Vol 34*.
- Ohio Department of Transportation. (2008). Preventive Maintenance/Repair Guidelines for Bridges and Culverts. Retrieved from [www.dot.state.oh.us: http://www.dot.state.oh.us/Divisions/Engineering/Structures/bridge%20operations%20and%20maintenance/PreventiveMaintenanceManual/BPMM/beams/sbeams.htm](http://www.dot.state.oh.us/Divisions/Engineering/Structures/bridge%20operations%20and%20maintenance/PreventiveMaintenanceManual/BPMM/beams/sbeams.htm)
- Pedro, A., Akhrawat, L., & Daqing, F. (2008). Stress Intensity Factors for Structural Steel I-beams. *Journal of Structural Engineering*.

- Rice, J. (1968). A path independent integral and the approximate analysis of strain concentration by notches and cracks. *Journal of Applied Mechanics*, 379-396.
- Roylance, D. (2001). *Introduction to fracture mechanics*. Cambridge, MA.
- Russo, F. M., Mertz, D. R., Frank, K. H., & Wilson, K. E. (2016). *Design and Evaluation of Steel Bridges for Fatigue and Fracture - Reference Manual*. Federal Highway Administration.
- Schreurs, P. (2012). *Fracture Mechanics*.
- Sharma, R. K., Ghosh, A., Bhachawat, D., Ingole, S., Balasubramanian, A., & Muktibodh, U. (2014). Assessment of Structural Integrity of Pressure Tubes during Cold Pressurization. *1st International Conference on Structural Integrity, ICONS*, 359 – 366.
- Sherman, R. J. (2016). *Standards to Control Fracture in Steel Bridges Through the Use of High-Toughness Steel and Rational Inspection*. West Lafayette, Indiana.
- Sun, C., & Jin, Z.-H. (2012). Elastic-Plastic Fracture Criteria. In C. J.-H. Sun, *Fracture Mechanics* (pp. 171-187). Elsevier.
- Tada, H., Paris, P., & Irwin, G. (2000). *The Stress Analysis of Cracks Handbook Third Edition*. Professional Engineering Publishing.
- Venkatachalam, G., Harichandran, R., Rajkumar, S., Dharmaraja, C., & Pandivelan, C. (2008). Determination of J-integral and stress intensity factor using the commercial FE software ABAQUS in austenitic stainless steel (AISI 304) plates. *International Journal of Advanced Manufacturing Technology*.
- Whitehead, J. (2015). *Probability of Detection Study for Visual Inspection of Steel*.
- Wright, W. J. (2015). *Steel Bridge Design Handbook: Bridge Steels and Their Mechanical Properties*. Washington D.C: Federal Highway Administration.

APPENDIX A

A.1 Model Development

A.1.1 Symmetry

Symmetry and anti-symmetry boundary condition help to reduce the model development and analysis time, especially when developing an FE model of a complex geometry comprising of a lot of components. A more simplified model of a structure having one or more reflective symmetry planes can be developed by taking advantage of symmetry boundary condition on the symmetrical edges. To apply the symmetry boundary condition, the support conditions have to be symmetric about the same plane, while the loading can either be symmetric, or anti-symmetric. On the symmetry plane, the perpendicular displacement vector, and the parallel rotational vector are zero. The opposite criteria will apply to the anti-symmetric plane.

An example of a tension plate with a hole in the center is explained in this section. The plate is symmetric about both the x and y-axis, hence only quarter portion was modeled for analysis. Figure 64 shows the quarter portion of the plate which will be used for analysis instead of a full-size plate.

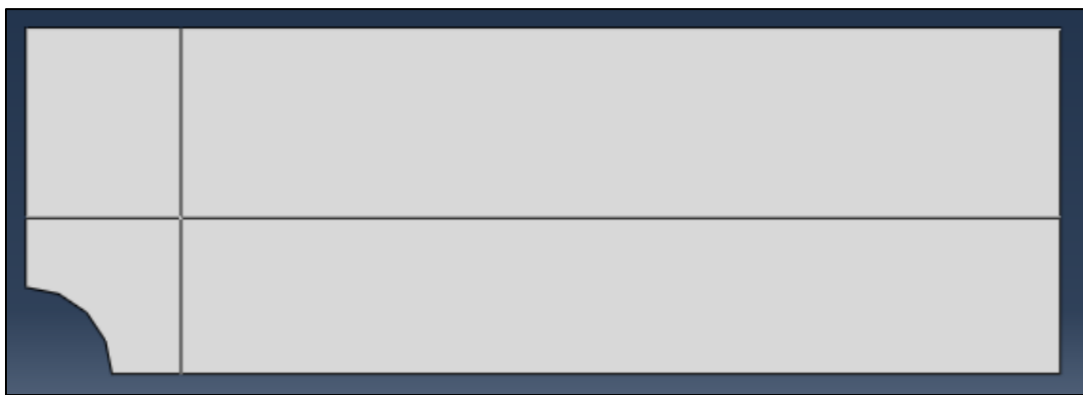


Figure 64: Quarter portion of the tension plate

Boundary condition ‘XSYMM’ (zero displacement along the x-axis and zero rotations along the y-axis and z-axis) has been applied to achieve x-axis symmetry while boundary condition ‘YSYMM’ (zero displacement along the y-axis and zero rotations along the x-axis and z-axis) has been applied to achieve y-axis symmetry. Figure 65 & Figure 66 below shows the symmetry boundary condition about the x-axis and y-axis respectively. Notice that the displacement or rotation at the flaw points (Holes or Cracks) are not zero. The quarter center-hole portion in this example.

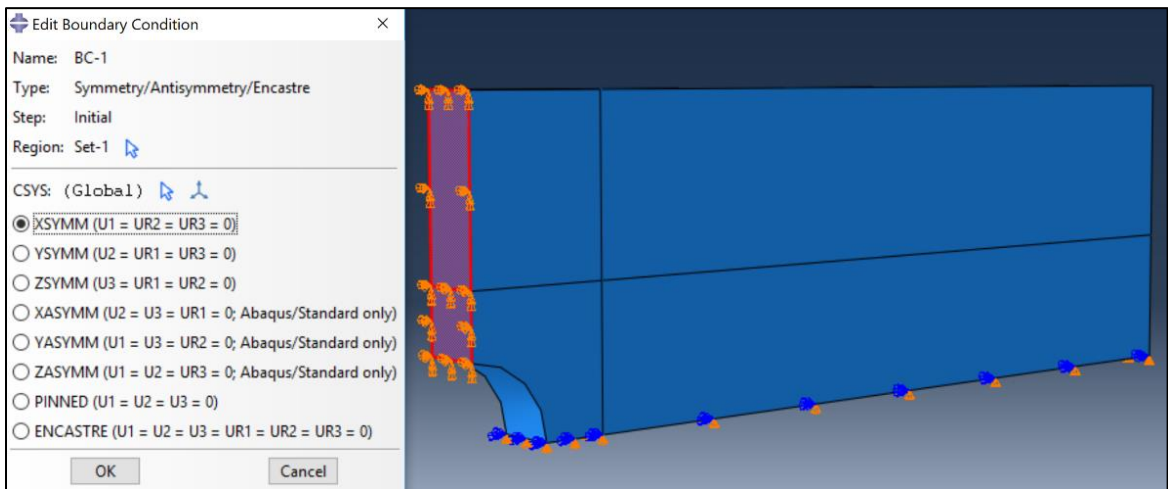


Figure 65: X-axis symmetry

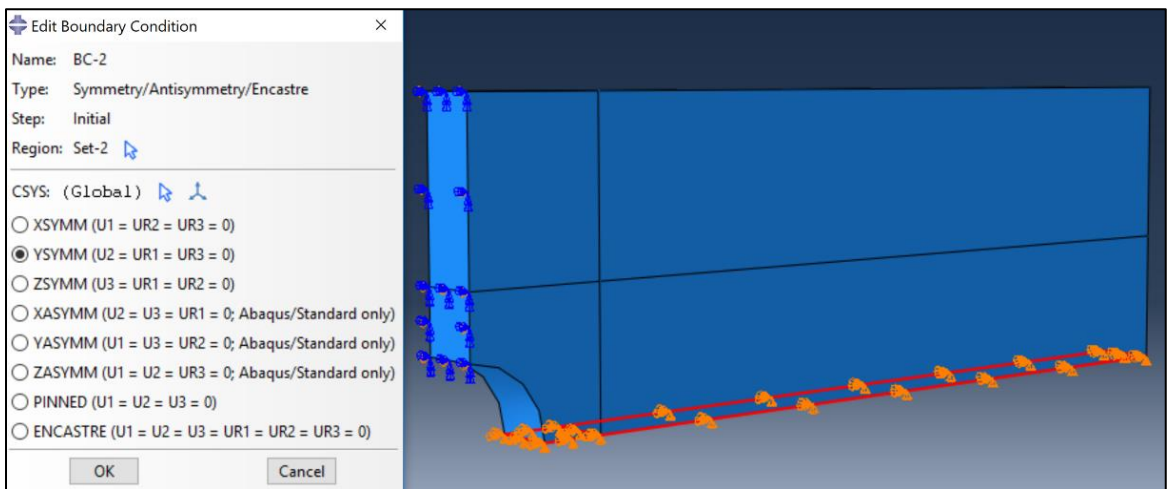


Figure 66: Y-axis symmetry

Figure 67 below shows the uniform load applied on the symmetric edge (X-axis) of the plate. In this example, a pressure of 5ksi is applied on the right edge. The negative sign indicates the tension force on the surface.

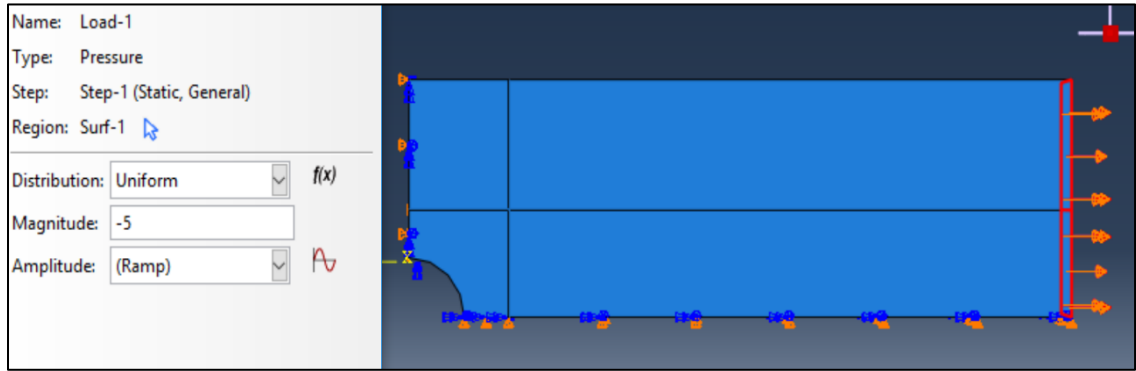


Figure 67: Tension loading

We only have the quarter portion of the plate which helps to finely mesh the part especially around the flaw or crack line. This will eventually help to increase the accuracy of the history outputs such as SIF, J-integral etc., Moreover, the analysis run time will be significantly reduced.

A.1.2 Modeling a Crack

Finite Element Analysis is one of the best approaches to study the crack growth behavior in a member. ABAQUS is a popular and useful software used to model and analyze the geometries with cracks. When the crack is very sharp the stress at the tip of the crack is theoretically infinite which is called as “Crack tip singularity”. Although, in reality, the cracks are not very sharp, they have definite thickness. However, it is difficult to measure the thickness and sketch it on the member cross-section. Instead, ABAQUS allows the user to simulate the crack using the ‘special tool’ under the ‘interaction module’. The special tool allows the user to create, and edit cracks.

Cracks can be simulated on a complete geometry as well as on a symmetric plane. If the crack is on a symmetric plane seam command is not used to define the crack and no symmetry boundary conditions are applied at the crack plane. The cracks can be of any nature like edge crack, center crack or double edge crack.

Assigning the seam

When the partition tool is used to represent a crack, the elements on each side of the crack planes are connected and share nodes. When we assign the seam, these element nodes will be separated. Under the interaction module, using special tool => crack => Assign seam, select the edge or face to assign the seam to represent a crack. The black solid line shown in Figure 68 shows the seam line representing the edge crack.

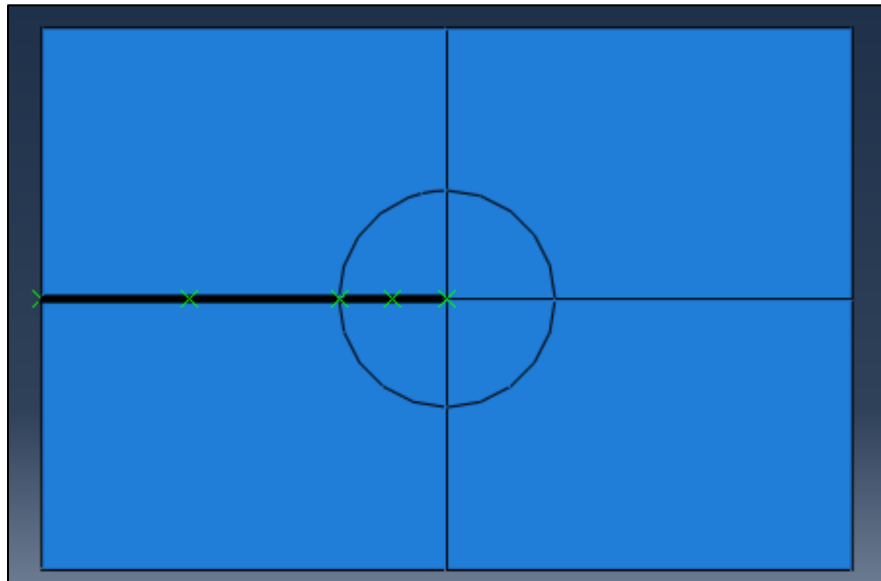


Figure 68: Seam line representing the edge crack

Defining the crack

After assigning the seam, a crack can be defined to request specific output. This can be done using the interaction module => special => crack => create or by double-clicking ‘Cracks’ in the model tree, under ‘Assembly’, ‘Engineering Features’. Give a name to the crack and select contour integral in the type as shown in Figure 69. The reason for selecting the contour integral type is that the requested output will be calculated for a layer of elements around the crack line. History output at each node for each contour around the crack line will be automatically specified after running the job.

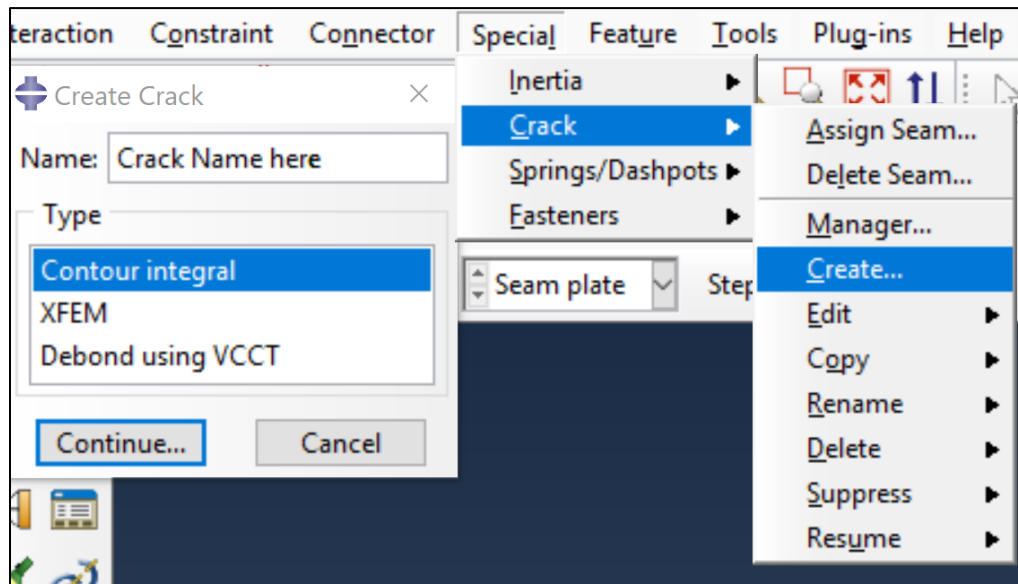


Figure 69: Crack Creation

The crack front determines the first layer of elements used to calculate the requested output value (Huizer, 2017). Crack extension direction can be assigned either by using normal to the crack plane option or using q vectors. Figure 70 shows the crack extension direction in red arrows defined using normal to crack plane option. If the crack is on the symmetry plane under the edit crack window check the box “On symmetry plane (half-crack model)” as shown in

Figure 70. If this option is used, no symmetry boundary conditions or seam are applied on the crack plane, allowing it to open under the applied load.

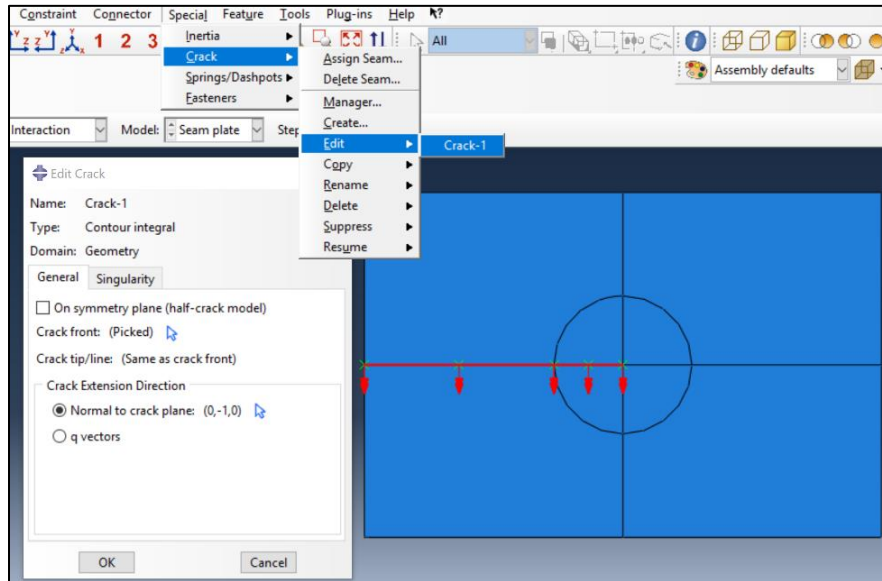


Figure 70: Edit crack options

If we are interested in finding the SIF of a model, defining the crack tip singularity is very important. This can be defined using the singularity tab located on the right side of the general tab under the edit crack window (Figure 71). Mid-side node parameter of 0.25 will be used and the nodes along the crack line will be constrained to move together by choosing “Collapsed element side, single node” option under degenerate element control at the crack line.

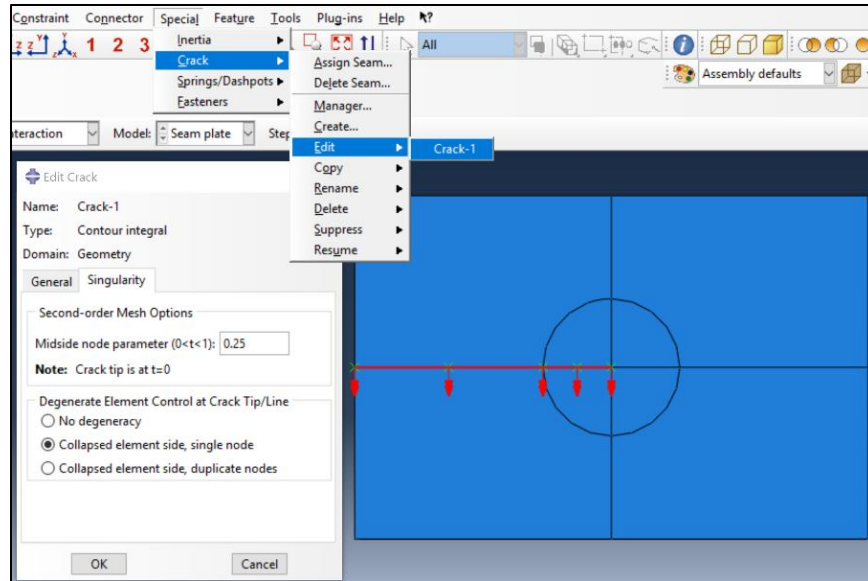



Figure 71: Crack-tip Singularity

Requesting history output

Crack-related history output can be created using the ‘history output request’ option. Under History Output Requests => domain => crack => choose the required crack name if there is more than one crack, as shown in Figure 72. Have at least eight contours for best results. Then, select a type of output required like J-integral or SIF. If there is more than one output, create separate history output requests for each one.

 Edit History Output Request

Name: H-Output-1

Step: load

Procedure: Static, General

Domain: Crack : Crack-1

Frequency: Every n increments n: 1

Timing: Output at exact times

Number of contours: 8

☐ Step for residual stress initialization values:

Type: ☐ J-integral
☐ Ct-integral
☐ T-stress
☒ Stress intensity factors

Crack initiation criterion: ☐ Maximum tangential stress
☒ Maximum energy release rate
☐ KII=0

Figure 72: History Output Request

After submitting the job and completing the analysis, under the results tab, history output can be obtained (Figure 73). Figure 74 shows the visualization of the edge cracked plate. The stress concentration and plastic deformation (plastic zone) around the crack tip can be observed.

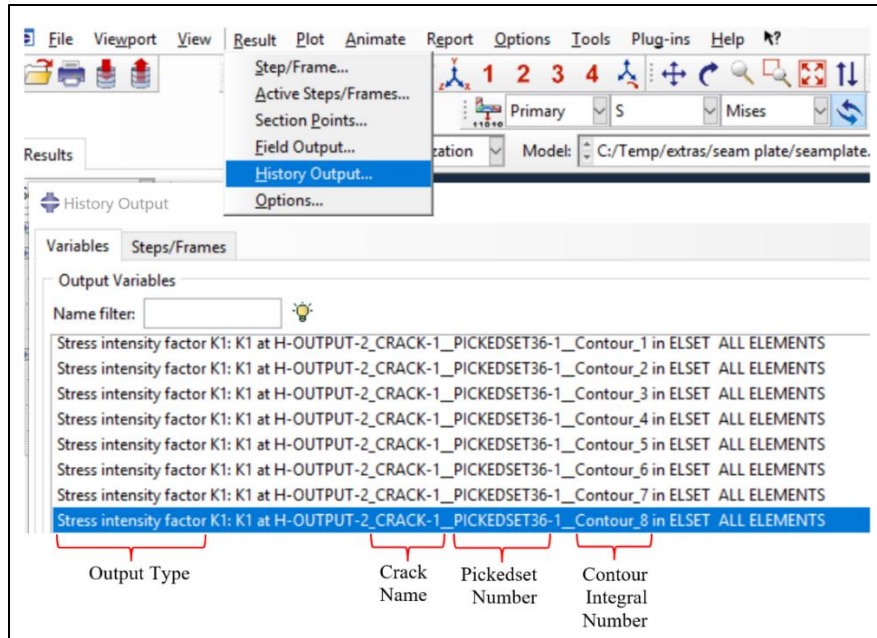


Figure 73: History Output

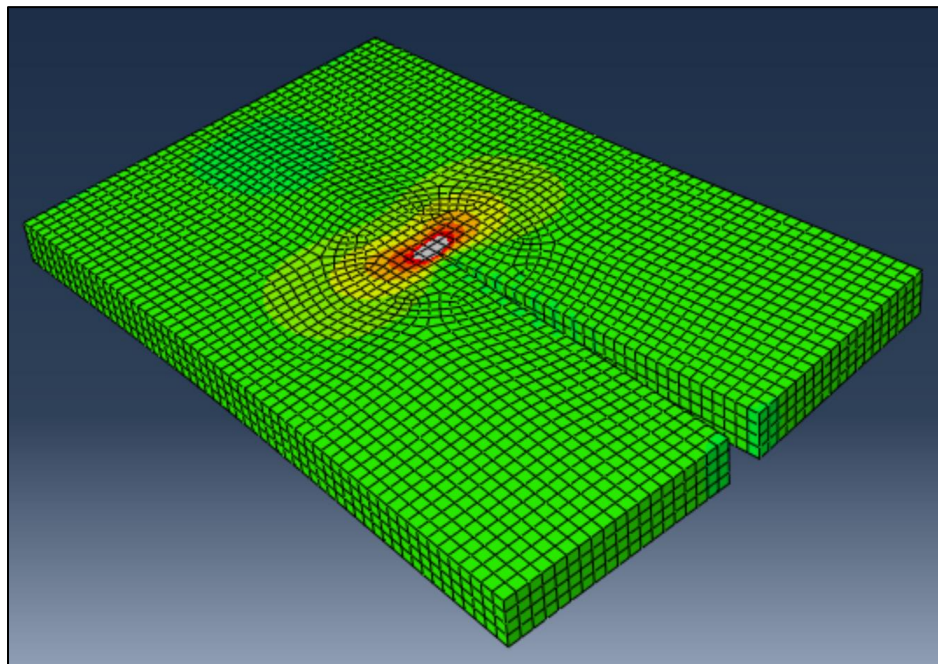


Figure 74: Visualization of Edge Cracked Plate

APPENDIX B

B.1 Handbook Solution for Benchmark Study Specimens

In the following section the calculation for handbook solution of benchmark study specimens are showed.

Axial Specimens

Specimen A1 – Edge Crack Profile

Plate Geometry

$$\text{Length} := 60 \text{ inch}$$

$$\text{Breadth} := 22 \text{ inch}$$

$$W := \text{Breadth}$$

$$\text{Thickness} := 1.5 \text{ inch}$$

$$\text{Crack_length} := 3 \text{ inch}$$

$$a := \text{Crack_length}$$

Material Properties

$$F_y := 50 \text{ ksi}$$

$$E := 29000 \text{ ksi}$$

$$\nu := 0.29$$

Geometry Factor Calculation Using the Handbook Solution

$$\alpha := \frac{a}{W}$$

$$\beta := 1.12 - 0.231(\alpha) + 10.55(\alpha)^2 - 21.73(\alpha)^3 + 30.29(\alpha)^4$$

Far-field Stress ' σ '

$$\sigma := 0.75 \cdot F_y = 37.5 \text{ ksi}$$

$$\text{SIF: } K_I := \sigma \cdot \sqrt{\pi \cdot a} \cdot \beta$$

$$\boxed{K_I = 142.76} \text{ ksi} \cdot \sqrt{\text{in}}$$

Specimen A2 – Double-Edge Crack Profile

Plate Geometry

Length := 60 inch

Breadth := 22 inch

W := Breadth

Thickness := 1.5 inch

Crack_length := 3 inch

a := Crack_length

Material Properties

Fy := 50 ksi

E := 29000 ksi

ν := 0.29

Geometry Factor Calculation Using the Handbook Solution

$$\alpha := \frac{a}{W}$$

$$\beta := \frac{1.122 - 0.561 \cdot (\alpha) - 0.205 \cdot (\alpha)^2 + 0.471 \cdot (\alpha)^3 - 0.19 \cdot (\alpha)^4}{\sqrt{1 - \alpha}} = 1.122$$

Far-field Stress ' σ '

$\sigma := 0.75 \cdot F_y = 37.5$ ksi

SIF: $K_I := \sigma \cdot \sqrt{\pi \cdot a} \cdot \beta$

$K_I = 129.184$

 ksi·√in

Specimen A3 – Center Crack Profile

Plate Geometry

Length := 60 inch

Breadth := 22 inch

W := Breadth

Thickness := 1.5 inch

Crack_length := 1.5 inch

a := Crack_length

Material Properties

Fy := 50 ksi

E := 29000 ksi

ν := 0.29

Geometry Factor Calculation Using the Handbook Solution

$$\alpha := \frac{a}{W}$$

$$\beta := \sec(\pi \cdot \alpha) = 1.023$$

Far-field Stress ' σ ' $\sigma := 0.75 \cdot F_y = 37.5 \text{ ksi}$

SIF: $K_I := \sigma \cdot \sqrt{\pi \cdot a} \cdot \beta$

$K_I = 83.309$

 ksi·√in

Specimen A4 – Edge Crack Profile

Plate Geometry

$$\text{Length} := 60 \text{ inch}$$

$$\text{Breadth} := 22 \text{ inch}$$

$$W := \text{Breadth}$$

$$\text{Thickness} := 1.5 \text{ inch}$$

$$\text{Crack_length} := 3 \text{ inch}$$

$$a := \text{Crack_length}$$

Material Properties

$$F_y := 70 \text{ ksi}$$

$$E := 29000 \text{ ksi}$$

$$\nu := 0.29$$

Geometry Factor Calculation Using the Handbook Solution

$$\alpha := \frac{a}{W}$$

$$\beta := 1.12 - 0.231(\alpha) + 10.55(\alpha)^2 - 21.73(\alpha)^3 + 30.29(\alpha)^4$$

Far-field Stress ' σ ' $\sigma := 0.75 \cdot F_y = 52.5 \text{ ksi}$

SIF: $K_I := \sigma \cdot \sqrt{\pi \cdot a} \cdot \beta$

$K_I = 199.864$

 ksi·√in

Specimen A5 –Edge Crack Profile

Plate Geometry

Length := 60 inch

Breadth := 14 inch

W := Breadth

Thickness := 2.5 inch

Crack_length := 3 inch

a := Crack_length

Material Properties

Fy := 50 ksi

E := 29000 ksi

ν := 0.29

Geometry Factor Calculation Using the Handbook Solution

$$\alpha := \frac{a}{W}$$

$$\beta := 1.12 - 0.231(\alpha) + 10.55(\alpha)^2 - 21.73(\alpha)^3 + 30.29(\alpha)^4$$

Far-field Stress ' σ '

$$\sigma := 0.75 \cdot F_y = 37.5 \text{ ksi}$$

SIF: $K_I := \sigma \cdot \sqrt{\pi \cdot a} \cdot \beta$

$$\boxed{K_I = 161.748 \text{ ksi} \cdot \sqrt{\text{in}}}$$

Bending Specimens

Specimen B2 – Edge Crack Profile

Plate Geometry Length $s := 480 \text{ in}$

Breadth $b := 3 \text{ in}$

Depth $d := 12 \text{ in}$

Material Properties $F_y := 50 \text{ ksi}$

$E := 29000 \text{ ksi}$

$\nu := 0.29$

Far-field Stress 'σ'

Neutral – Axis $y := \frac{d}{2} = 6 \text{ in}$ MOI $I := \frac{b \cdot d^3}{12} = 432 \text{ in}^4$

Load $P := 15 \text{ kips}$ Moment $M := P \cdot \frac{s}{3} = 2400 \text{ kip-in}$

Stress $\sigma := \frac{M \cdot y}{I} = 33.333 \text{ ksi}$

Geometry Factor Calculation Using the Handbook Solution

Crack Length $a := 3 \text{ in}$

$$\alpha := \frac{a}{d} = 0.25$$

$$\beta := \frac{1}{\pi} \cdot \frac{\left[1.99 - \alpha \cdot (1 - \alpha) \cdot \left(2.15 - 3.93 \cdot \alpha + 2.7 \cdot \alpha^2 \right) \right]}{(1 + 2 \cdot \alpha) \cdot (1 - \alpha)^{\frac{3}{2}}} = 0.568$$

SIF: $K_I := \sigma \cdot \sqrt{\pi \cdot a} \cdot \beta$

$K_I = 58.156$

 ksi·√in